COMPREHENSIVE ANALYSIS OF GLOBAL MID OCEAN RIDGE AND MARIANA CONVERGENT MARGIN HYDROTHERMAL SYSTEMS

TECTONICS, FLUID CHEMISTRY AND VENT BIOTA

by

Diluni Ayeshika Wimalaratne Hetti Pathirannehelage

APPROVED BY SUPERVISORY COMMITTEE:

Dr. Robert J. Stern, Chair

Dr. Thomas Brikowski

Dr. Juan Gonzalez

Dr. Carlos Aiken

Through the trenches up to the ridges

You made my journey a success

…

To my little Neth, Sachith, family, friends and mentors

COMPREHENSIVE ANALYSIS OF GLOBAL MID OCEAN RIDGE AND MARIANA CONVERGENT MARGIN HYDROTHERMAL SYSTEMS TECTONICS, FLUID CHEMISTRY AND VENT BIOTA

by

DILUNI AYESHIKA WIMALARATNE HETTI PATHIRANNEHELAGE, BS, MS

DISSERTATION

Presented to the Faculty of

The University of Texas at Dallas

in Partial Fulfillment

of the Requirements

for the Degree of

DOCTOR OF PHILOSOPHY IN

GEOSCIENCES

THE UNIVERSITY OF TEXAS AT DALLAS

May 2020

ACKNOWLEDGMENTS

I would like to thank Dr. Frank Konietschke and Asanka M. Gunawardana of the Department of Mathematical Sciences at the University of Texas at Dallas for their guidance in statistical analysis.

April 2020

COMPREHENSIVE ANALYSIS OF GLOBAL MID OCEAN RIDGE AND MARIANA CONVERGENT MARGIN HYDROTHERMAL SYSTEMS

TECTONICS, FLUID CHEMISTRY AND VENT BIOTA

Diluni Ayeshika Wimalaratne Hetti Pathirannehelage, PhD
The University of Texas at Dallas, 2020

Supervising Professor: Robert J. Stern

This study is a multidisciplinary data integration and metadata analysis for mid-ocean ridge (MOR) and Mariana intra oceanic convergent margin hydrothermal vents including fluids and biota. We compiled separate databases for MOR and Mariana hydrothermal vent parameters and their vent biota using published and on-line information managed by government agencies and other research institutes. The vent parameter databases are compiled under the categories of setting, vent field name, vent field number, name, latitude, longitude, alias, vent sites, smoker type and chimney composition, host rocks, full spreading rate, depth, temperature, pH, total Fe, $(^3He/^4He)/R_a$, CO_2, CH_4, H_2, H_2S, SO_4^{2-} ions, chlorinity, operations and references. MOR database for vent parameters includes 449 individual hydrothermal vents grouped into 73 vent fields at global divergent margins. The vent organism database of MOR vents includes 672 species belong to 72 individual vents. Mariana vent summary database includes 47 individual hydrothermal vents belong to four different tectonic settings: the forearc (FAR), arc (ARC), backarc (BAB) and the southern Mariana trough (SMT). Database for Mariana biota include vent animals for 31 vents of the above settings.

We considered vent depth, fluid temperature, pH, total Fe, Mn, helium isotopic ratio (($^3He/^4He)/R_a$), fluid gases (CO_2, CH_4, H_2, H_2S), SO_4^{2-} ions and chlorinity of the fluids for statistical analysis. In addition to these parameters, for MOR vents full spreading rate was also considered for statistical analysis. To overcome non-linear data distributions and small number of observations for some vent parameters, we used purely nonparametric statistical procedures. We assessed vent fluid parameters first for correlations with key parameters spreading rate (for MOR only), summit depth, fluid temperature and fluid chlorinity. Second, we compared different segments (MOR segments and Mariana tectonic settings) based on vent parameters. Similarities between the vent organisms in different tectonic segments were assessed using Sörensen similarity indices; for MOR vents at both genera and species levels; and for Mariana only for genus level. Our results for MORs show that even if MOR hydrothermal systems are associated with simple divergent margin tectonism, they are remarkably similar despite having differences in both fluid chemistry and biota distribution regardless of the ocean and the rate of spreading. Vent fluid temperature, pH, Fe, Mn, CO_2, H_2, SO_4^{2-} ion and chlorinity are independent of the spreading rate. Fluid temperature does control pH, Fe and H_2S. Brine separation might influence gases such as helium isotopic ratio and CO_2 in venting fluids. Highest similarities of the macro organisms are seen in the Indian Ocean ridges and the greatest differences are observed in the Pacific Ocean ridges. Integration of tectonics, fluid chemistry and vent biota of Mariana convergent margin vents demonstrate that Mariana vent groups are more diverse than global mid-ocean ridge vents and that the southernmost Marianas most resembles mid-ocean ridge (MOR) type venting, the other tectonic groups are quite different than MOR vents.

TABLE OF CONTENTS

LIST OF FIGURES

LIST OF TABLES

LIST OF ABBREVIATIONS

ANOVA	Analysis of Variance
ARC	Arc
BAB	Backarc Basin
CIR	Central Indian Ridge
EPG	East Pacific - Galapagos
EPR	East Pacific Rise
EOL	Encyclopedia of Life
EXR	Explorer Ridge
FAR	Forearc
GKR	Gakkel Ridge
GSC	Galapagos Spreading Center
GOR	Gorda Ridge
HOV	Human Occupied Vehicle
JAMSTEC	Japan Agency for Marine-Earth Science and Technology
JFR	Juan de Fuca Ridge
KOR	Kolbeinsey ridge
MGDS	Marine Geoscience Data System
MAR	Mid Atlantic Ridge
MCR	Mid Cayman Rise
MOR	Mid Ocean Ridge
MHR	Mohn’s Ridge

NOAA	National Oceanic and Atmospheric Administration
NEP	Northeast Pacific Ridges
n/a	Not Available
PMEL	Pacific Marine Environmental Laboratory
ROV	Remotely Operated Vehicle
RKR	Reykjanes Ridge
SMT	Southern Mariana Trough
SWIR	Southwest Indian Ridge
WHOI	Woods Hole Oceanographic Institution
WoRMS	World Register of Marine Species

CHAPTER 1

GLOBAL MID OCEAN RIDGE HYDROTHERMAL VENTS AND THEIR BIOTA

1.1.ABSTRACT

This study is a multidisciplinary data integration and metadata analysis for mid-ocean ridge hydrothermal vents including fluids and biota. Our new vent database includes 449 individual hydrothermal vents grouped into 73 vent fields at global divergent margins using published and on-line information. The vent organism database includes 671 species belong to 72 individual vents. Current understanding of hydrothermal vents along the global mid-ocean ridge (MOR) network indicates that vent distribution is independent of spreading rate and are associated with unique animal communities. To overcome non-linear data distributions and small number of observations for some vent parameters, we used purely nonparametric statistical procedures. We assessed vent fluid parameters first for correlations with key parameters spreading rate, summit depth, fluid temperature and fluid chlorinity. Second, we compared different MOR segments based on vent parameters. Our results indicate that there are many moderate correlations ($0.8 > \tau > 0.45$) between key parameters and other fluid parameters. Fluid temperature does not show correlations to spreading rate and depth. Central Indian Ridge (CIR) show significantly higher concentrations of Fe and chlorinity compared with East Pacific Rise (EPR) and Northeast Pacific Ridges (NEP). Fluid temperature of NEP vents are also significantly different from EPR, MAR and CIR vents. Sörensen similarity indices were computed for seven geographic provinces (NEP, EPR, GSC, MCR, MAR, CIR and SWIR) of MOR hydrothermal vents at both genera and species levels. Similarities obtained for species is much lower than that for genera. Results show at both genera and species levels the highest similarities are seen in the ridges of the Indian ocean (CIR vs SWIR).

Overall, the data show that even if MOR hydrothermal systems are associated with simple divergent margin tectonism, they are remarkably similar despite having differences in both fluid chemistry and biota distribution regardless of the ocean and the rate of spreading.

1.2.INTRODUCTION

Mid-ocean ridge hydrothermal systems are sites of complex interactions between magmatic, tectonic, hydrological, chemical and biological subsystems. Four decades of seafloor investigations have occurred since the first vent was discovered at the Galapagos spreading center (Corliss et al., 1979). We now know much more about seafloor hydrothermal systems, especially at mid-ocean ridges, and we are also learning about hydrothermal systems in other settings: backarc basins, arcs, forearcs, and hot spots. Exploration for these vents has been conducted by means of water column surveys and/or manned submersibles or remotely operated vehicles equipped with photographic imaging, acoustic sonars and robotic/towed cameras and/or robotic samplers etc. However, many of the seafloor environments where these vents are likely to exist remain poorly surveyed and there are still many seafloor hydrothermal vents to be discovered and much more to learn. This study summarizes our current state of knowledge about mid-ocean ridge (MOR) hydrothermal systems. These hydrothermal systems are simpler and better known than those at convergent margins and hotspots. There is also more data to compile and make sense of for MOR vents than for any other type of seafloor hydrothermal system.

MOR vents generally occur in newly formed young oceanic crust of the neovolcanic zone (Kelley et al., 2001). An exception to this is the Lost City hydrothermal field where low temperature venting occurs through older oceanic crust about 15 km away from the spreading axis

(Kelley et al., 2001). There are many studies of vents at different MOR segments addressing different aspects. These studies can be categorized as 1) hydrothermal plumes (Baker et al., 1995; Baker & Urabe, 1996; Baker et al., 2001; Baker et al, 2008; Lupton et al, 1999); 2) sub-seafloor fluid-rock interactions (Von Damm and Bischoff, 1987; Massoth et al., 1989; Butterfield et al., 1990; Gamo, 1995; Alt, 1995; Tivey, 1995; 2007); 3) chemistry and evolution of hydrothermal fluids (Butterfield, 2000; Von Damm, 1990, 2000); 4) biogeography and ecology of vent communities (Lutz et al., 1993; Gebruk et al., 1997; Van Dover, 1988, 2002; Anderson et al., 2014; Tarasov et al., 2005; Beedessee et al., 2013); 5) seafloor mineralization processes (Rona, 1984; Hannington et al., 2011); and 6) submarine eruptions, geothermal studies and seafloor mapping (Baker et al., 2012; Rubin et al., 2012). Information about the six types of study are scattered throughout the scientific literature, and lack of comprehensive overviews impedes further study and analysis of MOR hydrothermal vent systems. Previous synthesis efforts are 20 years ago and MOR hydrothermal research has advanced significantly since then. These older efforts include fluid geochemistry databases for different ridges (Von Damm, 1990; Gamo, 1995; Butterfield, 2000). Such an effort is also reflected in the work by Lutz et al., (1993) and Van Dover et al., (2002). Karson et al., (2015), Kelley et al., (2002) and Fornari & Embley (1995) reviewed the essence of submarine hydrothermal venting and related processes.

The present study is motivated by the need for a multidisciplinary data integration approach to better understand MOR seafloor hydrothermal systems. In contrast to primary data analysis of site-specific observations and models, our secondary data analysis consists of data compilation and integration to better understand these geo-chemo-biological systems (Glass 1976). In such an effort, it is important to use databases and search methods in meta-analysis of existing research

data (Whiting et al. 2008). Here we present a metadata analysis for MOR hydrothermal vents including fluids and biota and statistically analyze these to elucidate hidden patterns and relationships among the different ridge segments. Our database includes data reported in peer-reviewed literature for vent fluid chemistry, host rock geology, operations history and vent biology for 449 individual hydrothermal vents in global mid ocean ridges.

1.3.GEOLOGICAL SETTINGS

MOR hydrothermal venting has been discovered at ridges with a wide range of spreading rates from ultra-fast to ultraslow. Many plume signals and vent fields have been found along the East Pacific Rise (EPR), Galapagos Spreading Center (GSC), Juan de Fuca Ridge (JFR), Explorer Ridge (EXR) and Gorda Ridge (GOR) in the Pacific Ocean; Mid Cayman Rise (MCR) in the Caribbean sea; Reykjanes Ridge (RKR), Mohn's Ridge (MHR), Kolbeinsey ridge (KOR), and Mid Atlantic Ridge (MAR) in the Atlantic Ocean; Gakkel Ridge (GKR) in the Arctic Ocean; and the Central Indian Ridge (CIR), Southwest Indian Ridge (SWIR) and Southeast Indian Ridge (SEIR) in the Indian Ocean (Fig. 1.1). Spreading rates mentioned below are full spreading rates. Possible vent fields (Fig. 1.1a) are inferred from water column chemistry and some have been confirmed by submersible observations of the seafloor.

1.3.1. Pacific Ocean Spreading Ridges

a. Juan de Fuca Ridge (JFR), Explorer Ridge (EXR), and Gorda Ridge (GOR)

These three ridge segments (A in Fig. 1.1a) in the NE Pacific are treated together as NEP and discussed from N to S; they are unusually well-studied because the ridge is so close to the U.S.and

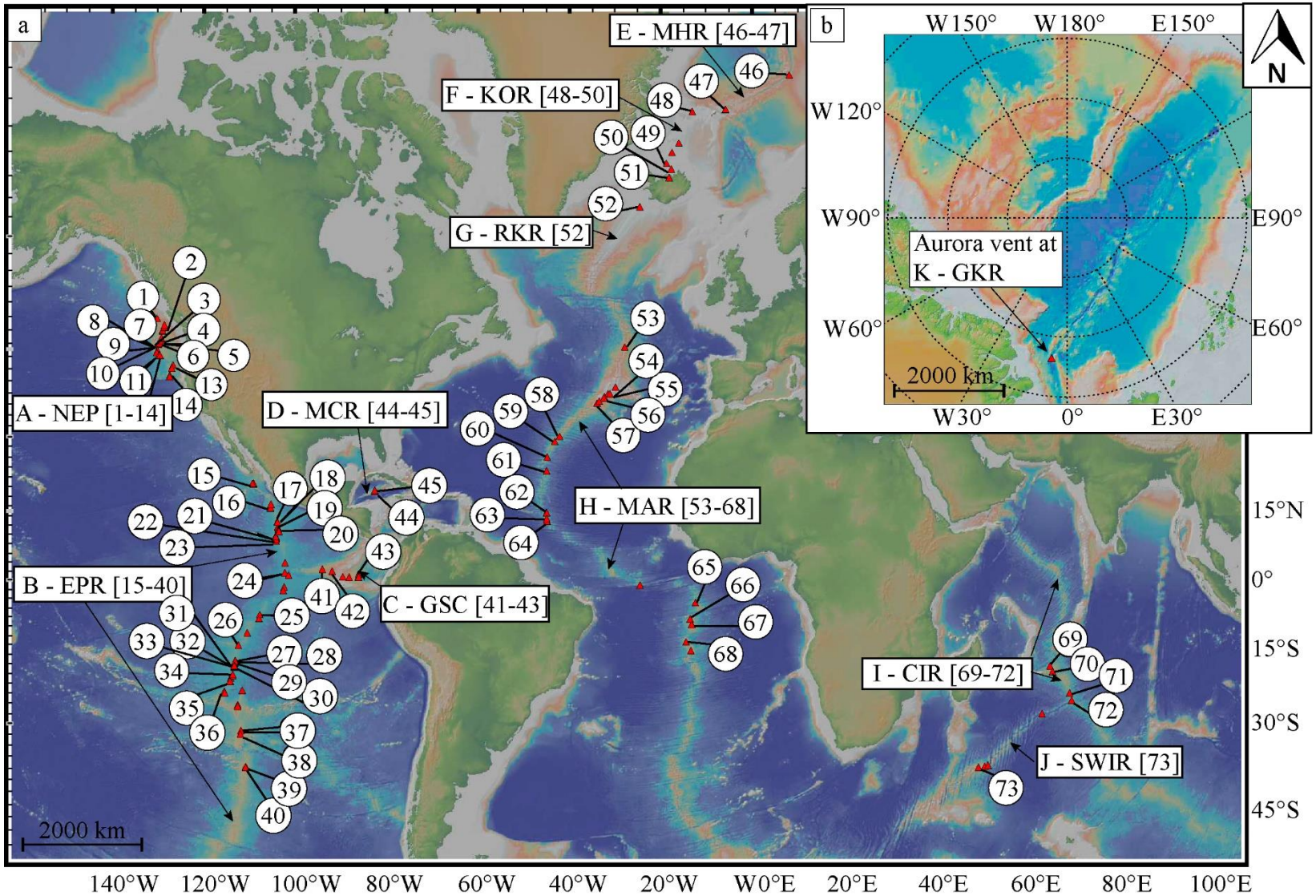
a
b
A - NEP [1-14]
B - EPR [15-40]
C - GSC [41-43]
D - MCR [44-45]
E - MHR [46-47]
F - KOR [48-50]
G - RKR [52]
H - MAR [53-68]
I - CIR [69-72]
J - SWIR [73]
Aurora vent at
K - GKR
2000 km
W150°
W180°
E150°
W120°
W90°
W60°
W30°
0°
E30°
E60°
E90°
N
15°N
0°
15°S
30°S
45°S
140°W
120°W
100°W
80°W
60°W
40°W
20°W
W0°E
20°E
40°E
60°E
80°E
100°E

Fig. 1.1: Locations of the active hydrothermal vents of the global mid ocean ridges (a) 1-71 represent documented and potential vent fields observed along the global mid ocean ridge segments (b) Documented vent field of the Gakkel Ridge in the Arctic. 1- EXR, Magic Mountain; 2- JFR, Middle Valley; 3- JFR, Endeavour Field; 4- JFR, Not Dead Yet; 5- JFR, Flow area; 6- JFR, Floc area; 7- JFR, Co-Axial; 8- JFR, Source site; 9- JFR, Axial CASM; 10- JFR, Axial Ashes; 11- JFR, North Cleft; 12- JFR, South Cleft; 13- GOR, Sea Cliff; 14- GOR, N Escanaba; 15- EPR, 21 N; 16- EPR, Teotihuacan; 17- EPR, 13 N; 18- EPR, 13 N, Marginal High; 19- EPR 11 N; 20- EPR, Feather Duster Field; 21- EPR 9° 50'N; 22- EPR 9° 47'N; 23- EPR 9 40'N; 24- EPR, Aha Field; 25- EPR, 7 25'S; 26- EPR, RM04; 27- EPR, RM24; 28- EPR, RM23; 29- EPR, 17 44'S; 30- EPR, RM29; 31- EPR, 18 15'S; 32- EPR, RM28; 33- EPR, Animal Farm; 34- EPR, 21 S; 35- EPR, Rapa Nui Field; 36- EPR, 23 30'S; 37- EPR, Nolan's Nook; 38- EPR, Saguaro Field; 39- EPR, 37 48'S Axial Dome; 40- EPR, 37 40'S Axial Dome; 41- GSC, Navidad; 42- GSC, Iguanas-Pinguinos; 43- GSC, Rose Garden; 44-MCR, Von Damm; 45-MCR, Beebe; 46- MHR, Loki's Castle; 47- MHR, Soria Moria Field; 48- KOR, Kolbeinsey Field; 49- KOR, Kolbeinsey Ridge; 50- KOR, Grimsey Field; 51- KOR, Eyjafjördur vent field; 52- RKR, Steinaholl Vent Field; 53- MAR, Moytirra; 54- MAR, Mogued Gwen; 55- MAR, Menez Gwen; 56- MAR, Lucky Strike; 57- MAR, Rainbow; 58- MAR, Lost City; 59- MAR, Broken Spur; 60- MAR, TAG Field; 61- MAR, Snakepit; 62- MAR Logatchev; 63- MAR, Semyenov; 64- MAR, Ashadze; 65- MAR, 4 48'S; 66- MAR, Nibelungen; 67- MAR, Lilliput; 68- MAR, Zouyu ridge; 69- CIR, Dodo Field; 70- CIR, Solitaire Field; 71- CIR, Edmond Field; 72- CIR, Kairei Field; 73- SWIR, Longqi Field. (b) Documented vent field of the Gakkel Ridge in the Arctic. Figure made with GeoMapApp (www.geomapapp.org).

Canada. These segments separate the Juan de Fuca and Explorer plates from the Pacific plate. The Explorer Ridge is the northern continuation of the JFR off the west coast of Canada. It consists of the Southern Explorer Ridge and several smaller ridge segments along its about 130 km length. One major hydrothermal field (Magic Mountains) has been discovered in the Southern Explorer Ridge segment, which has high temperature venting and associated biology (Butterfield, 2000). The Juan de Fuca Ridge shows intermediate spreading rates with an average full spreading rate of about 60 mm/yr (Normark et al., 1983). This ridge has been extensively explored and hydrothermal venting has been located along its ~500 km length (Gamo et al., 1995; Butterfield et al., 1997). Important venting sites are the Ashes vent field (Gamo, 1995), Middle Valley (Gamo, 1995), Main Endeavor (Shanks et al., 1995; Butterfield et al., 1994), Floc site, Flow site, Source site (Butterfield

et al., 1997) and North Cleft fields (Gamo, 1995). The Gorda Ridge spreading center lies offshore of Oregon and northern California. GOR is ~300 km long and is bounded by the Mendocino fracture zone on the south and the Blanco fracture zone on the north (Zierenberg et al., 1993). GOR spreads faster in the north and slower in the south (Zierenberg et al., 1993), averaging about 60 mm/yr. Hydrothermal activity has been located at several places along the ridge axis, such as the Sea Cliff Field, Northern and Southern Escanaba fields with high temperatures and low pH vents (Butterfield, 2000; Von Damm et al., 2006).

b. East Pacific Rise (EPR)

The EPR spreading center (B in Fig. 1.1a) can be traced from the Gulf of California to near 55° S, 130° W where it joins the Pacific-Antarctic Ridge. The EPR has the fastest spreading rate on Earth. It is about 8900 km long with several overlapping spreading centers and is interrupted by several transform faults along its length (McGuire, 2008). The EPR separates the Pacific Plate to the west from the North America, Cocos, Nazca and Antarctic Plates to the east. The spreading rate changes along the EPR, slower in the north (~49 mm/yr) and fastest in the south where it adjoins the Nazca Plate (134-158 mm/yr; (DeMets et al., 1990). Many hydrothermal vent fields are known between 21°N to 37°S. About 26 possible vent fields have been found; among them EPR 9ºN, EPR 13°N, EPR 21°N and Rehu-Marka are the best studied, and multiple high temperature vents have been identified in those fields.

c. Galapagos Spreading Center (GSC)

The E-W trending GSC (C in Fig. 1.1a) marks the boundary between the Nazca Plate to the south and the Cocos Plate to the north (Haymon et al., 2007). GSC is about 2000 km long and bounded in the west by the EPR and to the east by the Panama Fracture Zone (Pedersen et al., 2001). GSC has an intermediate spreading rate (Sinton et al., 2003) with full spreading rates varying from 45 mm/yr at 98°W to 63 mm/yr at 86°W (DeMets et al., 1990). GSC is where the first deep sea hydrothermal vent was found by John Corliss and the ALVIN team in 1977. Including the first vent site, the Rose Garden vent field. GSC hosts two other possible vent fields: Iguanas-Pinguinos and Navidad fields.

1.3.2. Atlantic and Arctic Ocean Spreading Ridges

a. Mid Atlantic Ridge (MAR), Reykjanes Ridge (RKR), Kolbeinsy Ridge (KOR), and Mohn's Ridge (MHR)

The Mid-Atlantic Ridge system extends from a junction with the Gakkel Ridge (Mid-Arctic Ridge) northeast of Greenland southward to the Bouvet Triple Junction in the South Atlantic. In our analysis we treated the MAR (H in Fig. 1.1a) and its continuations to the north -the Reykjanes Ridge (RKR; G in Fig. 1.1a), Kolbeinsey Ridge (KOR; F in Fig. 1.1a) and Mohn's Ridge (MHR; E in Fig. 1.1a); these are described below from S to N. MAR is a well-studied slow-spreading ridge (20-40 mm/yr full rate). Many hydrothermal venting sites have been discovered between 45°N to 33°S along the ridge. The initial discoveries were the Trans-Atlantic Geotraverse (TAG) and Snake Pit fields in 1985 (Rona et al., 1986; Douville et al., 2002). Subsequently, numerous other fields were also discovered, such as Lucky Strike (Langmuir et al., 1997), Broken Spur

(Murton et al., 1995), Menez Gwen (Fouquet et al., 1994), Logatchev (Sudarikov et al., 2000) and Rainbow (Fouquet et al., 1997; Charlou et al., 2000). All together there are about 16 possible vent fields along the length of about 11850 km until it meets the RKR. The RKR is the northern continuation of the MAR and continues inland in Iceland. The RKR separates the North American and Eurasian plates at about 19 mm/yr. The submarine portion of the ridge is about 1450 km long and hosts the active Steinaholl vent field at 350 m below sea level, much shallower than typical MOR vents. KOR is the continuation of the MAR to the north of Iceland. It is bounded to the south by the Tjörnes fracture zone and to the north by the Jan Mayen fracture zone (Johnson et al., 1972) and is about 540 km long (Pedersen et al., 2010). KOR spreads at an average full rate of about 20 mm/yr (Pedersen et al., 2010) and hosts a few active hydrothermal vent fields including Kolbeinsey, Grimsey and Eyjafjördur. North of KOR is the MHR, which is about 550 km long (Pedersen et al., 2010). MHR is bounded to the south by the Jan Mayen fracture zone and continues north along the Knipovich Ridge. The average full spreading rate for the MHR is 15 mm/yr (Pedersen et al., 2010) oblique to the ridge axis. MHR hosts two known high temperature vent fields, Loki's Castle and Soria Moria.

b. Mid Cayman Rise (MCR)

MCR (D in Fig. 1.1a) is an ultraslow spreading ridge (15-17 mm/yr) (McDermott et al., 2018) extending 110 km (Connelly et al., 2012) between North American plate to the north and the Caribbean plate to the south. To its east lies the Gonave microplate. It is the world's deepest seafloor spreading center and its depth ranges from 4,200 to > 6,000 m. Hydrothermal activities were first discovered through water column studies in 2010, and four hydrothermal vent fields

have been discovered. Von Damm field and Bebee (or Piccard) vent fields are active and activity of Walsh and Europa vents are inferred through water column studies (German et al.,2010; Connelly et al.,2012; Kinsey et al., 2013).

c. Gakkel Ridge (GKR)

The Gakkel Ridge in the Arctic Ocean separates the North American and Eurasian plates. It is the slowest spreading (6-12 mm/yr) and one of the least explored divergent boundaries in the world (Edmonds et al., 2003). GKR (K in Fig. 1.1b) extends about 1600 km from Lena Trough near Greenland to Laptev Sea Rift near Russia (Pedersen et al., 2010). The ridge axis is very deep, generally 4700–5300 m, within a well-developed rift valley with volcanic activity in some regions (Cochran et al., 2003). Water column studies indicate that the GKR hosts 9 potential hydrothermal vent sites (Edmonds et al., 2003; Pedersen et al., 2010).

1.3.3. Indian Ocean Spreading Ridges

a. Central Indian Ridge (CIR)

The intermediate spreading (~50 mm/yr) CIR lies (I in Fig. 1.1a) between the African Plate and the Indo-Australian Plate. It is bounded in the north by Owen transform fault and in the south by the Rodrigues triple junction. The axial ridge is about 4500 km long and has 500–1000 m of relief (Son et al., 2014) and its morphology reflects characteristics of slow to intermediate ridges. CIR has been intensively explored since 2000 and four hydrothermal vent fields (e.g., Kairei, Edmond, Solitaire and Dodo vent fields) have been visually confirmed between 6°N and 25°S and many other plumes have been reported (Okino et al., 2015).

b. Southwest Indian Ridge (SWIR)

SWIR (J in Fig. 1.1a) separates the African Plate to its north and the Antarctic Plate to its south and shows slow to ultraslow spreading rates (~14 mm/yr) along the 7700 km long ridge axis (Sauter et al., 2010). SWIR extends from the Bouvet triple junction in the southern Atlantic Ocean to the Rodrigues triple junction in the Indian Ocean. The easternmost part of this ridge represents the deepest of the MOR system (Sauter et al., 2010). This segment also has some high temperature venting around 49.6°N (Ji et al., 2017) and many plumes of probable hydrothermal origin are known from along the SWIR. The best-known field discovered so far is the Lonqi hydrothermal vent field (Li et al., 2015).

1.4.METHODS

In this study we treat a vent as an individual fissure in the seafloor which issues chemically altered fluids. A vent field is a closely associated group of multiple vents typically < 10 km^2 in area; vent fields are typically separated from each other by tens to hundreds of kilometers along seafloor spreading centers (Copley et al., 2016). Possible vent fields are named based on the above definition, along the axis as a linear field or on top of a volcano as a planar field. When naming the fields, most cited or most popular names in literature and InterRidge Vents Database Ver. 3.4 are used.

1.4.1. Data Sources

Data generated from multiple research expeditions from the 1970s to present were compiled into a database which has 449 individual vents grouped into 73 vent fields (EPR: 26; NEP: 14; GSC: 3; MCR: 2; MAR: 16; RKR: 1; KOR: 4; MHR: 2; GOR: 3; SWIR: 1; CIR: 4). The data used in

this compilation come from two sources: 1) peer-reviewed geoscientific literature; 2) websites managed by government agencies and ocean research institutes published in English. Very few studies contain all the information we want to consider in our statistical analysis. Those with little or no information in their measured fluid parameters are included for locality and other relevant information. The reference list covers only the citations used in the text and tables. A full listing of the references used in supplementary tables are provided in the supplementary documents. The internet sources used in the database are listed below:

1. InterRidge vents database 3.3 (http://vents-data.interridge.org/), which is hosted by Peking University, Beijing, China. This website provides a comprehensive list of active and inferred (unconfirmed) active submarine hydrothermal vent fields all over the world.

2. Marine Geoscience Data System (MGDS), which gives access to marine geoscience research data acquired throughout the oceans and adjoining continental margins (http:// www.marine-geo.org/portals/ndsf/).

3. Woods Hole Oceanographic Institution (WHOI), underwater vehicle information especially ROV operations and HOV Alvin dive operations (http://www.whoi.edu/main/ underwater vehicles).

4. World Register of Marine Species (WoRMS) database provides an authoritative and comprehensive list of names of marine organisms, including information on synonymy (http://www.marinespecies.org).

1.4.2. Statistical Analysis of Vent Parameters

In this metadata analysis we reviewed in excess of 900 publications that reference hydrothermal vent studies (Table S1). The non-biological parameters we compiled include spreading rate, vent depth, fluid temperature, pH, total Fe, Mn, helium isotopic ratio, fluid gases (CO_2, CH_4, H_2, H_2S), SO_4^{2-} ions and chlorinity of the fluids. We understand that measurements of vent fluid parameters are sensitive to several factors, including sampling procedures and temporal changes in vent flow strength; we make no effort to correct for such effects. Spreading rate and vent depth are two important variables as differences in spreading rates result in different ridge morphology therefore variable vent depths are observed. The fluid temperature reflects the strength of the heat source. MOR vents potentially have at least four different types of heat sources: heat from the mantle, heat transfer from cooling crust and lithosphere, heat of serpentinization and magmatic heat transfer (Lowell, 2010). Mixing of normal seawater also affects vent fluid temperature. Vent fluid temperature alone cannot reveal the heat source but combining it with spreading rate and host rock geology can help reveal vent heat sources. pH is also important as this reflects subseafloor fluid-rock interactions and/or addition of magmatic gases in the deeper crust. Metals and sulfate ions also reflect fluid-rock interactions in the reaction zone. Helium isotopes, ^3He and ^4He, are important geochemical tracers of mantle and crustal inputs and elevated $^3He/^4He$ relative to atmosphere (Ra, where Ra = 1.40×10^{-6}) is an unambiguous indicator of hydrothermal activity. Other gases (CO_2, CH_4, H_2, H_2S) could be due to mantle or magma outgassing or produced via chemical reactions such as biological activity or serpentinization. Chlorinity reveals contributions of seawater in the hydrothermal fluid, the importance of phase separation (Butterfield et al., 1997), and precipitation or dissolution of chloride-bearing minerals (Seyfried et al., 1986; Von Damm,

1988) in the reaction zone. More details about these parameters and other compiled information are provided in supplementary Table S1.

Summary statistics of the 12 vent parameters reviewed in this study are given in Table 1.1. We assessed vent fluid parameters (e.g., temperature and chemistry) first for correlations with spreading rate, summit depth, fluid temperature and fluid chlorinity. Second, we compared different MOR segments based on vent parameters. Due to the small numbers of observations and the fact that data for all 12 parameters does not exist for all vents, we used purely nonparametric statistical procedures which provide robust and accurate statistical inference results in situations where the assumption of specific data distributions is questionable. Fluid concentrations used for the statistical analysis are corrected for background seawater or are at the concentration at which magnesium in solution is zero (Bischoff et al., 1975). Two approaches are described below.

Relationships between fluid parameters vs spreading rate (Fig. 1.2 and 1.3), depth (Fig. 1.4 and 1.5), temperature (Fig. 1.6 and 1.7) and chlorinity (Fig. 1.8 and 1.9) were assessed using Kendall's tau coefficient (τ). These correlations are reported along with the p-values (Table A1) so that we can assess whether these correlations exist at the 5% level of significance. Second, we compared the vent parameters of different MOR segments using rank based non-parametric Analysis of Variance (ANOVA). For multiple comparisons, the Bonferroni adjustment was applied (Brunner et al., 2016). Results are regarded as significant if $p<0.05$ (Table A2). Box Plots (Fig. 1.10, 1.11 and 1.12) were used to visualize the similarities and differences obtained from ANOVA.

1.4.3. Statistical Analysis of Vent Biota

The vent species database (Table S2) consists of organisms described from 72 individual vents of different MORs. These communities were subdivided based on the taxonomic levels (phylum, class, family, genus and species) and species absence and presence matrix are provided. Sörensen similarity coefficients; SS = 2a/(2a+b+c); which quantify the similarity of organisms found in two different habitats at their species and genus levels, were computed for seven geographic provinces (NEP, EPR, GSC, MCR, MAR, CIR and SWIR) considered in this study; a is the number of taxa common to the two provinces considered, b is the number of taxa exclusive to the first province, and c to the second province. Results are reported as percentage similarity; higher percentages indicate higher similarity of species/genera between the groups (Table A3).

Table 1.1: Summary statistics of the mid ocean ridge vent parameters.

Variable	MOR			Seawater Average
	n	Mean	1SD	
Depth (m bsl)	324	2427.60	683.40	n/a
Temperature (^{0}C)	251	272.27	115.44	[a]2
pH	159	4.51	1.53	[b]8.1
Total Fe (mM)	123	3.84	5.97	[b]$1x10^{-6}$
Mn (mM)	118	0.71	0.79	[b]$5x10^{-6}$
(^{3}He/^{4}He)/R_a	29	7.90	0.53	[c]$2x10^{-9}$
CO_2 (mM)	81	23.53	28.69	[c]2
CH_4 (mM)	68	1.19	4.05	[b]$4x10^{-4}$
H_2 (mM)	85	4.21	6.64	n/a
H_2S (mM)	133	8.49	12.90	[a]0
SO_4^{2-}(mM)	79	4.61	13.60	[b]28
Chlorinity (mM)	129	535.83	208.96	[a]538

*MOR-Mid Ocean Ridge; n – number of vents considered; n/a - not available.
[a]Butterfiel et al., 1997; [b]Mottl et al., 2003; [c]Toki et al., 2015.

1.5.RESULTS

Summary statistics of the vent parameters used in this study are given in Table 1.1. We report Kendall's correlation coefficients (τ) and corresponding p-values for the data in cases where we have at least 2 samples. We consider $\tau > 0.8$ to be a strong correlation, $0.8 > \tau > 0.45$ to be a moderate correlation, $0.45 > \tau > 0.25$ to be a weak correlation, and $0.25 > \tau$ to be no correlation; results were regarded as significant if $p<0.05$ (Table A1).

1.5.1. Analyses of Vent Parameters

Our results show that there are significant ($p<0.05$) depth differences between the ridges with different spreading rates (Table A2) however, vent depths do not correlate well with spreading rate (Fig. 1.2a). Slow spreading ridges (e.g., MAR) show a wider range of vent depths while fast spreading ridges (e.g., EPR) show a narrower depth range (Fig. 1.10a). 50% of MOR vents occur between 2200-2761 m bsl and the average depth is 2428±683 m bsl (Table 1.1). Vent depth does not correlate with other fluid parameters such as temperature (Fig. 1.4a), pH (Fig. 1.4b), total Fe (Fig. 1.4c), Mn (Fig. 1.4d), CO_2 (Fig. 1.4e), ($^3He/^4He)/R_a$ (Fig. 1.5a), H_2 (Fig. 1.5b), H_2S (Fig. 1.5c), SO_4^{2-} (Fig. 1.5d) and fluid chlorinity (Fig. 1.5e). Weak negative correlations exist between vent depth and CH_4 (Fig. 1.4f). Vent fluid temperatures vary between 2^0C-407^0C regardless of spreading rates (Fig. 1.10b). There is no correlation between spreading rate and fluid temperature (Fig. 1.2b). The mean fluid temperature is 272 ±115^0C and 50% of the vents are above 252^0C and below 351^0C (Table 1.1). Significant temperature differences exist between NEP vs EPR, MAR and CIR vents (Table A2). Venting temperatures are more or less the same for all other ridge segments. Fluid temperature moderately correlate with pH (Fig. 1.6a), H_2S (Fig. 1.7b) and weakly

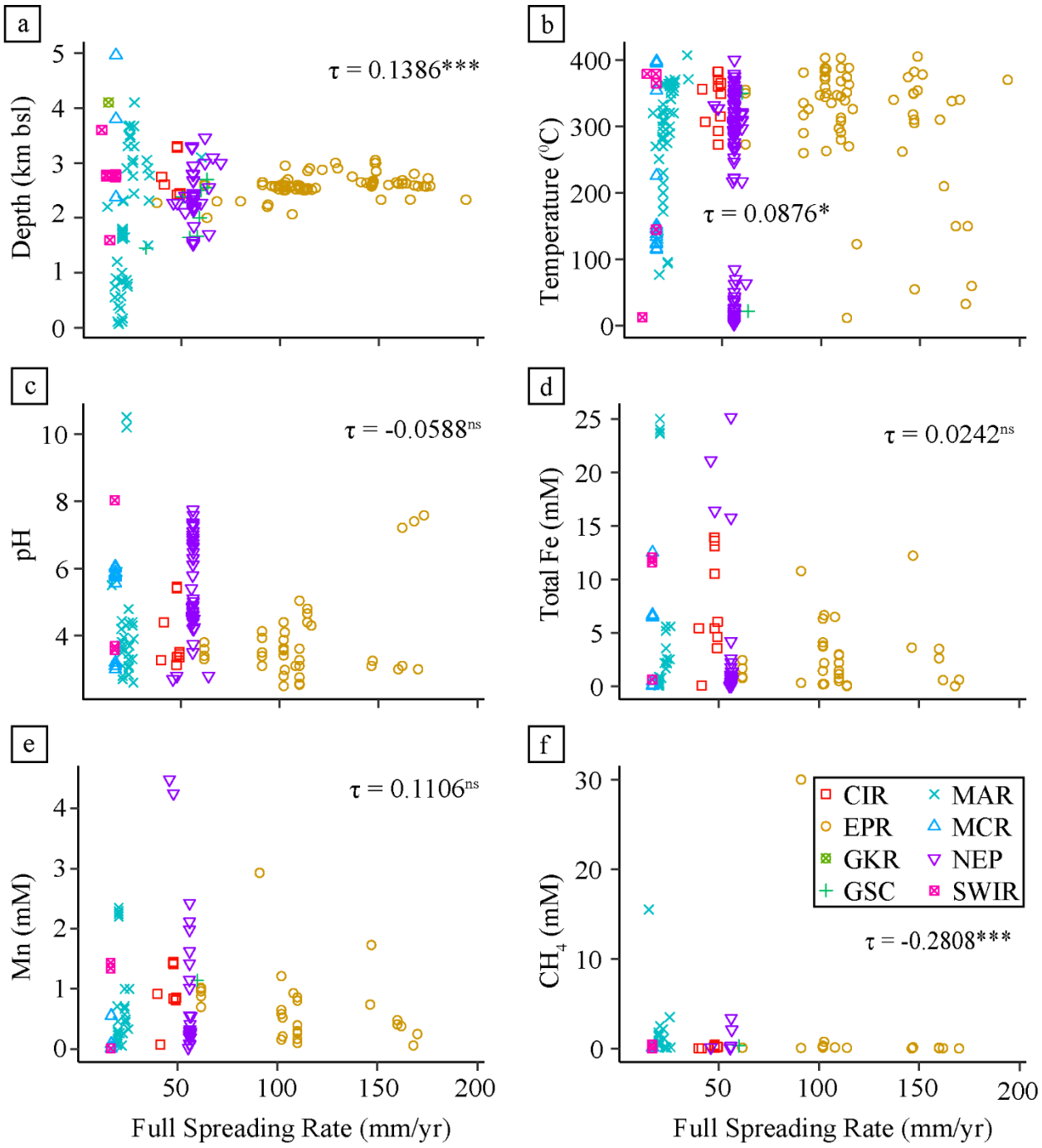

Fig. 1.2: Selected vent parameters vs. spreading rate. Kendall's tau correlations and corresponding p-values of (a) vent depth (b) fluid temperature (c) pH (d) total Fe (e) Mn (f) CH_4 vs spreading rate. CH_4 has a weak negative correlation to spreading rate. * Significant at $p < 0.05$, ** significant at $p < 0.01$, *** significant at $p < 0.001$, **** significant at $p < 0.0001$, ns – not significant.

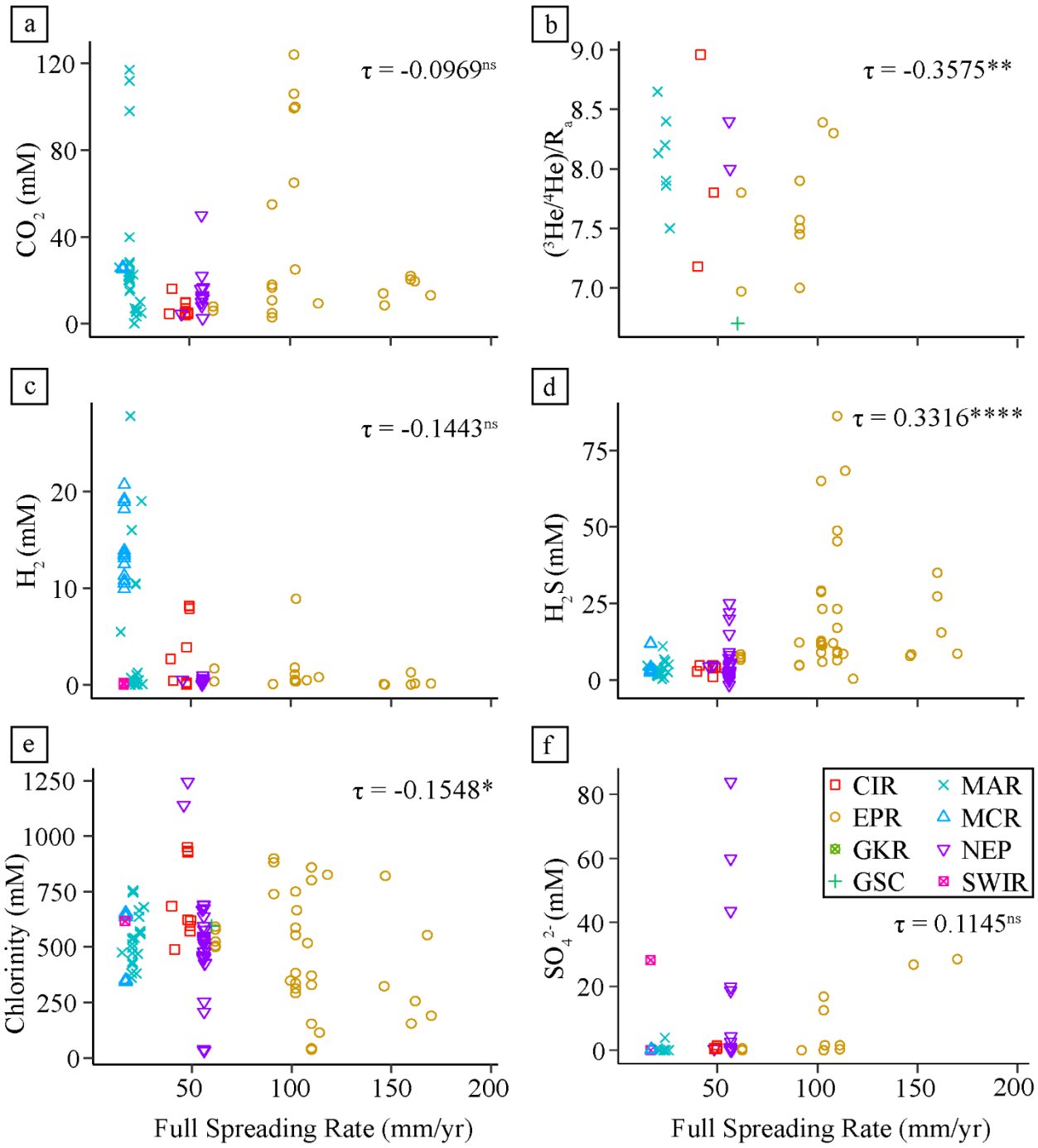

Fig. 1.3: Selected vent parameters vs. spreading rate. Kendall's tau correlations and corresponding p-values of (a) CO_2 (b) $(^3He/^4He)/R_a$ (c) H_2 (d) H_2S (e) Chlorinity (f) SO_4^{2-} ions vs spreading rate. Weak correlations are found for $(^3He/^4He)/ R_a$ and H_2S. * Significant at $p < 0.05$, ** significant at $p < 0.01$, *** significant at $p < 0.001$, **** significant at $p < 0.0001$, ns – not significant.

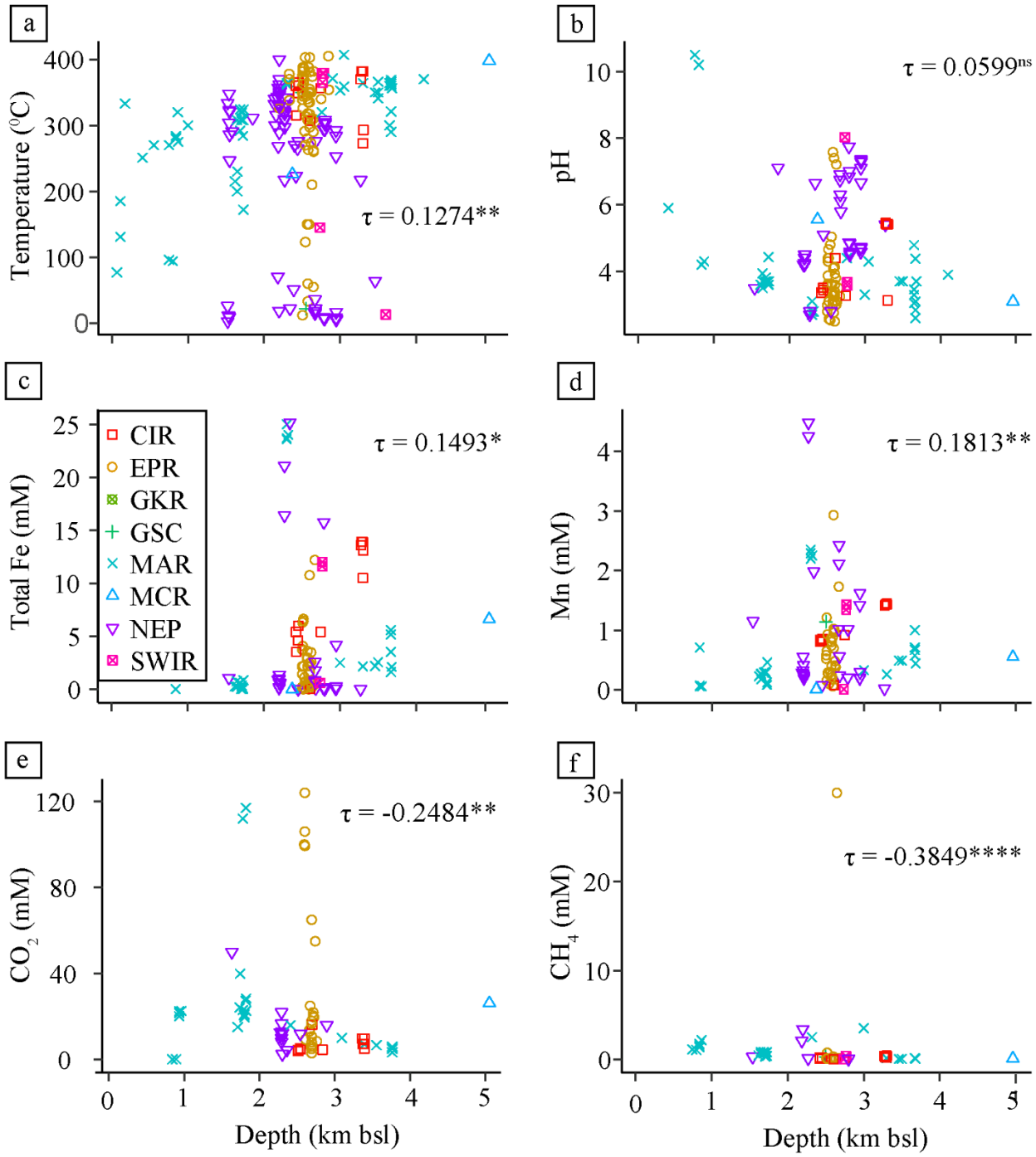

Fig. 1.4: Selected vent parameters vs. depth. Kendall's tau correlations and corresponding p-values of (a) fluid temperature (b) pH (c) total Fe (d) Mn (e) CO_2 (f) CH_4 vs depth. Weak significant correlation is found for CH_4 and a minor correlation for CO_2. * Significant at $p < 0.05$, ** significant at $p < 0.01$, *** significant at $p < 0.001$, **** significant at $p < 0.0001$, ns – not significant.

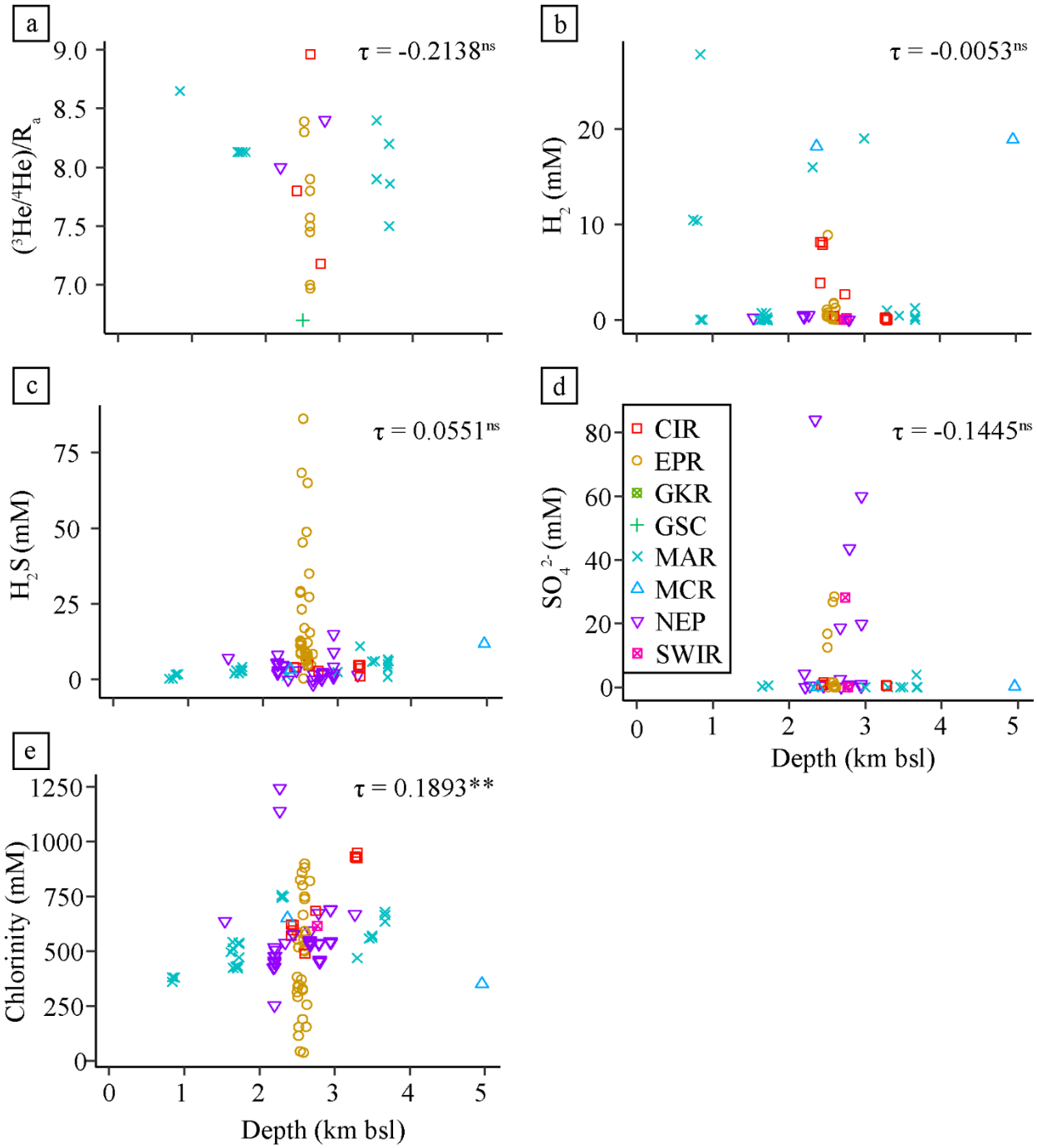

Fig. 1.5: Selected vent parameters vs. depth. Kendall's tau correlations and corresponding p-values of (a) $(^3He/^4He)/R_a$ (b) H_2 (c) H_2S (d) SO_4^{2-} ions (e) Chlorinity vs depth. $(^3He/^4He)/R_a$ shows a minor correlation. * Significant at $p < 0.05$, ** significant at $p < 0.01$, *** significant at $p < 0.001$, **** significant at $p < 0.0001$, ns – not significant.

correlate with total Fe (Fig. 1.6b) and ($^3He/^4He)/R_a$ (Fig. 1.6d). Other vent fluid parameters, Mn (Fig. 1.6c), CO_2 (Fig. 1.6e), CH_4 (Fig. 1.6f), H_2 (Fig. 1.7a), SO_4^{2-} (Fig. 1.7c) and chlorinity (Fig. 1.7d) do not correlate with temperature.

MOR vent fluids are more acidic than seawater except for a few cases such as Lost City (MAR) where basic fluids are observed. The pH of the vent fluids shows no correlation with spreading rate (Fig. 1.2c). Our results show that 50% of the vent fluids lie between pH 3.38 - 5.42 and the average pH is 4.51±1.53 (Table 1.1). Significant pH differences exist between EPR vs NEP, MCR and MAR vs NEP vent fluids (Table A2) (Fig. 1.10c). The total Fe concentration of the vent fluids show no correlation with spreading rate (Fig. 1.2d). However, Indian Ridges show a high concentration of Fe content compared to other ridge segments (Fig. 1.10d), and that difference is significant for CIR vs EPR, NEP (Table A2). The average total Fe concentration is 3.84±5.97 mM and 50% of the vents lie between 0.18-4.40 mM (Table 1.1). The Mn concentration is also high for Indian Ridge vents compared to others (Fig. 1.11a). Average Mn concentration is 0.71±0.79 mM, 50% of the vents are between 0.21-0.95 mM (Table 1.1). Spreading rate has no correlation to the Mn content of fluids (Fig. 1.2e). MCR vents show significantly different Mn concentrations to EPR, NEP and CIR vents (Table A2). The helium isotopic composition of MAR vs EPR and MCR vs EPR, NEP, MAR, CIR, SWIR vents differ significantly (Fig. 1.11b) (Table A2). This has a weak negative correlation with spreading rate (Fig. 1.3b). For He isotopic data, the average R/Ra is 7.90±0.53, with 50% of data between 7.57 and 8.20 (Table 1.1). Carbon dioxide has a minor negative correlation with depth (Fig. 1.4e) and shows no correlation to spreading rate (Fig. 1.3a), temperature (Fig. 1.6e) (Table A1). The average CO_2 is 24±29 mM and 50% of the data lie between 6.7 and 23 mM (Table 1.1). Moreover, CO_2 of the CIR vents differ significantly

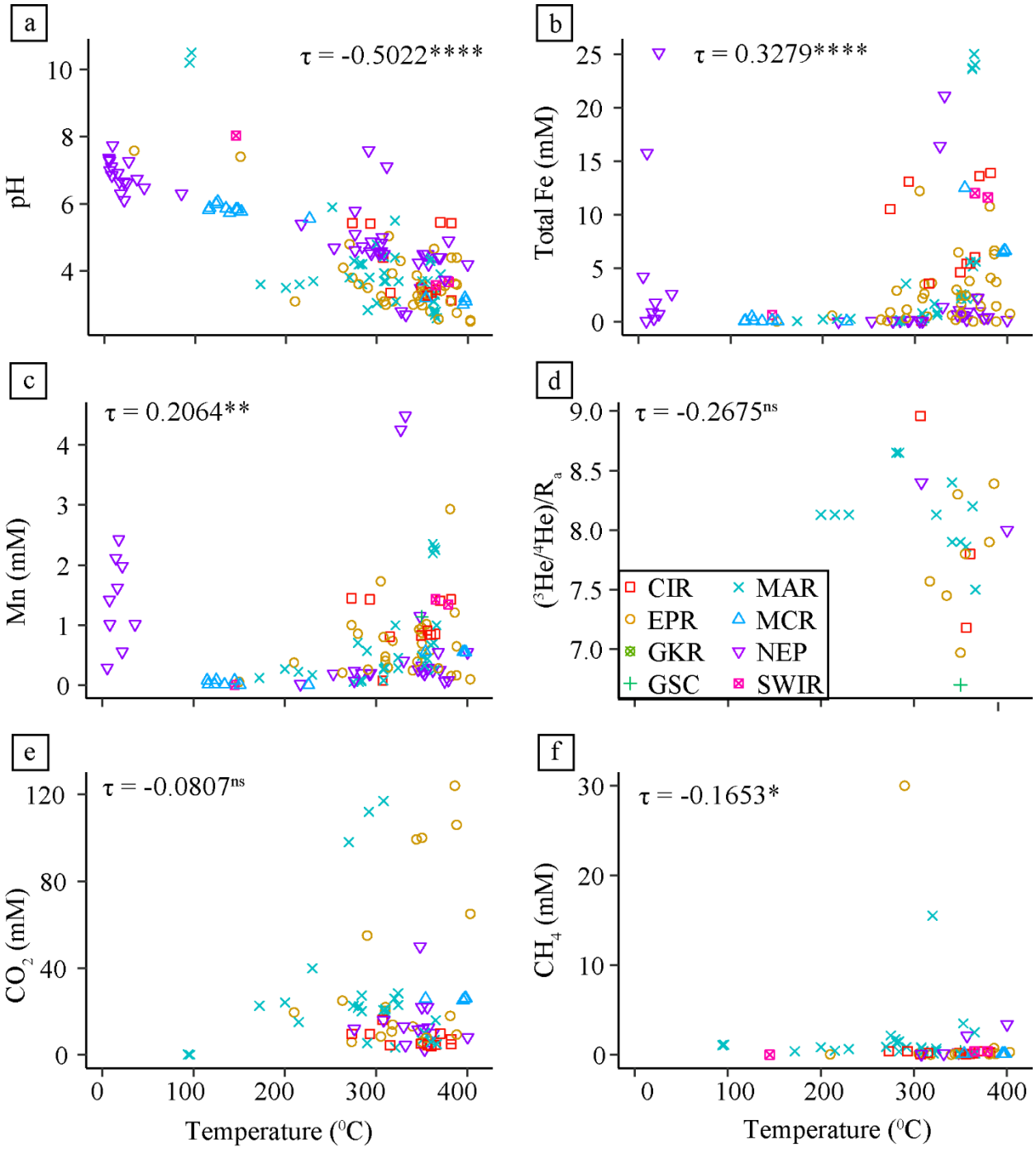

Fig. 1.6: Selected vent parameters vs. vent fluid temperature. Kendall's tau correlations and corresponding p-values of (a) pH (b) total Fe (c) Mn (d) $(^3He/^4He)/R_a$ (e) CO_2 (f) CH_4 vs temperature. Fluid pH has a moderate relationship with temperature. $(^3He/^4He)/R_a$ and total Fe have weak correlations. * Significant at $p < 0.05$, ** significant at $p < 0.01$, *** significant at $p < 0.001$, **** significant at $p < 0.0001$, ns – not significant.

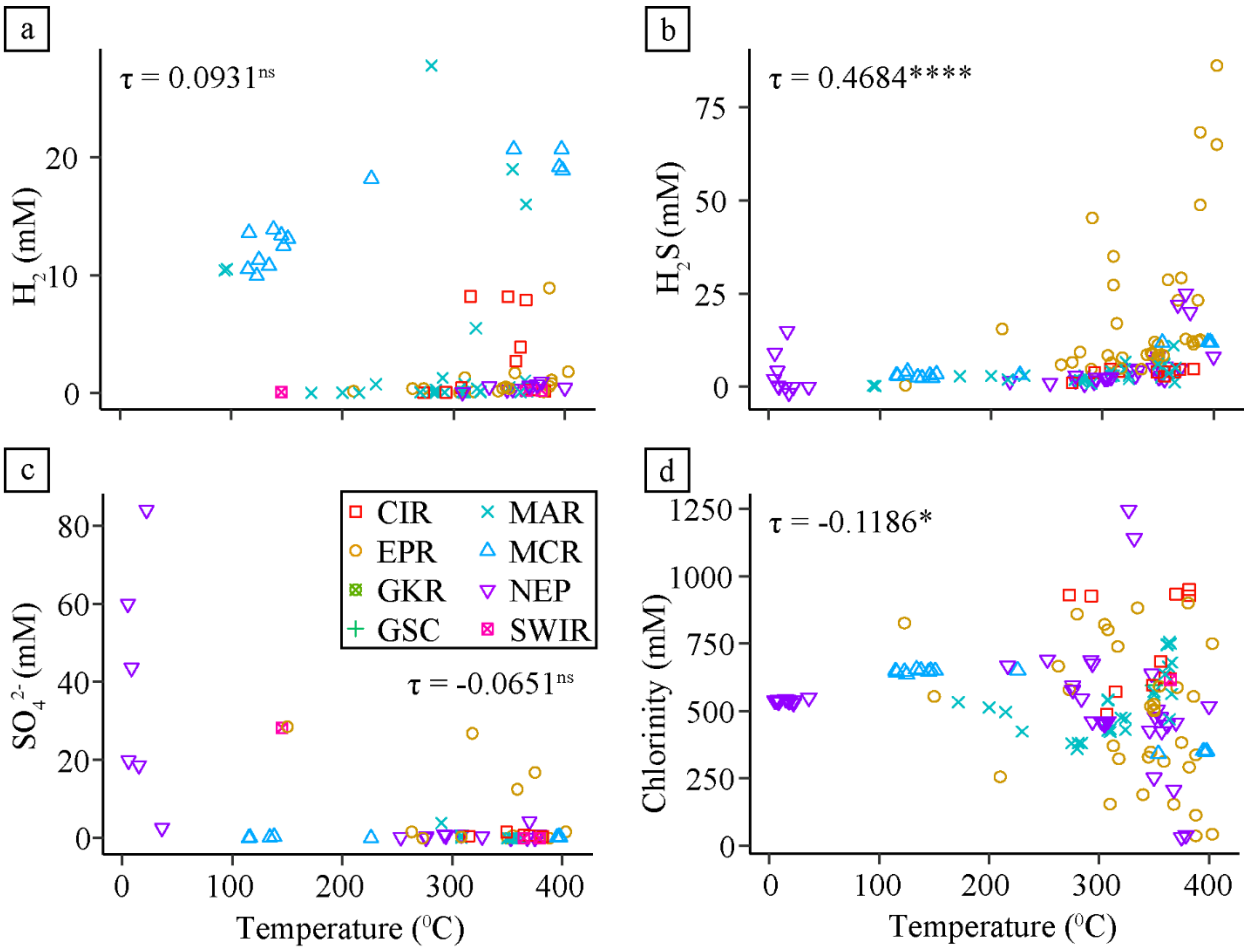

Fig. 1.7: Selected vent parameters vs. vent fluid temperature. Kendall's tau correlations and corresponding p-values of (a) H_2 (b) H_2S (c) SO_4^{2-} ions (d) Chlorinity vs temperature. Moderate correlation is found for H_2S. * Significant at $p < 0.05$, ** significant at $p < 0.01$, *** significant at $p < 0.001$, **** significant at $p < 0.0001$, ns – not significant.

from EPR, MCR and MAR vents (Table A2) (Fig. 1.11c). MCR vs NEP is also different for CO_2 (Table A2).

Methane concentration has a weak negative relationship with spreading rate (Fig. 1.2f). 50% of vents have CH_4 between 0.11 and 0.74 mM with a mean of 1.19±4.05 mM (Table 1.1). CH_4 content of MAR vs CIR, MCR and EPR are significantly different (Table A2) (Fig. 1.11d). H_2S of vent fluids differ significantly between EPR vs CIR, NEP, MCR and MAR (Table A2)

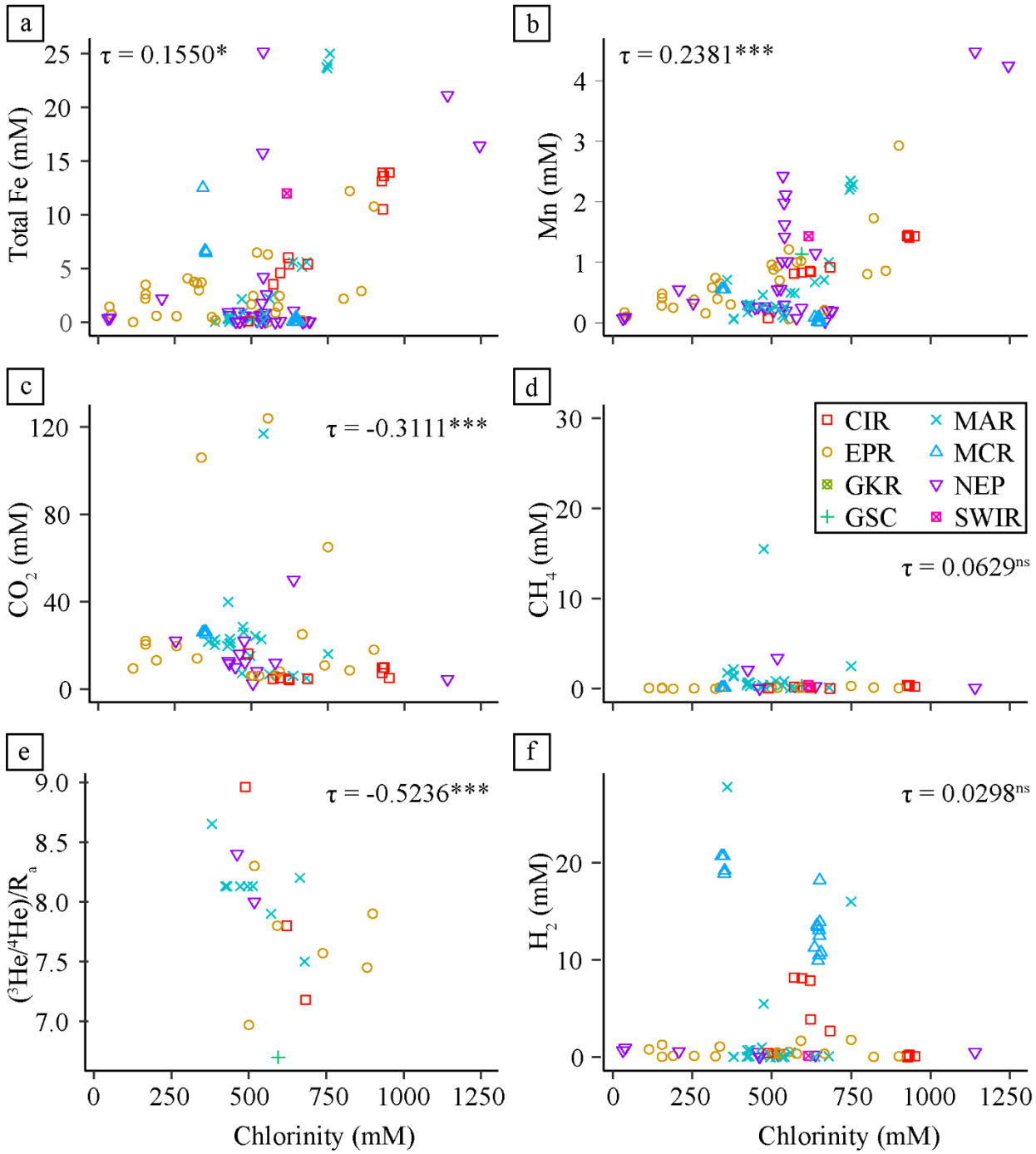

Fig. 1.8: Selected vent parameters vs. vent fluid chlorinity. Kendall's tau correlations and corresponding p-values of (a) total Fe (b) Mn (c) CO_2 (d) CH_4 (e) $(^3He/^4He)/R_a$ (f) H_2 vs chlorinity. Moderate negative correlation is found for $(^3He/^4He)/R_a$. Fluid CO_2 has a weak correlation. * Significant at $p < 0.05$, ** significant at $p < 0.01$, *** significant at $p < 0.001$, **** significant at $p < 0.0001$, ns – not significant.

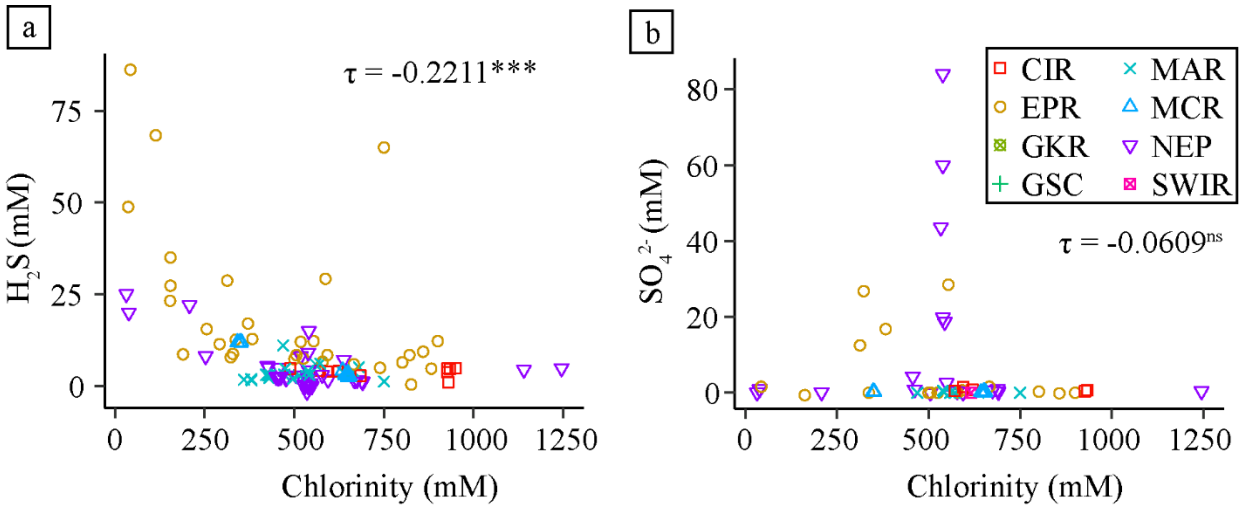

Fig. 1.9: Selected vent parameters vs. vent fluid chlorinity. Kendall's tau correlations and corresponding p-values of (a) H_2S (b) SO_4^{2-} ions vs chlorinity. Minor correlation is found for H_2S. * Significant at $p < 0.05$, ** significant at $p < 0.01$, *** significant at $p < 0.001$, **** significant at $p < 0.0001$, ns – not significant.

(Fig. 1.12b). H_2S also correlates with spreading rate (Fig. 1.3d) and temperature (Fig. 1.7b) and pH of the fluid. Mean H_2S is 8.48±12.91 mM with 50% of the data between 2.40 and 8.6 mM (Table 1.1); EPR vents appear to have elevated H_2S content relative to other ridges (Fig. 1.12b). Elevated hydrogen concentrations in MCR vents are significantly different from all other MOR segments; EPR, NEP, MAR, CIR and SWIR (Table A2) (Fig. 1.12a) and H_2 shows no correlation to spreading rate (Fig. 1.3c), depth (Fig.1.4b), temperature (Fig.1.7a) or chlorinity (Fig.1.8f). The average H_2 concentration is 4.21±6.64 mM with 50% of data between 0.10-8.15 mM (Table 1.1). Our results show that some MOR vent fluids are depleted in SO_4^{2-} ion compared to seawater in which average SO_4^{2-} concentrations are 28 mM (Table 1.1). Mean sulfate ion content is 6.28±15.56 mM and 50% of the vent data are between 0.005-1.59 mM. SO_4^{2-} content is indistinguishable between ridges (Table A2) (Fig. 1.12c) and it does not correlate with the spreading rate (Fig. 1.3f). Chlorinity of vent fluids show both enrichment and depletion compared to normal seawater (538

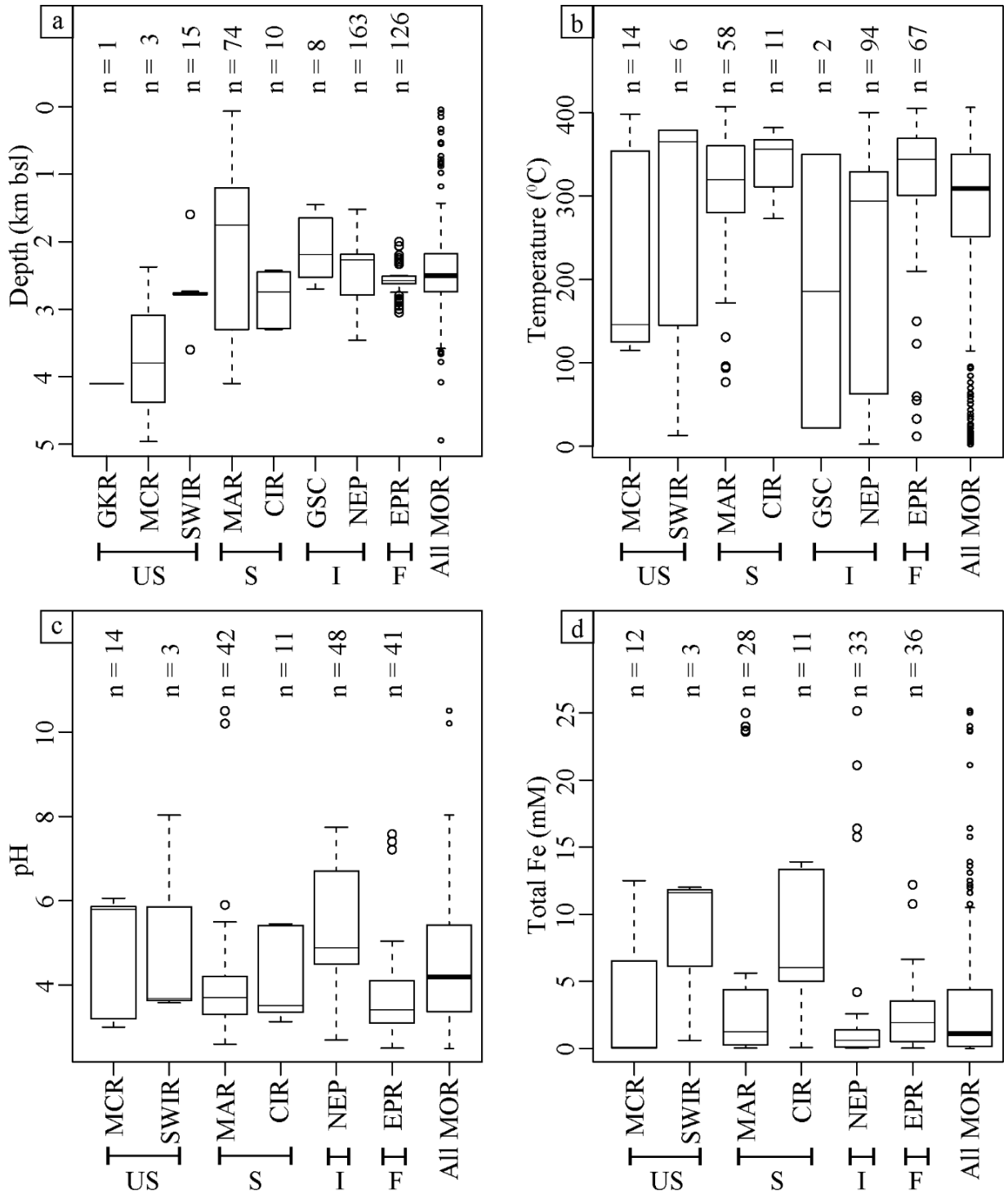

Fig. 1.10: Selected vent parameters grouped according to ridge segment spreading rate. Box and whisker plots for vent parameters (a) depth (b) temperature (c) pH (d) total Fe; n - represent the total number of individual vents considered.

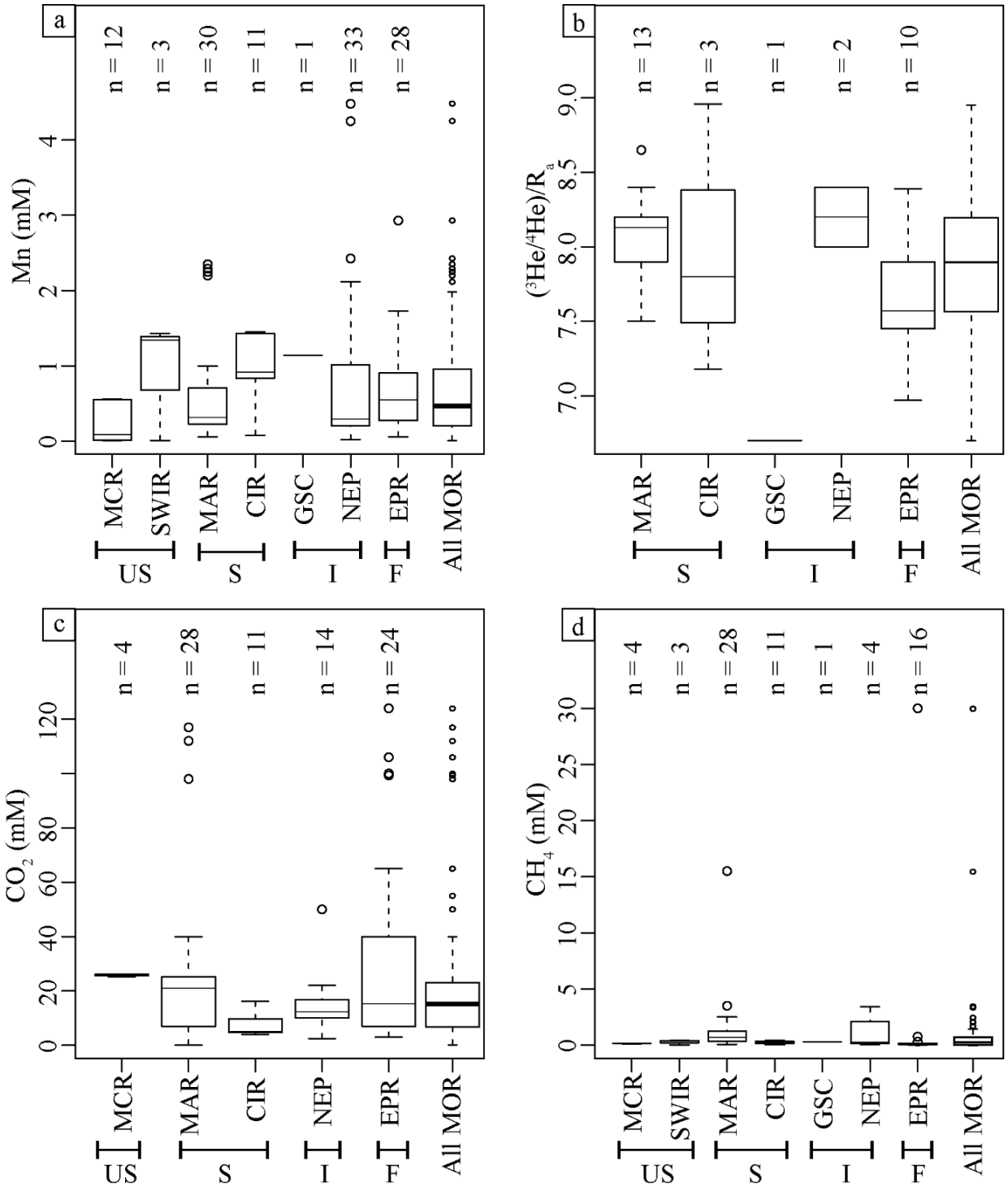

Fig. 1.11: Selected vent parameters grouped according to ridge segment spreading rate. Box and whisker plots for vent parameters (a) Mn (b) $(^3He/^4He)/R_a$ (c) CO_2 (d) CH_4; n - represents the total number of individual vents considered.

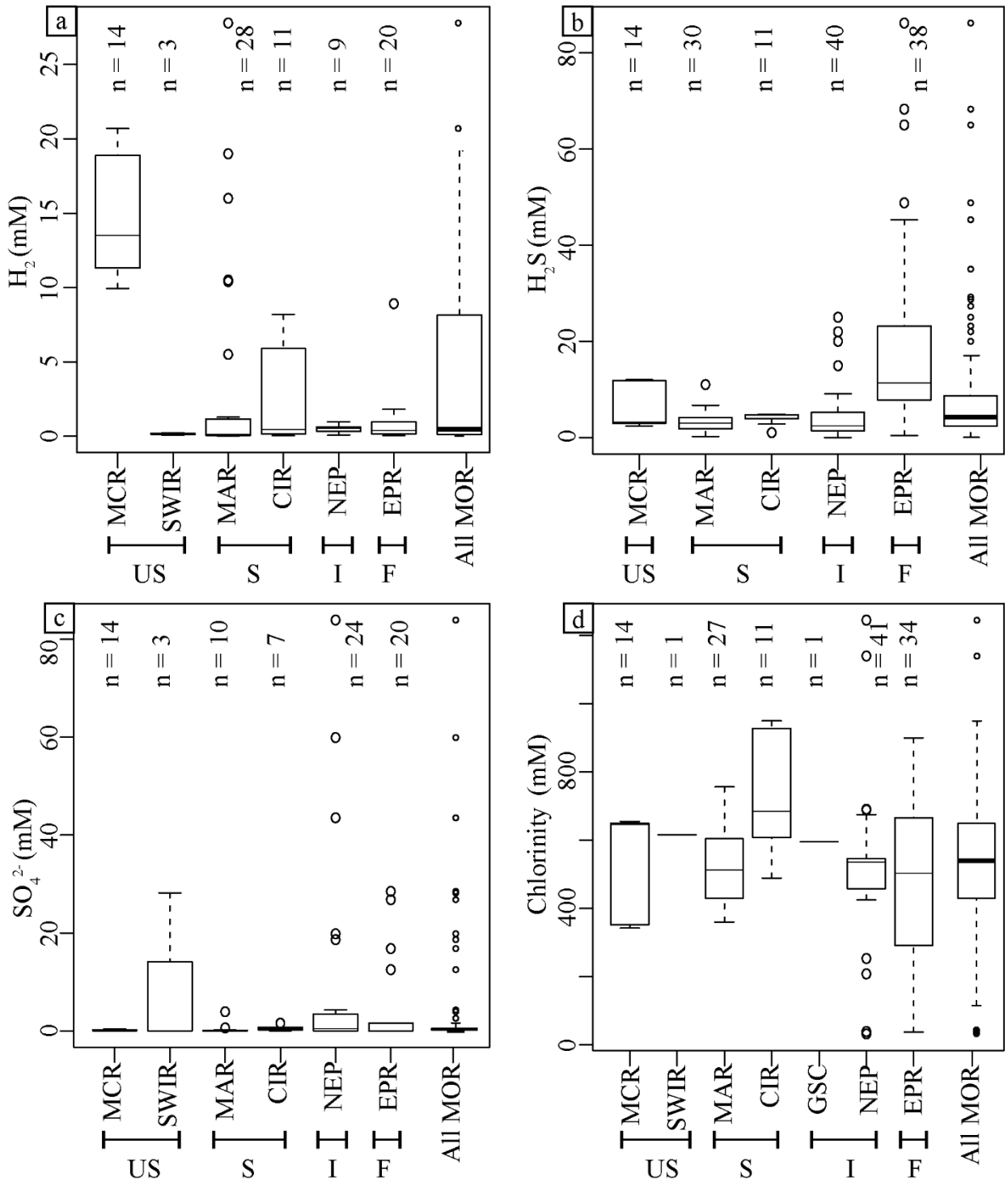

Fig. 1.12: Selected vent parameters grouped according to ridge segment spreading rate. Box and whisker plots for vent parameters (a) H_2 (b) H_2S (c) SO_4^{2-} ions (d) Chlorinity; n - represent the total number of individual vents considered.

mM Cl; Butterfield, et al., 1997). It shows moderate negative correlation with ($^3He/^4He)/R_a$ (Fig. 1.8e) and a weak negative correlation with CO_2. Mean chlorinity for MOR vents is 536±209 mM with 50% of data between 428 and 649 mM (Table 1.1). Chlorinity has no correlation with spreading rate (Fig. 1.3e), total Fe (Fig. 1.8a), Mn (Fig. 1.8b), CH_4 (Fig. 1.8d), H_2 (Fig. 1.8f), H_2S (Fig. 9a) or SO_4^{2-} ion (Fig. 1.9b). CIR ridge vent fluids are significantly enriched in chloride content relative to those of EPR, NEP, and MAR (Table A2) (Fig. 1.12d).

1.5.2. Similarity Analysis of Vent Biota

Similarity coefficients obtained for 7 MOR geographic provinces show that CIR vs SWIR has the highest similarity for genera (59%) and that for the species level is also high (14%) (Table A3). Overall EPR vent biota shares between 4%-28% of its genera with other ridges in this analysis (e.g., 24% with MAR, 23% with NEP and 28% with CIR etc.). Vents in the Central Indian Ridge also share 15%-59% of its genera with other ridge segments (e.g., 15% with GSC, 26% with MAR, 28% with EPR and 20% with NEP). Squat lobster of genus Munidopsis is shared between six geographic provinces except in MCR. In addition, polychaete worm belongs to genus Amphisamytha, shrimp belong to genus Alvinocaris, mussels belong to genus Bathymodiolus and sea snail of genus Lepetodrilus are shared in five of the seven biogeographic provinces.

However, similarity of species between the ridges is much lower compared to that of genera (e.g., 14% CIR vs SWIR, 6% EPR vs NEP, CIR, 5% CIR vs MAR, MCR, 4% MAR with EPR, 1% EPR with SWIR etc.). MAR shares none of its species with NEP.

1.6.DISCUSSION

Here we use our compiled data and statistical analysis to address four topics: 1) What if any effect does spreading rate and bathymetric depth have on hydrothermal fluid composition?; 2) What if any control does vent fluid temperature have on fluid compositions; 3) What is the most important control on MOR vent biota?; and 4) Why there are anomalous Fe and chlorinity found for vent fluids from the Central Indian Ridge ?

1.6.1. Effect of Spreading Rate and Summit Depth on Hydrothermal Fluid

In this study we evaluated hydrothermal vents from different mid ocean ridge segments for differences of hydrothermal fluids and biota. We obtained some statistically significant relationships among the fluid parameters for these ridges (Fig. 1.13). As MOR spreading rate controls ridge topography and depth we expected that hydrothermal systems would also be influenced by spreading rate, but this is mostly not observed. Only helium isotopic composition, methane and H_2S showed weak but statistically significant ($p<0.05$) correlations with spreading rate. The negative relationship between helium isotopic ratio and spreading rate might reflect different crustal thicknesses associated with different spreading rates as described by Chen (1992), in which thinner crust associated with slower spreading (3-8 km) favors mantle outgassing. This difference resulted in a significant difference between MAR and EPR helium isotopic ratios, in which MAR mean is above and EPR mean is below global mean for helium isotopic ratio respectively. However, both MAR and EPR lie between the 25th and 75th quartiles for the global MOR data, therefore we can assume that helium isotopic composition of the upper mantle is approximately homogeneous.

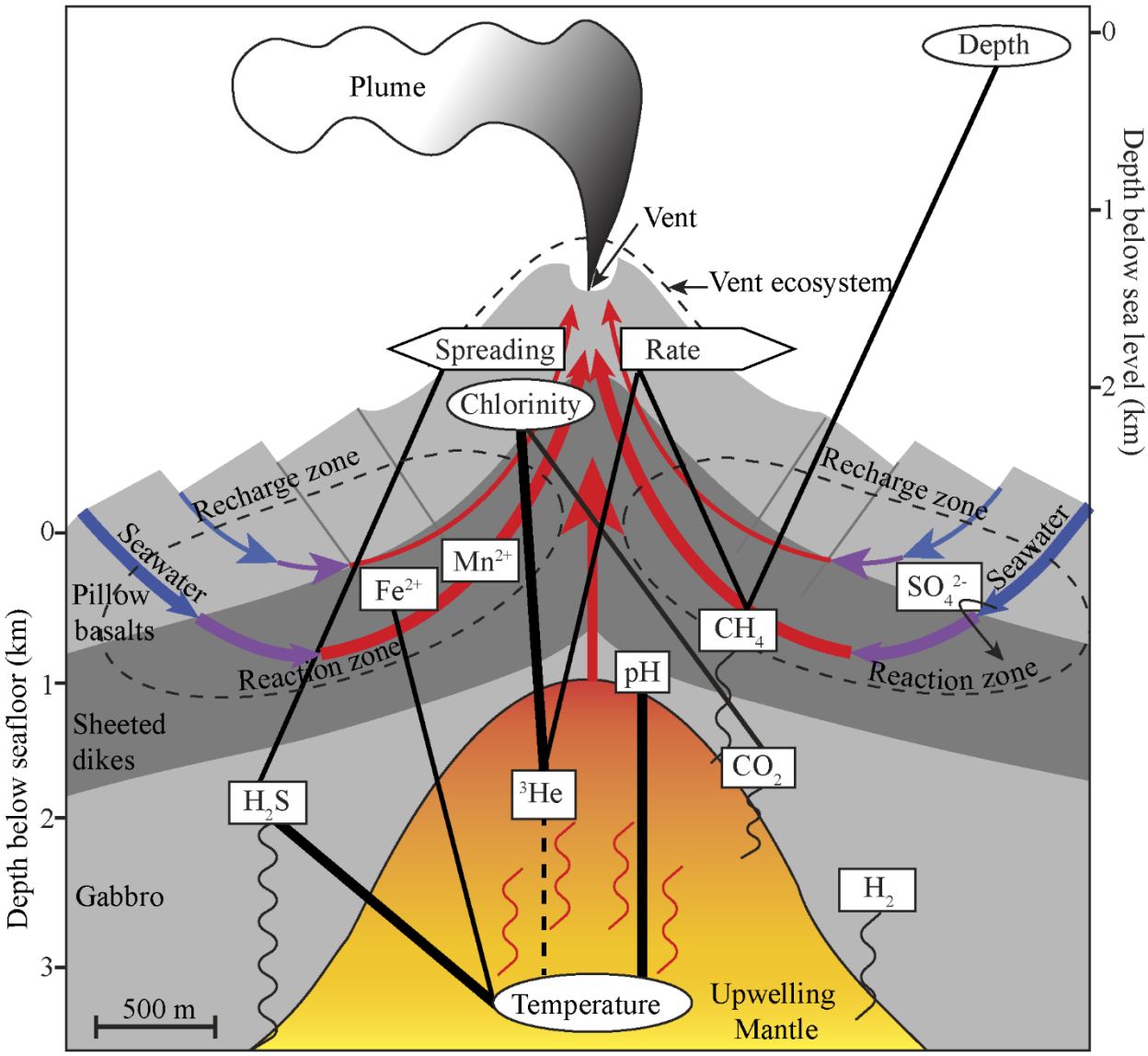

Fig. 1.13: Schematic representation of a hydrothermal vent of a fast spreading ridge; dark black lines - moderate (0.45< τ >0.8) -significant (p<0.05) correlations; black lines - weak (0.25< τ >0.45) -significant (p<0.05) correlations; dashed black lines - weak (0.25< τ >0.45) -marginally significant (p<0.06) correlations between vent parameters analyzed in this study.

The negative correlation between methane vs spreading rate and methane vs depth could be due to lithological differences. Slow spreading ridges like MAR expose more ultramafics due to the absence of a steady state magma chamber (Wetzel and Shock, 2000); serpentinization of these

rocks produce CH_4. As these deep slow ridges are barren of sediments, sedimentary derived CH_4 is minimal and significant methane production by biological processes is reduced (Bougault et al., 1993). In contrast, H_2S is produced by magmatic degassing and leached sulfur from the host rock, gives a positive correlation with both spreading rate and vent fluid temperature, indicating that high temperature fluids carry more magmatic gases and enhances elements leaching.

Significant depth differences between vents on different ridges reflect different spreading rates. Such differences exist between EPR compared to NEP, GSC, MAR, and SWIR. Slow spreading ridges have deep axial valleys (~ 2000 m relief) and a wide range of depths (Bougault et al., 1993) thus that depth difference interfere with the expected negative correlation between depths and spreading rate. This also affects the other fluid parameters, from MAR vents it is very clear that at greater depths fluids have higher temperatures, and they are also rich in metals. At shallow depths fluids are rich in gases. However, this generalization is not applicable to vents of EPR for which most of the fluid parameters show wide range of variation within a very narrow depth range.

1.6.2. Temperature and Chlorinity Controls on Fluid Compositions

Vent fluid temperature is statistically independent of spreading rate (Fig. 1.2b) although the mean for intermediate spreading rates are less than that for slow and fast spreading centers. The opposite relationship with spreading rate is observed for pH: Intermediate rate spreading ridges of the Northeast Pacific have high pH compared to vents of most other spreading ridges. Magmatic gases such as CO_2 and H_2S are released from upwelling mantle or degassing magmas and combine with modified seawater in sub-seafloor reaction zones. Such fluids become more acidic and could result

in a negative correlation between vent fluid temperature and pH. As H_2 and H_2S (Fischer et al., 2015) are notable gases among hydrothermal fluids, their abundance usually correlates with vent temperature (Fig. 1.7b). EPR vents have higher H_2S content compared to intermediate- and slow-spreading ridges. However, H_2 is not always magmatic, ultraslow spreading MCR vents contain anomalous concentrations of H_2 where magmatic input is at a minimum compared to fast spreading EPR. McDermott et al., (2018) describes a few pathways of H_2 production such as fluid-mineral equilibria and phase separation processes during high temperature, high-pressure seawater-mafic substrate alteration, precipitation of pyrite formed during fluid cooling and ascent to the seafloor. Metal dissolution is a function of temperature, low pH and chloride rich brines as shown by Douville et al., (2001). Dissolution of basalt to release metals increases as higher T and Cl-rich and lower pH seawater reacts with basalts at temperatures > 150° C, causing increased metal contents in vent fluids (Gamo, 1995) as evidenced by the positive correlation for total Fe vs temperature (Fig. 1.6b) and negative correlation vs pH (Table A1). Indian Ocean ridge vents show high total Fe content compared to other ridge segments (Fig. 1.10d). Differences are significant for CIR vs EPR and NEP and could be due to high chlorinity linked with hot fluids which intensify metal transport as shown by Von Damm et al., (2001). Chloride-rich brines are produced through gas-liquid phase separation beneath the seafloor (Gamo, 1995). This explains the minor positive relationships between chloride ion vs total Fe (Fig. 1.8a) and Mn (Fig. 1.8b). Chloride ion concentration of vent fluids can be enriched or depleted compared to normal seawater, with Cl- of 550 mM (Gamo, 1995). Sub-seafloor liquid phase separation also explains the negative correlations between chloride and gas components such as helium isotopes (Fig. 1.8e) and CO_2 (Fig. 1.8c).

1.6.3. Anomalous Fe and Chlorinity of Central Indian Ridge Vent Fluids

The observed higher total Fe and Chlorinity of CIR vent fluids compared to EPR and NEP ridges is noticeable and is also confirmed by ANOVA with p-values <0.05 for EPR and NEP compared with CIR (Table A2). This observation agrees with that of Von Damm et al., (2001), where they compared hot fluids of Edmond and Kairei fields, both in the CIR. They argued that the reason for high CIR Fe concentrations are due to high chlorinity coupled with hot fluids which leads to enhanced metal transport. Although the SWIR Longqi field also has Fe levels (12 mmol/kg) as high as CIR, we do not have enough observations for SWIR-Longqi chlorinity therefore we cannot assess whether or not high chlorinity is also responsible here.

1.6.4. Is geography the most important control on MOR vent biota?

Unlike terrestrial and shallow marine flora and fauna, deep sea hydrothermal vent ecosystems depend upon the chemosynthetic microbes which thrive on nutrient rich fluids emanating from active vents. As these vent systems are similar in their fluid temperatures and chemistry, we might also expect the organisms that are found in these environments to be similar. However, our results indicate that hydrothermal vent communities of different ridge segments corresponding to the 7 geographic provinces of MOR are not high. This is true for both species and genera but especially for species. Such low indices imply that the distribution of organisms is controlled by distance (Hessler and Lonsdale, 1991) and other geological and hydrological barriers as described by Tunnicliffe et al., (1996) and the minor differences in the availability of nutrients related to fluid composition as shown by ANOVA.

1.7.CONCLUSIONS

All mid-ocean ridges have simple divergent margin tectonics but with different rates of spreading resulting different morphologies such as axial ridges and valleys for slow-spreading ridges vs. axial highs for fast spreading ridges. Spreading rate also exerts strong controls on magma production, with basalt lavas dominating at fast-spreading ridges whereas more mantle peridotite is exposed at slow spreading ridges. Thus, we might expect that spreading rate and hydrothermal fluid parameters to show systematic variations. However, it appears that many fluid parameters such as vent fluid temperature, pH, Fe, Mn, CO_2, H_2, SO_4^{2-} ion and chlorinity are independent of spreading rate. Fluid temperature does control pH, Fe and H_2S. In addition, brine separation might influence gases such as helium isotopic ratio and CO_2 in venting fluids. All these differences might be related to local lithology, permeability, age of the hydrothermal system, depth to magma body etc.

Vent biota distribution among the ridges seems to be mostly be controlled by the distance (Hessler and Lonsdale, 1991) and other geological and hydrological barriers as described by Tunnicliffe et al., (1996) and the minor differences in the availability of nutrients related to fluid composition as shown by this study.

1.8.ACKNOWLEDGMENTS

We thank Dr. Frank Konietschke and Asanka M. Gunawardana of the Department of Mathematical Sciences, at the University of Texas at Dallas for their guidance in statistical analysis.

Appendix A: Statistical analyses of fluid parameters and vent organisms in global mid ocean ridge hydrothermal system.

Table A.1: Kendall's tau correlations and corresponding p-values of vent fluid parameters vs full spreading rate, depth, temperature and chlorinity

Variable	Statistics	Full Spreading Rate (mm/yr)	Depth (m bsl)	Temperature (^{0}C)	pH	Total Fe (mM)	Mn (mM)
Full Spreading Rate (mm/yr)	tau	1.0000	0.1386	0.0876	-0.0588	0.0242	0.1106
	p-value	****	***	*	ns	ns	ns
Depth (m bsl)	tau	0.1386	1.0000	0.1274	0.0599	0.1493	0.1813
	p-value	***	****	**	ns	*	**
Temperature (0C)	tau	0.0876	0.1274	1.0000	-0.5022	0.3279	0.2064
	p-value	*	**	****	****	*****	**
pH	tau	-0.0588	0.0599	-0.5022	1.0000	-0.3650	-0.2693
	p-value	ns	ns	****	****	****	****
Chlorinity (mM)	tau	-0.1548	0.1893	-0.1186	0.0775	0.1550	0.2381
	p-value	*	**	*	ns	*	***

Table A.1 (continued).

Variable	Statistics	(^{3}He/^{4}He) /Ra	CO_2 (mM)	CH_4 (mM)	H_2 (mM)	H_2S (mM)	SO_4^{2-} (mM)
Full Spreading Rate (mm/yr)	tau	-0.3575	-0.0969	-0.2808	-0.1443	0.3316	0.1145
	p-value	**	ns	***	ns	****	ns
Depth (m bsl)	tau	-0.2138	-0.2484	-0.3849	-0.0053	0.0551	-0.1445
	p-value	ns	**	****	ns	ns	ns
Temperature (^{0}C)	tau	-0.2675	-0.0807	-0.1653	0.0931	0.4684	-0.0651
	p-value	ns	ns	*	ns	****	ns
pH	tau	0.2815	-0.0355	0.3156	0.0405	-0.4175	0.0924
	p-value	ns	ns	***	ns	****	ns
Chlorinity (mM)	tau	-0.5236	-0.3111	0.0629	0.0298	-0.2211	-0.0609
	p-value	***	***	ns	ns	***	ns

§ ≥0.8 High correlation, ≤0.45-0.8> moderate correlation, ≤0.25-0.45> weak correlation, <0.25 no correlation; * Significant at $p < 0.05$, ** significant at $p < 0.01$, *** significant at $p < 0.001$, **** significant at $p < 0.0001$, ns – not significant.

Table A.2: p-Values of multiple comparisons for non-parametric Analysis of Variance (ANOVA) with Bonferroni corrections.

Comparison	Depth (m bsl)	Temperature (^{0}C)	pH	Total Fe (mM)	Mn (mM)	(^{3}He/^{4}He)/Ra
CIR, SWIR	ns	ns	ns	ns	ns	n/a
EPR, CIR	ns	ns	ns	**	ns	ns
EPR, GSC	*	ns	n/a	n/a	n/a	n/a
EPR, MAR	*	ns	ns	ns	ns	ns
EPR, NEP	****	****	****	ns	ns	ns
EPR, SWIR	****	ns	ns	ns	ns	n/a
GSC, CIR	ns	ns	n/a	n/a	n/a	n/a
GSC, SWIR	**	ns	n/a	n/a	n/a	n/a
MAR, CIR	ns	ns	ns	ns	ns	ns
MAR, GSC	ns	ns	n/a	n/a	n/a	n/a
MAR, NEP	ns	*	****	ns	ns	ns
MAR, SWIR	ns	ns	ns	ns	ns	n/a
MCR, CIR	ns	ns	ns	ns	***	n/a
MCR, EPR	ns	ns	ns	ns	*	n/a
MCR, GSC	ns	ns	n/a	n/a	n/a	n/a
MCR, MAR	ns	ns	ns	ns	ns	n/a
MCR, NEP	ns	ns	ns	ns	ns	n/a
MCR, SWIR	ns	ns	ns	ns	ns	n/a
NEP, CIR	**	*	ns	*	ns	ns
NEP, GSC	ns	ns	n/a	n/a	n/a	n/a
NEP, SWIR	ns	ns	ns	ns	ns	n/a

Table A.2 (continued).

Comparison	CO_2 (mM)	CH_4 (mM)	H_2S (mM)	SO_4^{2-} (mM)	H_2 (mM)	Chlorinity (mM)
CIR, SWIR	n/a	ns	n/a	ns	ns	n/a
EPR, CIR	*	ns	****	ns	ns	**
EPR, GSC	n/a	n/a	n/a	n/a	n/a	n/a
EPR, MAR	ns	**	****	ns	ns	ns
EPR, NEP	ns	ns	****	ns	ns	ns
EPR, SWIR	n/a	ns	n/a	ns	ns	n/a
GSC, CIR	n/a	n/a	n/a	n/a	n/a	n/a
GSC, SWIR	n/a	n/a	n/a	n/a	n/a	n/a
MAR, CIR	*	*	ns	ns	ns	**
MAR, GSC	n/a	n/a	n/a	n/a	n/a	n/a
MAR, NEP	ns	ns	ns	ns	ns	ns
MAR, SWIR	n/a	ns	n/a	ns	ns	n/a
MCR, CIR	*	ns	ns	ns	****	ns
MCR, EPR	ns	ns	**	ns	****	ns
MCR, GSC	n/a	n/a	n/a	n/a	n/a	n/a
MCR, MAR	ns	ns	ns	ns	****	ns
MCR, NEP	ns	ns	ns	ns	****	ns
MCR, SWIR	n/a	ns	n/a	ns	*	n/a
NEP, CIR	ns	ns	ns	ns	ns	**
NEP, GSC	n/a	n/a	n/a	n/a	n/a	n/a
NEP, SWIR	n/a	ns	n/a	ns	ns	n/a

*CIR-Central Indian Ridge; SWIR- Southwest Indian Ridge; EPR- East Pacific Rise; GSC- Galapagos Spreading Center; MCR- Mid Cayman Rise; MAR- Mid Atlantic Ridge; NEP- Northeast Pacific Ridges (Explorer Ridge/ Juan de Fuca Ridge and Gorda Ridge); # n/a - not available; § * Significant at $p < 0.05$, ** significant at $p < 0.01$, *** significant at $p < 0.001$, **** significant at $p < 0.0001$, ns – not significant.

Table A.3: Sörensen similarity indices for biogeographic provinces obtained from multivariate regression analysis.

	Setting	CIR	EPR	GSC	MAR	MCR	NEP	SWIR
Sörensen Indices for Species	CIR	100%	6%	n/a	5%	5%	1%	14%
	EPR	6%	100%	n/a	4%	3%	6%	2%
	MAR	5%	4%	n/a	100%	1%	0%	1%
	MCR	5%	3%	n/a	1%	100%	0%	0%
	NEP	1%	6%	n/a	0%	0%	100%	0%
	SWIR	14%	2%	n/a	1%	0%	0%	100%
Sörensen Indices for Genera	Setting	CIR	EPR	GSC	MAR	MCR	NEP	SWIR
	CIR	100%	28%	15%	26%	17%	20%	59%
	EPR	28%	100%	4%	24%	6%	23%	20%
	GSC	15%	4%	100%	4%	17%	3%	7%
	MAR	26%	24%	4%	100%	6%	14%	26%
	MCR	17%	6%	17%	6%	100%	6%	11%
	NEP	20%	23%	3%	14%	6%	100%	12%
	SWIR	59%	20%	7%	26%	11%	12%	100%

* CIR-Central Indian Ridge; EPR- East Pacific Rise; GSC- Galapagos Spreading Center; MCR- Mid Cayman Rise; MAR- Mid Atlantic Ridge; NEP- Northeast Pacific Ridges (Explorer Ridge/ Juan deFuca Ridge and Gorda Ridge); SWIR- Southwest Indian Ridge; # n/a - not available.

REFERENCES

Alt, J. C. (1995). Subseafloor Processes in Mid-Ocean Ridge Hydrothermal Systems. Seafloor Hydrothermal Systems: Physical, chemical, biological, and geological interactions, Geophysical Monograph 91, 85-114.

Anderson, R. E., Sogin, M. L., & Baross, J. A. (2014). Biogeography and ecology of the rare and abundant microbial lineages in deep-sea hydrothermal vents.

Baker, E. T., & Urabe, T. (1996). Extensive distribution of hydrothermal plumes along the superfast spreading East Pacific Rise, 13° 30′–18° 40′ S. Journal of Geophysical Research: Solid Earth, 101(B4), 8685-8695.

Baker, E. T., Chadwick Jr, W. W., Cowen, J. P., Dziak, R. P., Rubin, K. H., & Fornari, D. J. (2012). Hydrothermal discharge during submarine eruptions: The importance of detection, response, and new technology. Oceanography, 25(1), 128-141.

Baker, E. T., Cormier, M. H., Langmuir, C. H., & Zavala, K. (2001). Hydrothermal plumes along segments of contrasting magmatic influence, 15° 20′–18° 30′ N, East Pacific Rise: Influence of axial faulting. Geochemistry, Geophysics, Geosystems, 2(9).

Baker, E. T., Embley, R. W., Walker, S. L., Resing, J. A., Lupton, J. E., Nakamura, K. I., ... & Massoth, G. J. (2008). Hydrothermal activity and volcano distribution along the Mariana arc. Journal of Geophysical Research: Solid Earth, 113(B8).

Baker, E. T., German, C. R., & Elderfield, H. (1995). Hydrothermal plumes over spreading-center axes: Global distributions and geological inferences. Geophysical Monograph-American Geophysical Union, 91, 47-47.

Beedessee, G., Watanabe, H., Ogura, T., Nemoto, S., Yahagi, T., Nakagawa, S., ... & Marie, D. E. (2013). High connectivity of animal populations in deep-sea hydrothermal vent fields in the Central Indian Ridge relevant to its geological setting. Plos one, 8(12), e81570.

Bischoff, J. L., Clancy, J. J., & Booth, J. S. (1975). Magnesium removal in reducing marine sediments by cation exchange. Geochimica et Cosmochimica Acta, 39(5), 559-568.

Bougault, H., Charlou, J. L., Fouquet, Y., Needham, H. D., Vaslet, N., Appriou, P., ... & Silantiev, S. (1993). Fast and slow spreading ridges: structure and hydrothermal activity, ultramafic topographic highs, and CH4 output. Journal of Geophysical Research: Solid Earth, 98(B6), 9643-9651.

Brunner, E., Konietschke, F., Pauly, M., & Puri, M. L. (2016). Rank-based procedures in factorial designs: hypotheses about non-parametric treatment effects. Journal of the Royal

Statistical Society: Series B (Statistical Methodology). Journal of the Royal Statistical Society 79(5), 1463-1485.

Butterfield, D. A., Jonasson, I. R., Massoth, G. J., Feely, R. A., Roe, K. K., Embley, R. E., ... & Delaney, J. R. (1997). Seafloor eruptions and evolution of hydrothermal fluid chemistry. Philosophical Transactions of the Royal Society of London. Series A: Mathematical, Physical and Engineering Sciences, 355(1723), 369-386.

Butterfield, D. A., Massoth, G. J., McDuff, R. E., Lupton, J. E., & Lilley, M. D. (1990). Geochemistry of hydrothermal fluids from Axial Seamount hydrothermal emissions study vent field, Juan de Fuca Ridge: Subseafloor boiling and subsequent fluid-rock interaction. Journal of Geophysical Research: Solid Earth, 95(B8), 12895-12921.

Butterfield, D. A., McDuff, R. E., Mottl, M. J., Lilley, M. D., Lupton, J. E., & Massoth, G. J. (1994). Gradients in the composition of hydrothermal fluids from the Endeavour segment vent field: Phase separation and brine loss. Journal of Geophysical Research: Solid Earth, 99(B5), 9561-9583.

Butterfield, D.A. (2000): Deep ocean hydrothermal vents. In Encyclopedia of Volcanoes, Academic Press, 857–875.

Charlou, J. L., Donval, J. P., Douville, E., Jean-Baptiste, P., Radford-Knoery, J., Fouquet, Y., ... & Stievenard, M. (2000). Compared geochemical signatures and the evolution of Menez Gwen (37 50′ N) and Lucky Strike (37 17′ N) hydrothermal fluids, south of the Azores Triple Junction on the Mid-Atlantic Ridge. Chemical Geology, 171(1-2), 49-75.

Chen, Y. J. (1992). Oceanic crustal thickness versus spreading rate. Geophysical Research Letters, 19(8), 753-756.

Cochran, J. R., Kurras, G. J., Edwards, M. H., & Coakley, B. J. (2003). The Gakkel Ridge: Bathymetry, gravity anomalies, and crustal accretion at extremely slow spreading rates. Journal of Geophysical Research: Solid Earth, 108(B2).

Connelly, D. P., Copley, J. T., Murton, B. J., Stansfield, K., Tyler, P. A., German, C. R., ... & Hayman, N. (2012). Hydrothermal vent fields and chemosynthetic biota on the world's deepest seafloor spreading centre. Nature Communications, 3(1), 1-9.

Copley, J. T., Marsh, L., Glover, A. G., Hühnerbach, V., Nye, V. E., Reid, W. D. K., ... & Wiklund, H. (2016). Ecology and biogeography of megafauna and macrofauna at the first known deep-sea hydrothermal vents on the ultraslow-spreading Southwest Indian Ridge. Scientific reports, 6, 39158.

Corliss, J. B., Dymond, J., Gordon, L. I., Edmond, J. M., von Herzen, R. P., Ballard, R. D., ... & van Andel, T. H. (1979). Submarine thermal springs on the Galapagos Rift. Science, 203(4385), 1073-1083.

DeMets, C., Gordon, R. G., Argus, D. F., & Stein, S. (1990). Current plate motions. Geophysical Journal International, 101(2), 425-478.

Douville, E., Charlou, J. L., Oelkers, E. H., Bienvenu, P., Colon, C. J., Donval, J. P., ... & Appriou, P. (2002). The rainbow vent fluids (36 14′ N, MAR): the influence of ultramafic rocks and phase separation on trace metal content in Mid-Atlantic Ridge hydrothermal fluids. Chemical Geology, 184(1-2), 37-48.

Edmonds, H. N., Michael, P. J., Baker, E. T., Connelly, D. P., Snow, J. E., Langmuir, C. H., ... & Graham, D. W. (2003). Discovery of abundant hydrothermal venting on the ultraslow-spreading Gakkel ridge in the Arctic Ocean. Nature, 421(6920), 252.

Fischer, T. P., & Chiodini, G. (2015). Volcanic, magmatic and hydrothermal gases. In the Encyclopedia of Volcanoes (pp. 779-797). Academic Press.

Fornari, D. J., & Embley, R. W. (1995). Tectonic and volcanic controls on hydrothermal processes at the mid-ocean ridge: An overview based on near-bottom and submersible studies. Seafloor hydrothermal systems: Physical, chemical, biological, and geological interactions, 91, 1-46.

Fouquet, Y. (1997). Discovery and first submersible investigations on the Rainbow hydrothermal field on the MAR (36 14'N). Eos Transactions of American Geophysical Union, 78, 832.

Fouquet, Y., Charlou, J. L., Costa, I., Donval, J. P., Radford-Knoery, J., Pellé, H., ... & Tivey, M. K. (1994). A detailed study of the Lucky Strike hydrothermal site and discovery of a new hydrothermal site: Menez Gwen: Preliminary results of the DIVA1 cruise (5–29 May, 1994). InterRidge News, 3(2), 14-17.

Gamo, T. (1995). Wide variation of chemical characteristics of submarine hydrothermal fluids due to secondary modification processes after high temperature water-rock interaction: a review. Biogeochemical processes and ocean flux in the Western Pacific, 425-451.

Gebruk, A. V., Galkin, S. V., Vereshchaka, A. L., Moskalev, L. I., & Southward, A. J. (1997). Ecology and biogeography of hydrothermal vent fauna of the Mid-Atlantic Ridge. In Advances in Marine Biology (Vol. 32, pp. 93-144). Academic Press.

German, C. R., Bowen, A., Coleman, M. L., Honig, D. L., Huber, J. A., Jakuba, M. V., ... & de Lépinay, B. M. (2010). Diverse styles of submarine venting on the ultraslow spreading Mid-Cayman Rise. Proceedings of the National Academy of Sciences, 107(32), 14020-14025.

Glass, G. V. (1976). Primary, secondary, and meta-analysis of research. Educational researcher, 5(10), 3-8.

Hannington, M., Jamieson, J., Monecke, T., Petersen, S., & Beaulieu, S. (2011). The abundance of seafloor massive sulfide deposits. Geology, 39(12), 1155-1158.

Haymon, R. M., Baker, E. T., Resing, J. A., White, S. M., Macdonald, K. C., & Galapagos Team. (2007). Hunting for Hydrothermal Vents Along the Galápagos Spreading Center: Along the Galápagos Spreading Center. Oceanography, 20(4), 100-107.

Hessler, R. R., & Lonsdale, P. F. (1991). Biogeography of Mariana Trough hydrothermal vent communities. Deep Sea Research Part A. Oceanographic Research Papers, 38(2), 185-199.

Ji, F., Zhou, H., Yang, Q., Gao, H., Wang, H., & Lilley, M. D. (2017). Geochemistry of hydrothermal vent fluids and its implications for subsurface processes at the active Longqi hydrothermal field, Southwest Indian Ridge. Deep Sea Research Part I: Oceanographic Research Papers, 122, 41-47.

Johnson, G. L., Southall, J. R., Young, P. W., & Vogt, P. R. (1972). Origin and structure of the Iceland Plateau and Kolbeinsey Ridge. Journal of Geophysical Research, 77(29), 5688-5696.

Karson, J. A., Kelley, D. S., Fornari, D. J., Perfit, M. R., & Shank, T. M. (2015). Discovering the Deep: A Photographic Atlas of the Seafloor and Ocean Crust. Cambridge University Press.

Kelley, D. S., Baross, J. A., & Delaney, J. R. (2002). Volcanoes, fluids, and life at mid-ocean ridge spreading centers. Annual Review of Earth and Planetary Sciences, 30(1), 385-491.

Kelley, D. S., Karson, J. A., Blackman, D. K., FruÈh-Green, G. L., Butterfield, D. A., Lilley, M. D., ... & Rivizzigno, P. (2001). An off-axis hydrothermal vent field near the Mid-Atlantic Ridge at 30 N. Nature, 412(6843), 145.

Kinsey, J. C., & German, C. R. (2013). Sustained volcanically hosted venting at ultraslow ridges: Piccard hydrothermal field, Mid-Cayman Rise. Earth and Planetary Science Letters, 380, 162-168.

Langmuir, C., Humphris, S., Fornari, D., Van Dover, C., Von Damm, K. L. A. M., Tivey, M. K., ... & Fouquet, Y. (1997). Hydrothermal vents near a mantle hot spot: the Lucky Strike vent field at 37 N on the Mid-Atlantic Ridge. Earth and Planetary Science Letters, 148(1-2), 69-91.

Li, X., Ye, C., Wang, C., Tao, C., & Xiao, X. (2015). Chinese manned submersible JIAOLONG's scientific cruise in 2014-2015. In OCEANS 2015-MTS/IEEE Washington (pp. 1-4). IEEE.

Lowell, R. P. (2010). Hydrothermal circulation at slow spreading ridges: analysis of heat sources and heat transfer processes. Diversity of hydrothermal systems on slow spreading ocean ridges. Geophysical Monograph, 188, 11-26.

Lowell, R. P., Rona, P. A., & Von Herzen, R. P. (1995). Seafloor hydrothermal systems. Journal of Geophysical Research: Solid Earth, 100(B1), 327-352.

Lupton, J. E., Baker, E. T., & Massoth, G. J. (1999). Helium, heat, and the generation of hydrothermal event plumes at mid-ocean ridges. Earth and Planetary Science Letters, 171(3), 343-350.

Lutz, R. A., & Kennish, M. J. (1993). Ecology of deep-sea hydrothermal vent communities: A review. Reviews of Geophysics 31(3), 211-242.

Massoth, G. J., Butterfield, D. A., Lupton, J. E., McDuff, R. E., Lilley, M. D., & Jonasson, I. R. (1989). Submarine venting of phase-separated hydrothermal fluids at Axial Volcano, Juan de Fuca Ridge. Nature, 340(6236), 702-705.

McDermott, J. M., Sylva, S. P., Ono, S., German, C. R., & Seewald, J. S. (2018). Geochemistry of fluids from Earth's deepest ridge-crest hot-springs: Piccard hydrothermal field, Mid-Cayman Rise. Geochimica et Cosmochimica Acta, 228, 95-118.

McGuire, J. J. (2008). Seismic cycles and earthquake predictability on East Pacific Rise transform faults. Bulletin of the Seismological Society of America, 98(3), 1067-1084.
Murton, B. J., Van Dover, C., & Southward, E. (1995). Geological setting and ecology of the Broken Spur hydrothermal vent field: 29 10′ N on the Mid-Atlantic Ridge. Geological Society, London, Special Publications, 87(1), 33-41.

Normark, W. R., Morton, J. L., Koski, R. A., Clague, D. A., & Delaney, J. R. (1983). Active hydrothermal vents and sulfide deposits on the southern Juan de Fuca Ridge. Geology, 11(3), 158-163.

Okino, K., Nakamura, K., & Sato, H. (2015). Tectonic background of four hydrothermal fields along the Central Indian Ridge. In Subseafloor Biosphere Linked to Hydrothermal Systems (pp. 133-146). Springer, Tokyo.

Pedersen, R. B., & Furnes, H. (2001). Nd-and Pb-isotopic variations through the upper oceanic crust in DSDP/ODP Hole 504B, Costa Rica Rift. Earth and Planetary Science Letters, 189(3-4), 221-235.

Pedersen, R. B., Thorseth, I. H., Nygård, T. E., Lilley, M. D., & Kelley, D. S. (2010). Hydrothermal activity at the Arctic mid-ocean ridges. Washington DC American Geophysical Union Geophysical Monograph Series, 188, 67-89.

Rona, P. A. (1984). Hydrothermal mineralization at seafloor spreading centers. Earth-Science Reviews, 20(1), 1-104.

Rona, P. A., Klinkhammer, G., Nelsen, T. A., Trefry, J. H., & Elderfield, H. (1986). Black smokers, massive sulphides and vent biota at the Mid-Atlantic Ridge. Nature, 321(6065), 33.

Rubin, K. H., Soule, S. A., Chadwick Jr, W. W., Fornari, D. J., Clague, D. A., Embley, R. W., ... & Dziak, R. P. (2012). Volcanic eruptions in the deep sea. Oceanography, 25(1), 142-157.

Ryan, W. B., Carbotte, S. M., Coplan, J. O., O'Hara, S., Melkonian, A., Arko, R., ... & Bonczkowski, J. (2009). Global multi-resolution topography synthesis. Geochemistry, Geophysics, Geosystems, 10(3).

Sauter, D., & Cannat, M. (2010). The ultraslow spreading southwest Indian ridge. Diversity of Hydrothermal Systems on Slow Spreading Ocean Ridges, 88, 153-173.

Seyfried Jr, W. E., Berndt, M. E., & Janecky, D. R. (1986). Chloride depletions and enrichments in seafloor hydrothermal fluids: Constraints from experimental basalt alteration studies. Geochimica et Cosmochimica Acta, 50(3), 469-475.

Sinton, J., Detrick, R., Canales, J. P., Ito, G., & Behn, M. (2003). Morphology and segmentation of the western Galápagos Spreading Center, 90.5°–98° W: Plume-ridge interaction at an intermediate spreading ridge. Geochemistry, Geophysics, Geosystems, 4(12).

Son, J., Pak, S. J., Kim, J., Baker, E. T., You, O. R., Son, S. K., & Moon, J. W. (2014). Tectonic and magmatic control of hydrothermal activity along the slow-spreading Central Indian Ridge, 8° S–17° S. Geochemistry, Geophysics, Geosystems, 15(5), 2011-2020.

Sudarikov, S. M., & Roumiantsev, A. B. (2000). Structure of hydrothermal plumes at the Logatchev vent field, 14 45′ N, Mid-Atlantic Ridge: evidence from geochemical and geophysical data. Journal of Volcanology and Geothermal Research, 101(3-4), 245-252.

Tarasov, V. G., Gebruk, A. V., Mironov, A. N., & Moskalev, L. I. (2005). Deep-sea and shallow-water hydrothermal vent communities: two different phenomena? Chemical Geology, 224(1-3), 5-39.

Tivey, M. K. (1995). The influence of hydrothermal fluid composition and advection rates on black smoker chimney mineralogy: Insights from modeling transport and reaction. Geochimica et Cosmochimica Acta, 59(10), 1933-1949.

Tivey, M. K. (2007). Generation of seafloor hydrothermal vent fluids and associated mineral deposits. Oceanography, 20(1), 50-65.

Tunnicliffe, V., & Fowler, C. M. R. (1996). Influence of seafloor spreading on the global hydrothermal vent fauna. Nature, 379(6565), 531.

Van Dover, C. L. (2002). Community structure of mussel beds at deep-sea hydrothermal vents. Marine Ecology Progress Series, 230, 137-158.

Van Dover, C. L., Berg Jr, C. J., & Turner, R. D. (1988). Recruitment of marine invertebrates to hard substrates at deep-sea hydrothermal vents on the East Pacific Rise and Galapagos spreading center. Deep Sea Research Part A. Oceanographic Research Papers, 35(10-11), 1833-1849.

Von Damm, K. L. (1988). Systematics of and postulated controls on submarine hydrothermal solution chemistry. Journal of Geophysical Research: Solid Earth, 93(B5), 4551-4561.

Von Damm, K. L. (1990). Seafloor hydrothermal activity: black smoker chemistry and chimneys. Annual Review of Earth and Planetary Sciences, 18(1), 173-204.

Von Damm, K. L. (2000). Chemistry of hydrothermal vent fluids from 9–10 N, East Pacific Rise:"Time zero," the immediate posteruptive period. Journal of Geophysical Research: Solid Earth, 105(B5), 11203-11222.

Von Damm, K. L., & Bischoff, J. L. (1987). Chemistry of hydrothermal solutions from the southern Juan de Fuca Ridge. Journal of Geophysical Research: Solid Earth, 92(B11), 11334-11346.

Von Damm, K. L., Parker, C. M., Lilley, M. D., Clague, D. A., Zierenberg, R. A., Olson, E. J., & McClain, J. S. (2006). Chemistry of vent fluids and its implications for subsurface conditions at Sea Cliff hydrothermal field, Gorda Ridge. Geochemistry, Geophysics, Geosystems, 7(5).

Wetzel, L. R., & Shock, E. L. (2000). Distinguishing ultramafic-from basalt-hosted submarine hydrothermal systems by comparing calculated vent fluid compositions. Journal of Geophysical Research: Solid Earth, 105(B4), 8319-8340.

Whiting, P., Westwood, M., Burke, M., Sterne, J., & Glanville, J. (2008). Systematic reviews of test accuracy should search a range of databases to identify primary studies. Journal of clinical epidemiology, 61(4), 357-e1.

Zierenberg, R. A., Koski, R. A., Morton, J. L., & Bouse, R. M. (1993). Genesis of massive sulfide deposits on a sediment-covered spreading center, Escanaba Trough, southern Gorda Ridge. Economic Geology, 88(8), 2069-2098.

CHAPTER 2

HYDROTHERMAL AND COLD-SEEP VENTS IN THE MARIANA CONVERGENT MARGIN: TECTONICS, FLUID CHEMISTRY AND BIOLOGY

2.1.ABSTRACT

Hydrothermal vents and cold-seeps of the submarine convergent margins are diverse in their origins, physicochemical characteristics and biota and are poorly studied. Hydrothermal vents of the Mariana convergent margin represent an excellent and well-studied example. We compiled data for this system and distinguish four tectonic groups of vents: Forearc vents lie close to the trench, arc vents are associated with submarine volcanoes along or behind the magmatic front, and backarc basin vents are associated with the backarc basin spreading axis. A fourth setting is identified in the southern Mariana Trough where unusually strong extension obscures the distinction between forearc, arc, and backarc. Like any other hydrothermal system on Earth, vent activity in the submarine Mariana convergent margin is identified by hot fluids and/or smokers, degassing magma, diffuse flow, active chimney growth and anomalies observed in hydrothermal plumes. Based on fluid temperature and chemistry, four types of vents are identified as: smokers, degassing sulfur, degassing CO_2 and serpentinite-hosted cold seeps. Except the cold seeps, the other three are related to igneous activity. All four types of vents are associated with chimney structures and surrounding ecosystems. Forearc vents are associated with serpentine mud volcanoes and seep cold and alkaline fluids in contrast to arc-backarc basin vent fluids, which are typically hot and acidic. Depending on temperature and pH, fluids from all four vent types carry varying amounts of dissolved ions and gases such as CO_2, CH_4 and H_2S. Three types of chimneys are identified: carbonate and/or brucite chimneys are associated with cool alkaline forearc seeps

whereas hot, acidic vents build chimneys rich in sulfur, sulfate-sulfide in the arc, backarc basin, and Southern Mariana Trough. Integration of tectonics, fluid chemistry and vent biota demonstrate that Mariana vent groups are more diverse than global mid-ocean ridge vents and confirm the distinct nature of the southernmost Mariana vent systems, including biota, which most resemble those of the mid-ocean ridges.

2.2.INTRODUCTION

Submarine hydrothermal and cold-seep vents are seafloor fissures which release fluids and gases into the ocean. First discovered in 1977 at the Galapagos Spreading Center (Corliss et al., 1979), we now know that seafloor hydrothermal systems are key components of the Earth system. Venting acts as an important mechanism that Earth's mantle loses heat (Lowell et al., 1995; Stein and Stein, 1994) and these fluids buffer seawater chemistry (Lupton et al., 2008). Venting is associated with unique deep-water ecosystems, comprising extremophile Archaea, Bacteria and larger animals (Van Dover et al, 2002). Venting can produce economic ore deposits, for example volcanogenic massive sulfides produced by ancient hydrothermal activity (Moore et al., 1990).

Seafloor hydrothermal activity along mid-ocean ridges have been studied and increasingly understood. More recently, research on hydrothermal vents at convergent plate boundaries (submarine arc-trench-backarc systems) is being carried out. The Mariana convergent margin provides an excellent example of an intra-oceanic convergent plate margin, built on oceanic crust and thus mostly lie below sea level (Stern, 2010). In recent years the hydrothermal activity of this convergent margin has been studied in some detail. In the mid 1990's only a handful of Mariana hydrothermal vents were known (Alt et al., 1993; Fryer et al., 1992; Stern et al., 1993). At that

time, scientists had only recently discovered (via ALVIN diving in 1987 (Craig, 1987)) hydrothermal vents and communities in Mariana trough, backarc basin spreading axis at 18°N (Fryer, 1990); no hydrothermal vents associated with submarine arc volcanoes had yet been discovered. Cold seeps associated with some forearc serpentinite mud volcanoes were suspected since the study of Fryer et al. (1985) but geoscientists were only beginning to study them. Today, largely through the expeditions by NOAA's Pacific Marine Environmental Laboratory (PMEL) and the Japan Agency for Marine-Earth Science and Technology (JAMSTEC), we know at least 47 vents (Fig. 2.1) in the Mariana convergent margin system. Through astonishing discoveries made on several expeditions (e.g., presence of sulfur lake at arc volcano Daikoku) we are learning that vents in intra-oceanic arc systems are as important as those on MOR but show much more variability.

The Mariana arc-backarc system has a diversity of hydrothermal vents that occur over a greater depth range than found for mid-ocean ridge vents (Fig. 2.2) from near sea-level to ~6500m and show a greater diversity of vent fluid temperatures, vent and chimney compositions, and associated ecosystems. Some Mariana vents are similar to MOR vents in being dominated by recirculated seawater, especially at backarc basin and some arc vents. Other Mariana vents also show significant differences with MOR vents, especially in the forearc and other arc volcanoes. Because the Mariana convergent margin is a non-accretionary system, vent fluids are little affected by the dewatering of sediments in the accretionary prism, in contrast to regions of thick sediments (e.g., Nankai, Cascadia). Therefore, the compositions of forearc vent fluids provide more information about fluids derived from the devolatilization of the subducting slab (Fryer, 1996; Sakai et al., 1990). Another difference from MOR vents is that significant inputs are made by

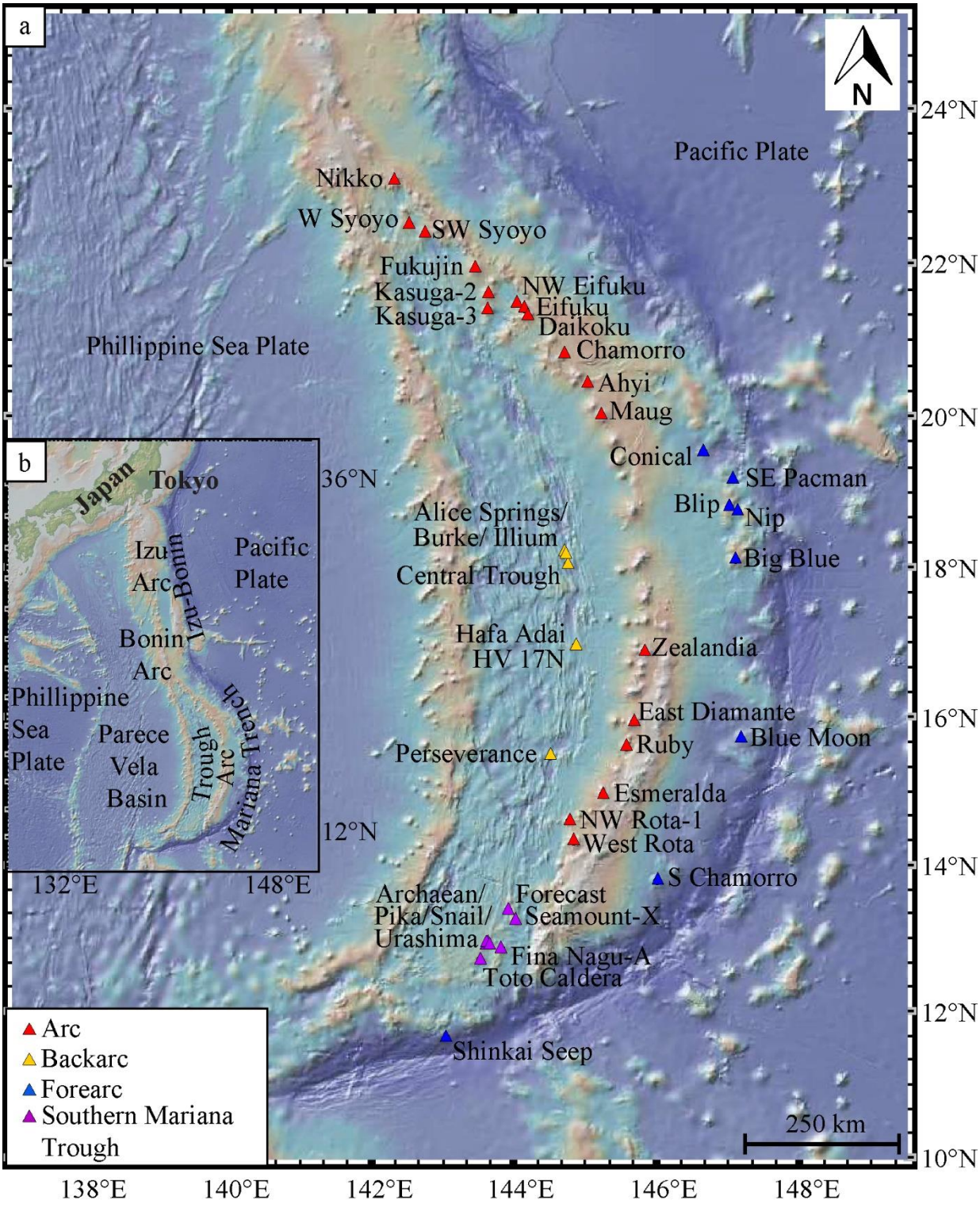

Fig. 2.1: Locality map of active known and inferred hydrothermal vents in the Mariana arc system. Figure made with GeoMapApp (www.geomapapp.org).

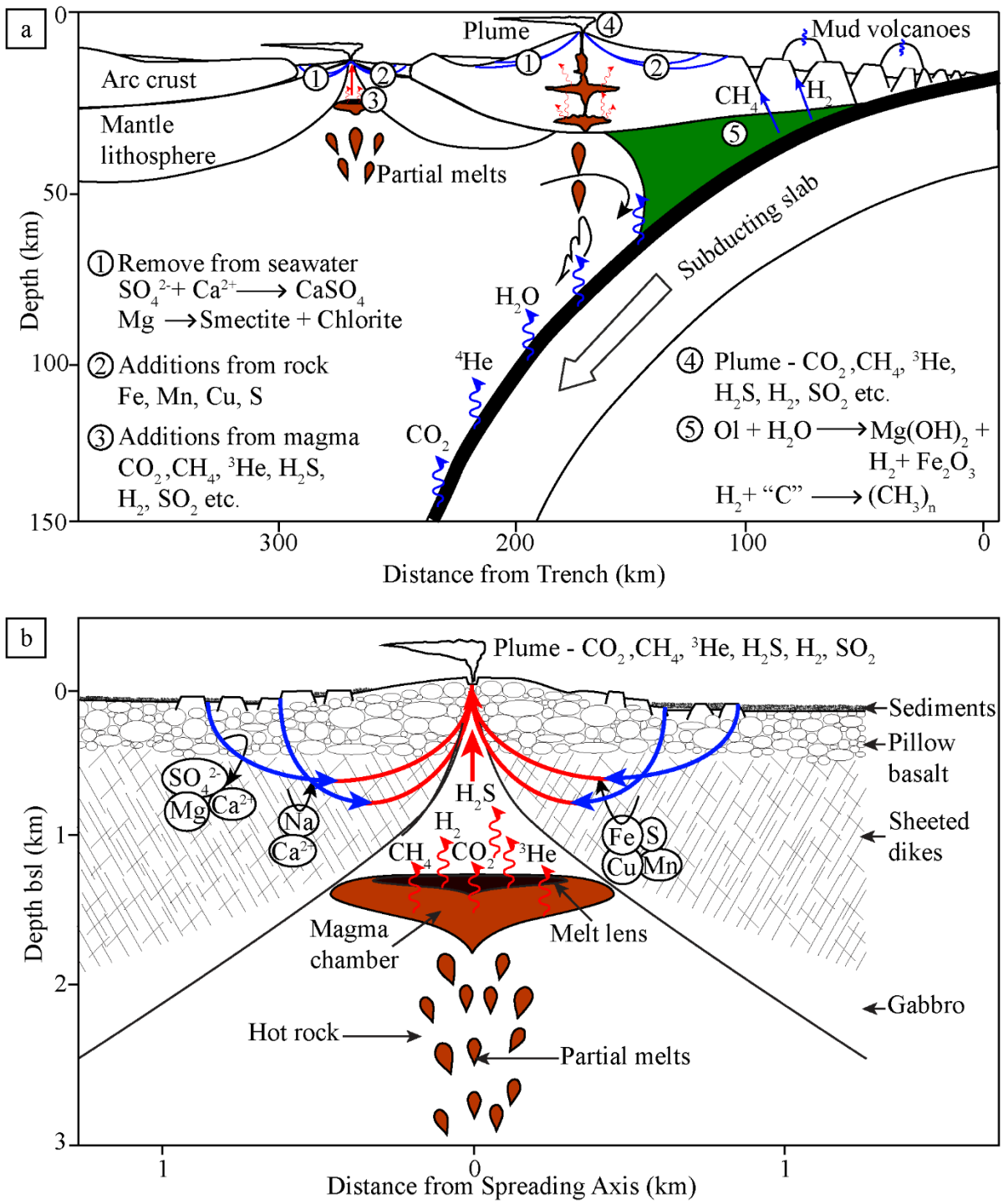

Fig. 2.2: Comparison of subseafloor processes and mantle interactions in divergent and convergent margin hydrothermalism (a) processes operating in Mariana convergent margin; green colored area represents the serpentinized mantle; Ol-olivine; C-carbon (adapted from Stern, 2002) (b) processes operating in mid ocean ridges (divergent margin).

degassing arc magmas. Additionally, understanding the diversity of convergent margin vent biota in the Marianas is a first step towards understanding how the wide range of convergent margin hydrothermal vents influences biological diversity.

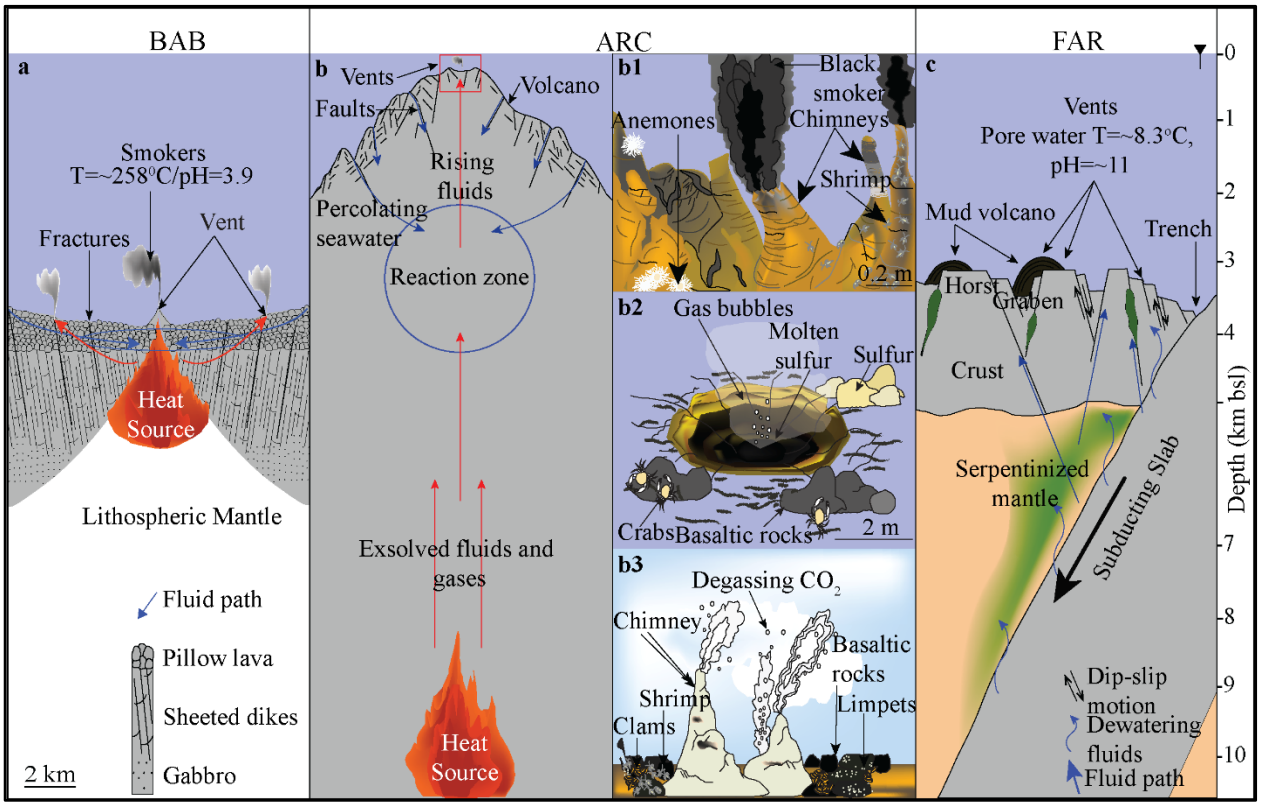

Fig. 2.3: Sketches of different types of vents in the Marianas and their tectonic settings (a) Backarc basin (BAB) setting and vents (b) Arc settings and 3 types of arc vents: (b1) Smoker type (found in arc, backarc basin, and southernmost Marianas) (b2) Degassing sulfur type venting (only found in arc vents) (b3) Degassing CO_2 type venting (only found in arc vents) (c) Forearc setting and cold seeps. Note typical water depths are approximated.

We identify three main tectonic settings of Mariana convergent margin vents: backarc basin (Fig. 2.3a), arc (Fig. 2.3b) and forearc (Fig. 2.3c), each with a distinctive style of venting. In addition, a fourth setting of hydrothermal activity is identified in the far south, where the distinction between arc, backarc basin, forearc is obscured by very active extension (Ribeiro et al., 2013; Stern et al., 2013; Stern et al., 2014). These four tectonic settings share four different types

of vents: hot fluids and/or smokers, degassing sulfur, degassing CO_2, and serpentinite-hosted cold seeps. These distinctive venting styles also share three different types of chimneys: carbonate and/or brucite chimneys, sulfur and sulfide-sulfate chimneys (Fig. 2.4).

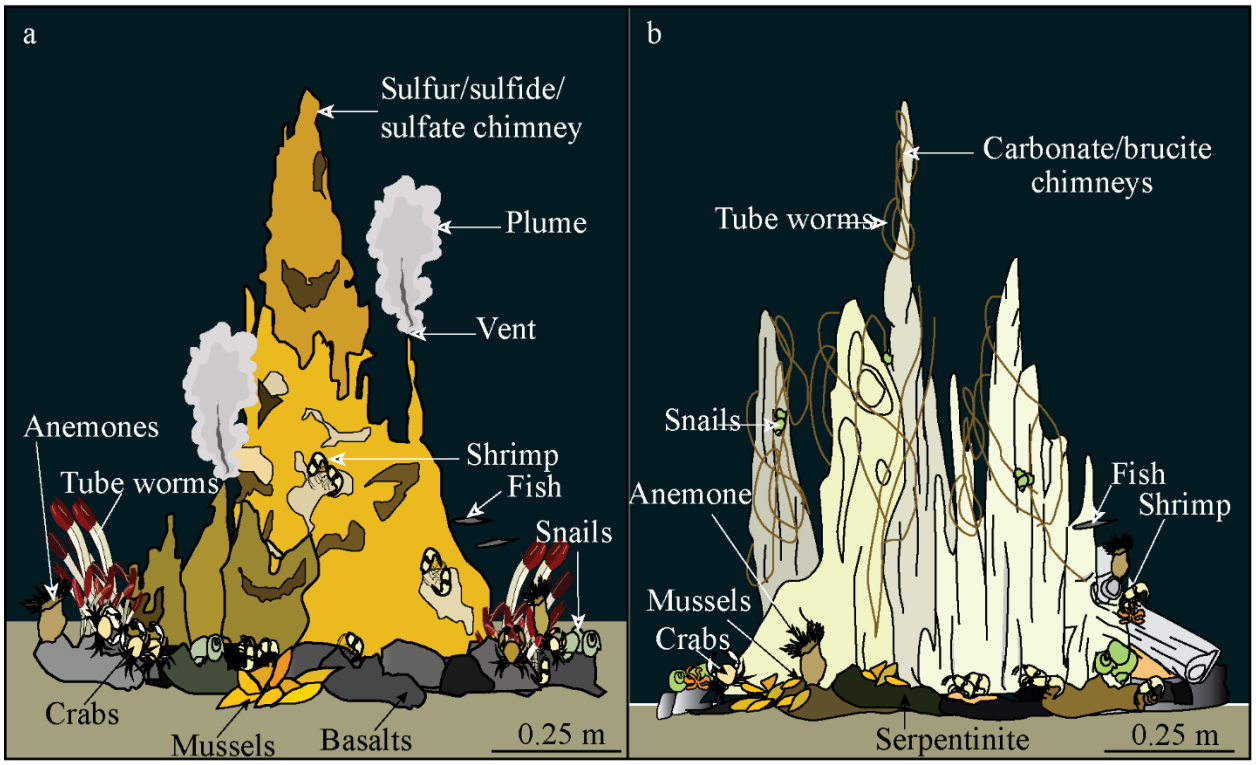

Fig. 2.4: Schematic representation of communities around two endmember chimney types (a) Smoker chimney (arc, backarc, and southernmost Marianas) (b) Carbonate and/or brucite chimneys in the forearc.

The present study is inspired by the need for a multidisciplinary data integration approach to elucidate hidden patterns and relationships among Mariana hydrothermal systems (forearc, arc and backarc) in comparison with MOR vent systems for both hydrothermal fluids and biota. Our data compilation and meta data analysis is intended further stimulate coordinated studies of vents of this and other intra-oceanic convergent margins. This compilation should also serve as baseline

information for the Mariana Trench Marine National Monument, which protects Mariana vents and their communities https://www.fws.gov/refuge/mariana_trench_marine_national_monument/

2.3.GEOLOGICAL SETTING

The Mariana convergent margin is an intra-oceanic convergent margin (Fryer et al., 1999) where the western edge of the Pacific Plate is subducted beneath the Philippine Sea Plate (Stern et al., 2002). The Marianas is the southern part of the Izu-Bonin-Mariana (IBM) arc system, which extends over 2800 km from Tokyo, Japan to Guam, USA (Stern et al, 2003). The Mariana convergent margin can be subdivided across strike into four sub regions: trench, fore-arc, volcanic arc and actively spreading back-arc. The rate of subduction is about 7 cm per year (Plank and Langmuir, 1993) and the angle of subduction varies from 12^0 to nearly vertical at about 100 km depth (Shipboard Scientific Party, 1990).

The Mariana forearc (Fig. 2.3c) is the region between the trench and the magmatic arc and in most places is about 200 km wide (Stern et al., 2003). Forearc serpentinite seamounts are found in the outer forearc which is more deformed, between 50 km to 120 km from the trench, where they occur either as horst blocks or as diapirs that extrude serpentinite (Shipboard Scientific Party, 1990), whereas the inner forearc (away from the trench) is less deformed (Stern, 2010). The presence of serpentinite mud volcanoes suggests that the mantle beneath the outer forearc is largely serpentinized (Stern and Smoot, 1998). Active mud volcanoes are associated with vents on their summits, which form carbonate, silicate or sometimes brucite chimneys (Ohara et al., 2012; Fryer and Mottl, 1992).

The Mariana volcanic arc (Fig. 2.3b) lies west of the forearc and is not older than 3-4 Ma (Stern et al., 2003). Large arc volcanoes are subaerial and smaller ones are submarine. Most submarine volcano summits are shallower than 300 m below sea level (Embley et al., 2004) but some have summits that lie as deep as 2000 mbsl. Most of these volcanoes are active or dormant (Bloomer et al., 1989) and still host magma bodies or have warm interiors. About a third of the arc seamounts are hydrothermally active (Baker et al., 2008) with chimneys that range from a few centimeters to a few meters high composed of sulfide, oxide and sulfate minerals. For an example, the Black Forest vent field of E. Diamante caldera contains sphalerite-rich chimneys are up to 7 m high (Embley et al., 2007).

The Mariana convergent margin has an actively spreading backarc basin known as the Mariana Trough (Fig. 2.3c). According to Stern et al., (2003), formation of the Mariana Trough happened sometime after 10 Ma. The backarc basin (BAB) is about 1300 km long and up to 270 km wide (Fryer, 1996; Hawkins et al., 1990; Anderson et al., 2017). Backarc basin rifting initiated about 6.5 Ma with a full spreading rate of 2.5 cm/y (Fryer, 1996). Near 18°N, the spreading axis shows an axial rift morphology typical of slow seafloor spreading (Fryer, 1995). The basin narrows northwards and the rift axis intersect the arc at Nikko Seamount near 24ºN (Smoot, 1990). BAB hydrothermal vents are concentrated along the axial rift (Baker et al., 2017). These vents eject hot fluids with low pH supported by high CO_2 concentrations (Toki et al., 2015). The chimneys associated with these vents are made up of sulfide (e.g., sphalerite, chalcopyrite) and sulfate (e.g., barite) minerals (Iwaida et al., 2005).

The southern termination is very different from the northern termination. The simple geometry of the convergent margin, with well-defined forearc, magmatic arc, and BAB disappears southwest

of Guam. This region is actively extending and is adjacent to the deepest point on the Earth's solid surface, the Challenger Deep. Because of strong extension, large volcanoes of the magmatic arc are missing and the forearc is narrow and tectonically active. Hydrothermal vents in this region are deeper than in the volcanic arc.

2.4.METHODS

2.4.1. Data Sources

Database (Table S3) includes data from multiple research expeditions for 47 known and suspected vents (Fig. 2.1) in the Mariana system accessed from peer-reviewed literature and websites managed by government agencies and ocean research institutes. The database for biota includes vent animals for 31 vents belong to the four different tectonic settings (Table S4). Some vents are inferred only from surface investigations, but others have been visited on the seafloor by remotely operated vehicles (ROV) or human occupied vehicles (HOV). Very few vents contain all the information we have considered in our statistical analysis therefore, depending on the analyses we treated them accordingly. Locality information and other available information are provided for vents with little or no information in their measured fluid parameters. A full listing of the references and the online databases used are provided in the supplementary documents. The reference list covers only the citations used in the text and tables. The following internet sources were used:

1. Encyclopedia of Life (EOL) provides information about life, from deep marine trenches to high mountain ranges (http://eol.org/).

2. InterRidge vents database 3.3 (http://vents-data.interridge.org/), which is hosted by Peking University, Beijing, China. This website provides a comprehensive list of active and inferred (unconfirmed) active submarine hydrothermal vent fields all over the world.
3. Japan Agency for Marine-Earth Science and Technology (JAMSTEC) provides many deep-sea photos and videos taken by submersibles such as Shinkai 6500 and Kaiko (http://www.godac.jamstec.go.jp/jedi/e/).
4. Marine Geoscience Data System (MGDS), which gives access to marine geoscience research data acquired throughout the oceans and adjoining continental margins (http://www.marine-geo.org/portals/ndsf/).
5. National Oceanic and Atmospheric Administration (NOAA), Ocean Exploration and Research Program, Submarine Ring of Fire expeditions carried out in 2003, 2004, 2006 and 2014 (http://oceanexplorer.noaa.gov/explorations/explorations.html), and Okeanos Explorer expeditions carried out in 2016 (http://oceanexplorer.noaa.gov/okeanos/explorations/ex1605/welcome.html). Additional information about these expeditions are available on the Pacific Marine Environmental Laboratory (PMEL), Earth-Oceans Interactions Program web site: https://www.pmel.noaa.gov/eoi/marianas_site.html
6. Smithsonian Institution National Museum of Natural History Global Volcanism Program (http://volcano.si.edu/search_volcano.cfm) database, which provides information about Holocene volcanism including submarine volcanoes.

7. Woods Hole Oceanographic Institution (WHOI), underwater vehicle information especially ROV operations and HOV Alvin dive operations (http://www.whoi.edu/main/underwater-vehicles).
8. World Register of Marine Species (WoRMS) database provides an authoritative and comprehensive list of names of marine organisms, including information on synonymy (http://www.marinespecies.org).

2.4.2. Statistical Analyses of Vent Parameters

We considered vent depth, fluid temperature, pH, total Fe, Mn, helium isotopic ratio (($^3He/^4He$)/Ra), fluid gases (CO_2, CH_4, H_2, H_2S), SO_4^{2-} ions and chlorinity of the fluids for statistical analysis. Summit depth is an important variable as bathymetry changes drastically over these four settings. Combination of heat generating processes; heat from the mantle, heat transfer from cooling crust and lithosphere, and magmatic heat transfer (Lowell, 2010) are possible in three of the four tectonic settings (arc, BAB and SMT), except for forearc vents where heat of serpentinization is dominating. The observed temperatures divide the vents into two groups, cold (nearest bottom water temperature, which is often ~2°C) water seeps in the forearc (including SMT) and hot (>>0°C) vents in the arc, BAB and SMT. Therefore, temperature is a key variable for evaluating these vents. Parameters like pH, metals and sulfate ions reflect subseafloor fluid-rock interactions in the reaction zone. In addition to fluid-rock interactions, pH of the fluids reveals addition of magmatic gases in the deeper crust. Mantle and crustal signatures of hydrothermal fluids can be easily traced by elevated $^3He/^4He$ relative to atmosphere (reported as R/Ra). CO_2, CH_4, H_2 and H_2S reflect three main sources: 1) mantle or magma outgassing, 2) biochemical

reactions, 3) serpentinization. Seawater is the main source of chlorinity in hydrothermal fluids and is modified through phase separation (Butterfield et al., 1997), and precipitation or dissolution of chloride-bearing minerals (Seyfried et al., 1986; Von Damm, 1988) in the reaction zone. More details about these parameters and other compiled information are provided in supplementary Table S3.

Summary statistics of the 12 vent parameters reviewed in this study are given in Table 2.1. In this metadata analysis we first assessed vent fluid parameters (e.g., temperature and chemistry) for existing correlations between vent fluid parameters vs vent depth, fluid temperature and fluid chlorinity. Second, we compared these fluid parameters with global MOR hydrothermal vent data. Because of non-Gaussian data distributions, small numbers of observations and the fact that data for all 12 parameters does not exist for all vents, we used purely nonparametric statistical procedures. This provides robust and accurate statistical inferences in situations where the assumption of specific data distributions is questionable. Fluid concentrations used for the statistical analysis are corrected for background seawater or are at the concentration at which magnesium in solution is zero (Bischoff et al., 1975). Two approaches are described below.

Relationships between fluid parameters vs depth (Fig. 2.5 and 2.6), temperature (Fig. 2.7 and 2.8) and chlorinity (Fig. 2.9 and 2.10) were assessed using Kendall's tau coefficient (τ) along with the p-values (Table B.1) so that we can assess whether these correlations exist at the 5% level of significance. Then we compared the vent parameters of the four Mariana tectonic settings and MOR vents using rank based non-parametric Analysis of Variance (ANOVA). For multiple comparisons, the Bonferroni adjustment was applied (Brunner et al., 2016), and results are

regarded as significant if $p<0.05$ (Table B.2). Box Plots (Fig. 2.11, 2.12 and 2.13) were used to visualize the similarities and differences obtained from ANOVA.

2.4.3. Statistical Analysis of Vent Biota

We compiled vent animals for 31 vents belong to the four different Mariana tectonic settings (Table S4). These communities were first subdivided based on the basic cellular arrangement (prokaryotic vs. eukaryotic) followed by the taxonomic levels (phylum, class, family, genus and species). Sörensen similarity coefficients, which quantify the similarity of organisms found in two different habitats at their genera was computed for above geographic provinces and 7 MOR geographic provinces; $SS = 2a/(2a+b+c)$; a is the number of taxa common to the two provinces considered, b is the number of taxa exclusive to the first province, and c to the second province. Results are reported as percentage similarity; higher percentages indicate higher similarity of genera between the groups (Table B.3).

2.4.4. Statistical Analysis of Chimney Compositions

We classified chimneys into three different categories based on chemistry: carbonate and/or brucite, sulfur and sulfide-sulfate chimneys (Table S3). Proportions of each chimney type present in the four tectonic settings and the MOR vents are illustrated using pi-charts (Fig. 2.14).

2.5.RESULTS

Summary statistics of the vent parameters used in this study are given in Table 2.1. We report Kendall's correlation coefficients (τ) and corresponding p-values for the data in cases where we have at least 2 samples. We consider $\tau > 0.8$ to be a strong correlation, $0.8 > \tau > 0.45$ to be a moderate correlation, $0.45 > \tau > 0.25$ to be a weak correlation, and $0.25 > \tau$ to be no correlation; results were regarded as significant if $p<0.05$ (Table B.1). Similar ranges are used to describe negative correlations. In addition to correlation coefficients, we report adjusted p-values for multiple comparisons between Mariana vent groups (arc, FAR, SMT, BAB) and MOR vents (East Pacific Rise, Mid Cayman Rise, Galapagos Spreading Center, NE Pacific, Mid-Atlantic Ridge, Central Indian Ridge, and SW Indian Ridge) from rank-based non-parametric ANOVA procedures. Results were regarded as significant if $p<0.05$ (Table B.2).

2.5.1. Analyses of Vent Parameters

Summit depth distribution of the four tectonic settings show significant differences, for example between BAB vs arc, SMT; arc vs SMT, FAR (Table B.2). Furthermore MOR vent depths differ from BAB, arc and FAR vents; SMT vents show similar depth ranges to MOR vents (Fig. 2.11a). The deepest mean depth (Table 2.1) is observed in BAB (3488±242 mbsl), significantly deeper than the average for MOR vents (2428±683 mbsl). Vent depth has a moderate correlation with fluid CO_2 (Fig. 2.5e), CH_4 (Fig. 2.5f) and H_2S (Fig. 2.6c). Fluid temperature (Fig. 2.5a), total Fe (Fig. 2.5c), ($^3He/^4He$)/Ra (Fig. 2.6a), H_2 (Fig. 2.6b), SO_4^{2-} ions (Fig. 2.6d) and chlorinity (Fig. 2.6e) show weak correlations to depth (Table B.1). Other fluid parameters such as pH (Fig. 2.5b), Mn (Fig. 2.5d), and show minor correlations with vent depth.

Table 2.1: Summary statistics of the Mariana and mid ocean ridge vent parameters.

Variable	ARC			BAB			FAR		
	n	mean	1SD	n	mean	1SD	n	mean	1SD
Depth (m bsl)	18	646.61	578.00	13	3488.38	241.58	7	3270.43	1317.52
Temperature (^{0}C)	11	116.05	94.54	11	258.30	114.47	2	8.25	7.42
pH	7	4.25	2.35	1	3.90	n/a	8	10.95	1.49
Total Fe (mM)	12	0.00	0.00	1	0.01	n/a	5	0.00	0.00
Mn (mM)	13	0.00	0.00	1	0.25	n/a	5	0.00	0.00
(^{3}He/^{4}He)/R_a	8	7.05	0.67	1	8.60	n/a	0	n/a	n/a
CO_2 (mM)	4	2498.98	4401.36	1	41.10	n/a	1	26.00	n/a
CH_4 (mM)	4	0.01	0.01	0	n/a	n/a	2	13.50	16.26
H_2 (mM)	4	3.87	7.62	0	n/a	n/a	0	n/a	n/a
H_2S (mM)	18	0.00	0.00	1	2.50	n/a	5	0.42	0.52
SO_4^{2-}(mM)	2	29.75	2.90	1	0.60	n/a	7	3.00	6.71
Chlorinity (mM)	2	525.50	14.85	1	557.00	n/a	7	432.29	109.02

Table 2.1. (continued).

Variable	SMT			MOR		
	n	mean	1SD	n	mean	1SD
Depth (m bsl)	8	2480.13	700.81	324	2427.60	683.40
Temperature (^{0}C)	7	238.21	120.40	251	272.27	115.44
pH	7	3.96	2.17	159	4.51	1.53
Total Fe (mM)	6	2.90	3.28	123	3.84	5.97
Mn (mM)	6	1.21	0.85	118	0.71	0.79
(^{3}He/^{4}He)/R_a	5	8.08	0.34	29	7.90	0.53
CO_2 (mM)	6	43.52	25.41	81	23.53	28.69
CH_4 (mM)	6	0.03	0.04	68	1.19	4.05
H_2 (mM)	4	0.36	0.20	85	4.21	6.64
H_2S (mM)	4	3.88	3.05	133	8.49	12.90
SO_4^{2-}(mM)	7	2.89	7.11	79	4.61	13.60
Chlorinity (mM)	6	575.50	60.92	129	535.83	208.96

*n – number of vents considered; SD – standard deviation; ARC – arc; BAB – backarc; FAR – forearc; SMT – southern Mariana trough; MOR – mid ocean ridge vents.

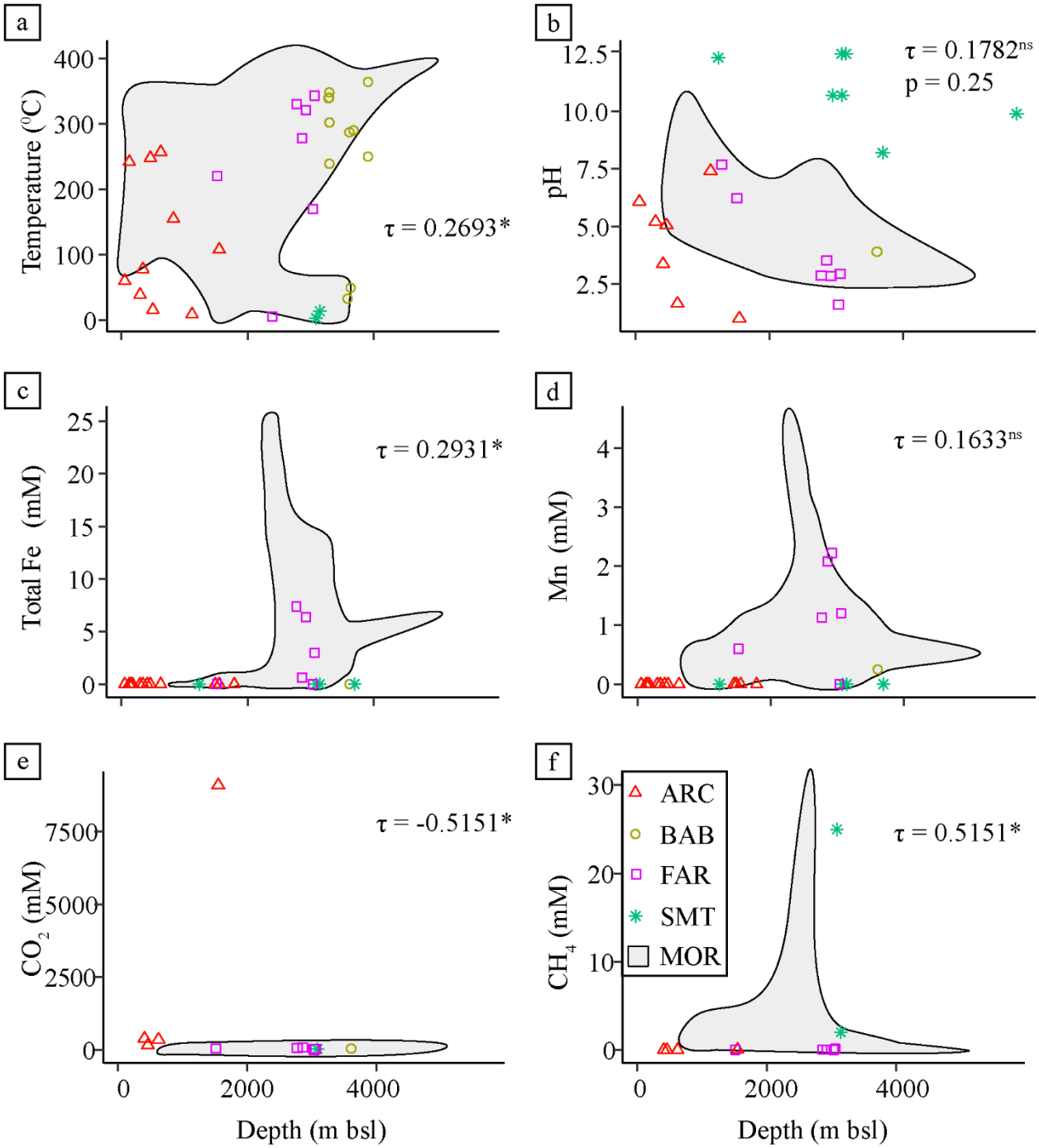

Fig. 2.5: Selected vent parameters vs. depth. Kendall's tau correlations and corresponding p-values of (a) fluid temperature (b) pH (c) total Fe (d) Mn (e) CO_2 (f) CH_4 vs depth. Moderate correlations are found for CO_2 and CH_4. Weak correlation is found for temperature and total Fe. * Significant at $p < 0.05$, ** significant at $p < 0.01$, *** significant at $p < 0.001$, **** significant at $p < 0.0001$, ns – not significant.

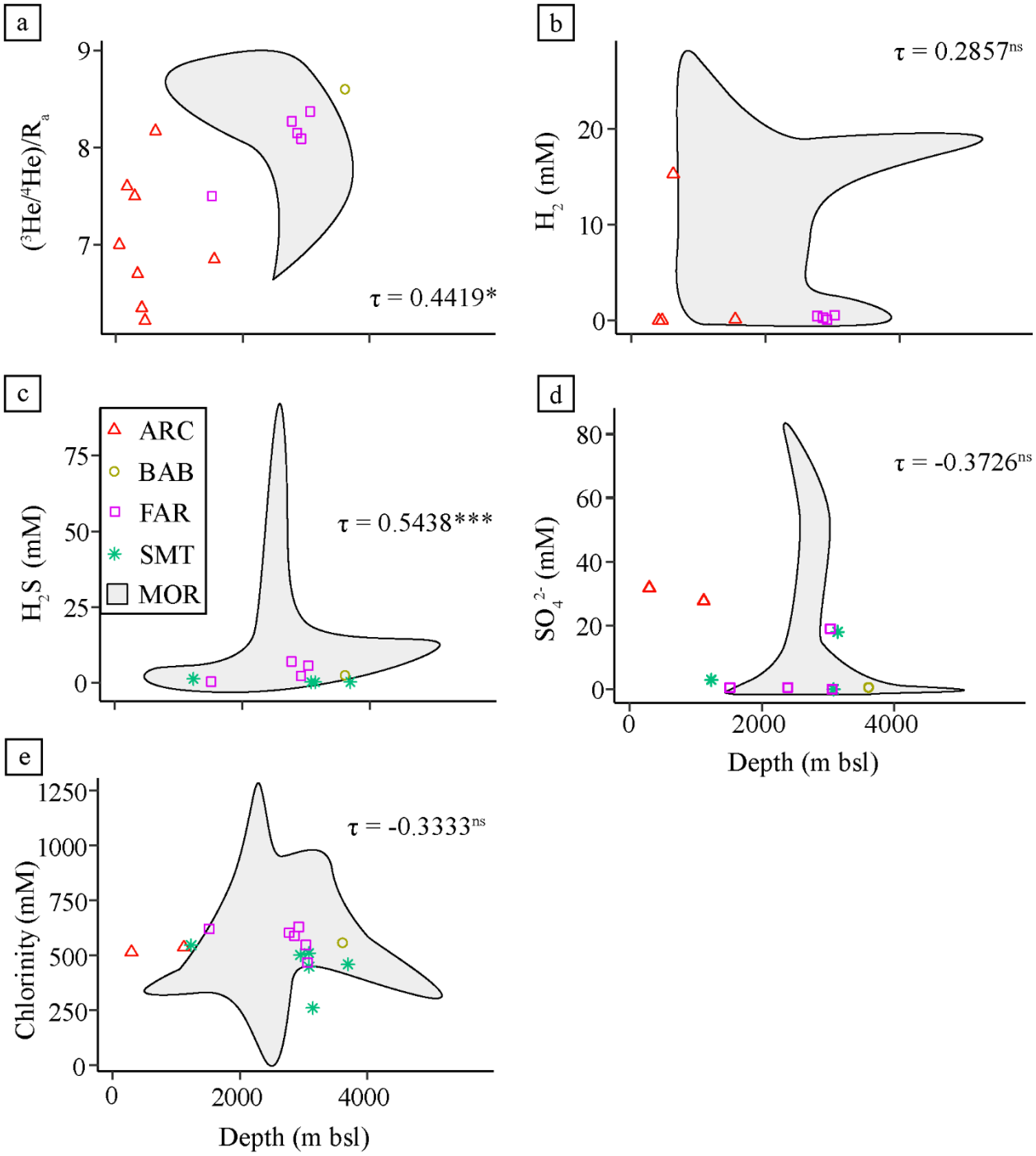

Fig. 2.6: Selected vent parameters vs. depth. Kendall's tau correlations and corresponding p-values of (a) $(^3He/^4He)/R_a$ (b) H_2 (c) H_2S (d) SO_4^{2-} ions (e) chlorinity vs depth. Moderate correlation is found for H_2S. Weak correlations are found for $(^3He/^4He)/R_a$, H_2, SO_4^{2-} ions and chlorinity. * Significant at $p < 0.05$, ** significant at $p < 0.01$, *** significant at $p < 0.001$, **** significant at $p < 0.0001$, ns – not significant.

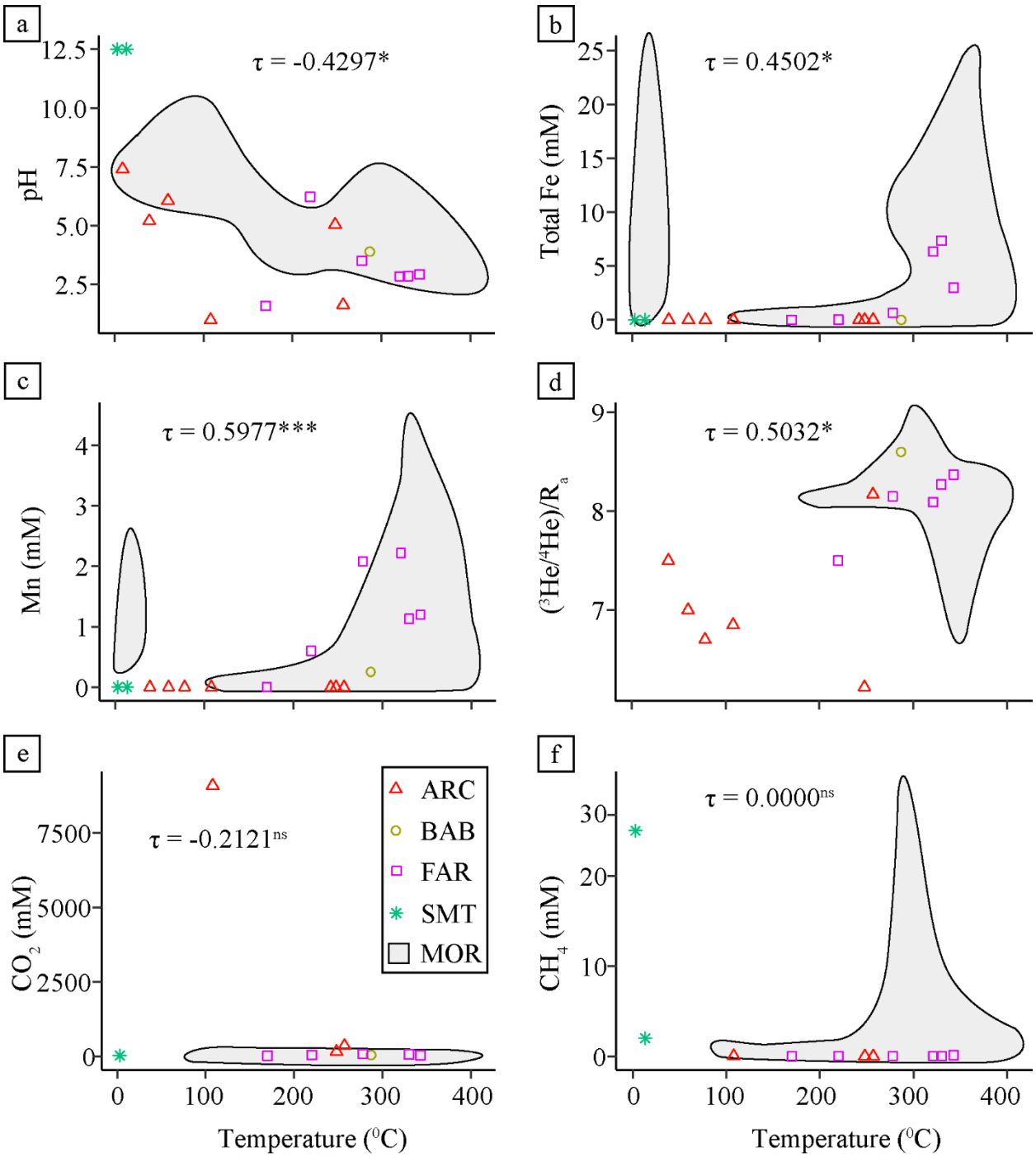

Fig. 2.7: Selected vent parameters vs. vent fluid temperature. Kendall's tau correlations and corresponding p-values of (a) pH (b) total Fe (c) Mn (d) $(^3He/^4He)/R_a$ (e) CO_2 (f) CH_4 vs temperature. Moderate correlation exists for total Fe, Mn and $(^3He/^4He)/R_a$. Weak correlations is found for fluid pH. * Significant at $p < 0.05$, ** significant at $p < 0.01$, *** significant at $p < 0.001$, **** significant at $p < 0.0001$, ns – not significant.

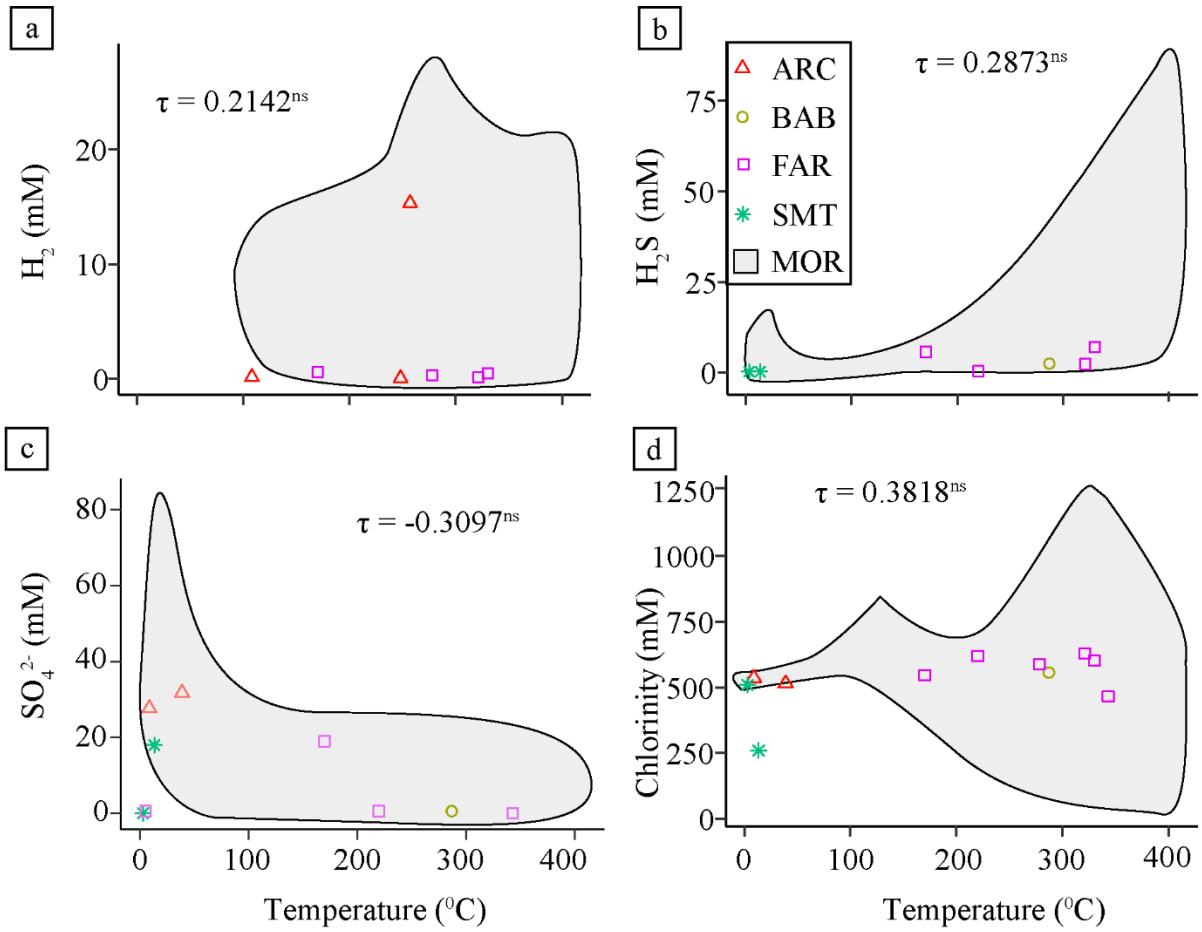

Fig. 2.8: Selected vent parameters vs. vent fluid temperature. Kendall's tau correlations and corresponding p-values of (a) H_2 (b) H_2S (c) SO_4^{2-} ions (d) Chlorinity vs temperature. Weak correlations are found for H_2S, SO_4^{2-} ions and chlorinity. * Significant at $p < 0.05$, ** significant at $p < 0.01$, *** significant at $p < 0.001$, **** significant at $p < 0.0001$, ns – not significant.

Vent fluid temperature possess a weak relationship to depth (Fig. 2.5a), however temperature has moderate correlations with total Fe (Fig. 2.7b), Mn (Fig. 2.7c) and ($^3He/^4He$)/Ra (Fig. 2.7d). Weak correlations exist for fluid pH (Fig. 2.7a), H_2S (Fig. 2.8b), SO_4^{2-} ions (Fig. 2.8c) and chlorinity (Fig. 2.8d). Fluid gases CO_2 (Fig. 2.7e), CH_4 (Fig. 2.7f), and H_2 (Fig. 2.8a) do not correlate with fluid temperature. Temperature differences among the four tectonic settings are insignificant, however arc and FAR mean temperatures significantly lower than MOR vents (Table

B.2) (Fig. 2.11b). Highest mean temperature (Table 2.1) is observed in BAB vents (258±114^{0}C) and the lowest is in FAR vents (8±7^{0}C). Even the hottest Mariana vent fluids are about 14^{0}C cooler than the average MOR fluids (272±115^{0}C). pH of BAB, SMT and arc vent fluids are lower than seawater and not significantly different from MOR vent fluids (Table B.2). However FAR fluids are more basic (Fig. 2.11c) and are different from arc, SMT and MOR (Table B.2). Fluid pH also has a moderate correlation to chlorinity (Table B.1) and weak correlations to Mn, CH_4, and H_2 (Table B.1). Chlorinity shows moderate correlations to pH, Mn (Fig. 2.9b) and H_2 (Fig. 2.9f). Weak relationships are found for total Fe (Fig. 2.9a), (^{3}He/^{4}He)/Ra (Fig. 2.9e), CH_4 (Fig. 2.9d) and H_2S (Fig. 2.10a). Fluid CO_2 (Fig. 2.9c) and SO_4^{2-} ions (Fig. 2.10b) do not correlate with chlorinity. Chlorinity between SMT vs FAR are significantly different (Table B.2). Average chlorinities for four settings show both enrichment and depletion with respect to seawater chlorinity (538 mM Cl; Butterfield, et al., 1997), FAR fluids have considerably depleted mean chlorinity (Table 2.1).

SMT vent fluids show high total Fe content compared to other settings (Fig. 2.11d) (Table 2.1), and that difference is significant for SMT vs arc (Table B.2). The average total Fe concentration for SMT is 2.9±3.3 mM and that for MOR is 3.84±5.97 mM (Table 2.1). Arc and FAR has very low total Fe concentrations (Fig. 2.11d) compared to MOR and their difference is statistically significant (Table B.2). We see a similar trend for fluid Mn (Fig. 2.12a) of which the average for SMT fluid is 1.2±0.85 mM (Table 2.1) and is more than the average for MOR, however that difference is not significant (Table B.2). Significantly different Mn levels exist between MOR vs arc, FAR and arc vs SMT (Table B.2). The (^{3}He/^{4}He)/Ra ratio of arc and MOR vents differ significantly (Fig. 2.12b) (Table B.2). Mean for arc is slightly lower (7.05±0.66) than that of MOR. SMT has slightly greater (8.08±0.34) (^{3}He/^{4}He)/Ra ratio than MOR (7.90±0.53) (Table 2.1).

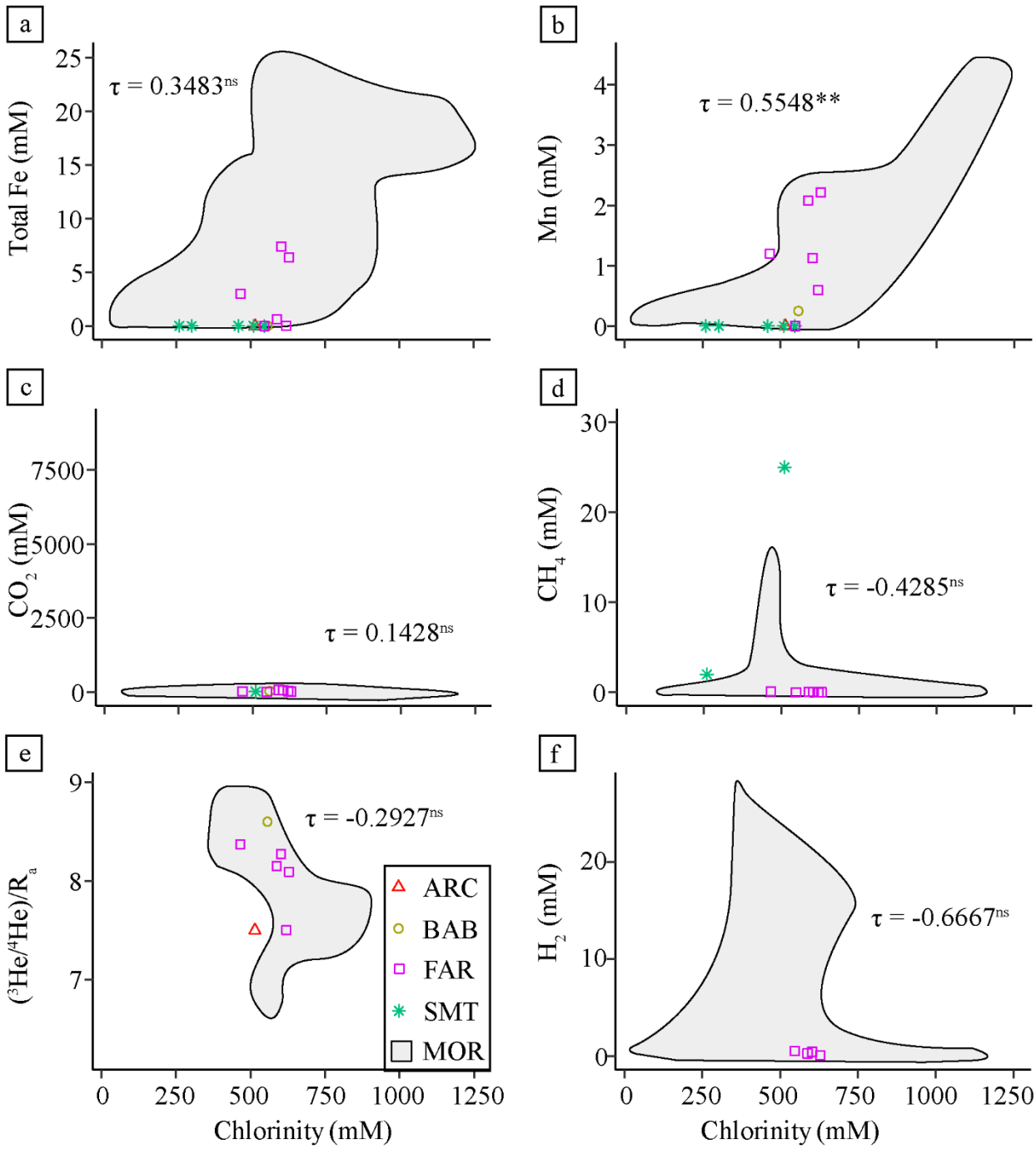

Fig. 2.9: Selected vent parameters vs. vent fluid chlorinity. Kendall's tau correlations and corresponding p-values of (a) total Fe (b) Mn (c) CO_2 (d) CH_4 (e) $(^3He/^4He)/R_a$ (f) H_2 vs chlorinity. Moderate correlations are found for Mn and H_2. Weak correlations are found for total Fe, CH_4 and $(^3He/^4He)/R_a$. * Significant at $p < 0.05$, ** significant at $p < 0.01$, *** significant at $p < 0.001$, **** significant at $p < 0.0001$, ns – not significant.

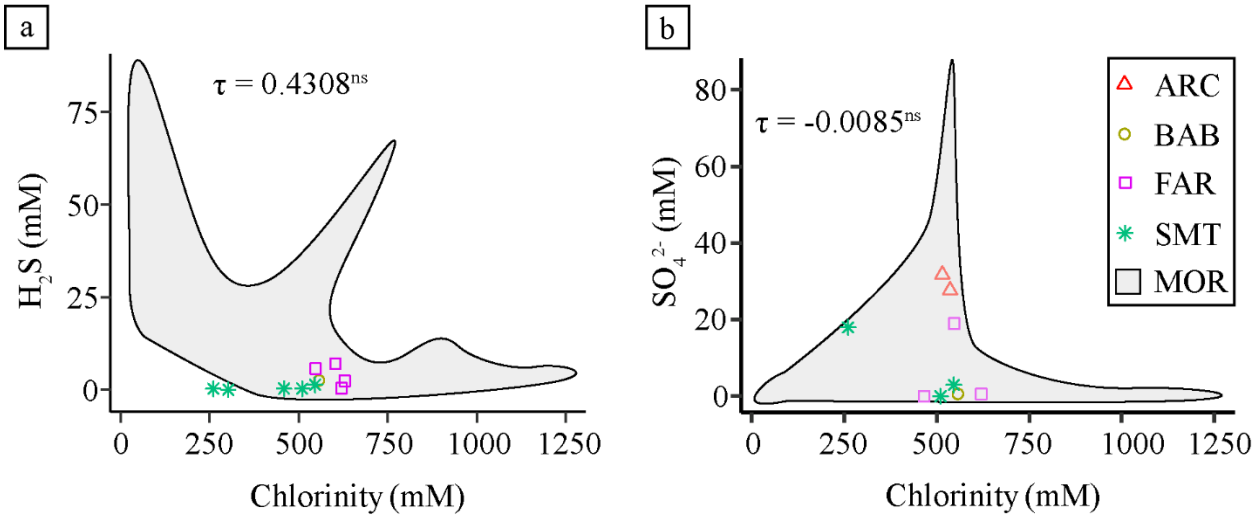

Fig. 2.10: Selected vent parameters vs. vent fluid chlorinity. Kendall's tau correlations and corresponding p-values of (a) H_2S (b) SO_4^{2-} ions vs chlorinity. A weak correlation is found for H_2S. * Significant at $p < 0.05$, ** significant at $p < 0.01$, *** significant at $p < 0.001$, **** significant at $p < 0.0001$, ns – not significant.

Carbon dioxide of the SMT and arc are significantly different from MOR vent fluids (Table B.2; Fig. 2.12c). The average for both SMT (43.5±25.4 mM) and arc ($2.5x10^3$±$4.4x10^3$ mM) is higher than the MOR fluids (23.5±28.7 mM) (Table 2.1). Hydrogen concentrations for all for settings and the MOR vents are statistically indistinguishable (Table B.2, Fig. 2.13a). The average H_2 concentration for arc vent fluids is 3.87±7.62 mM, lower than the MOR average (Table 2.1). Methane concentration of MOR vs arc and SMT are significantly different (Table B.2; Fig. 2.12d). Highest average is observed in FAR fluids (Table 2.1) and is greater than the MOR fluids. H_2S of vent fluids differ significantly between FAR and MOR (Table B.2; Fig. 2.13b). Average H_2S is highest for SMT (3.88±3.05 mM) and is higher than that of MOR (8.5±12.9 mM) (Table 2.1). Our results show that FAR and SMT fluids are depleted in SO_4^{2-} ions (Table 2.1, Fig. 2.13c) compared

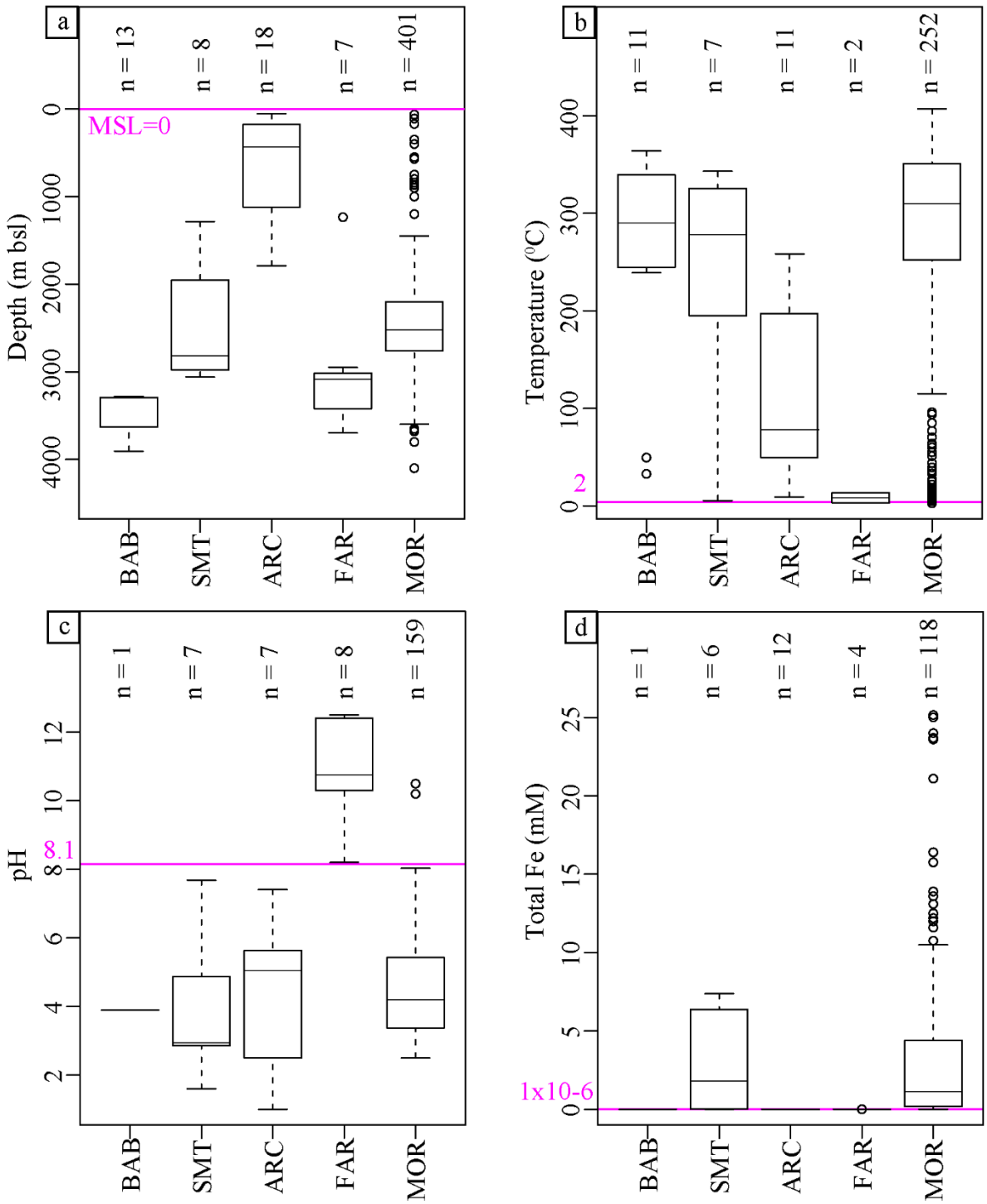

Fig. 2.11: Selected vent parameters grouped according to ridge segment spreading rate. Box and whisker plots for vent parameters (a) depth (b) temperature (c) pH (d) total Fe; n - represent the total number of individual vents considered. MSL- Mean Sea Level.

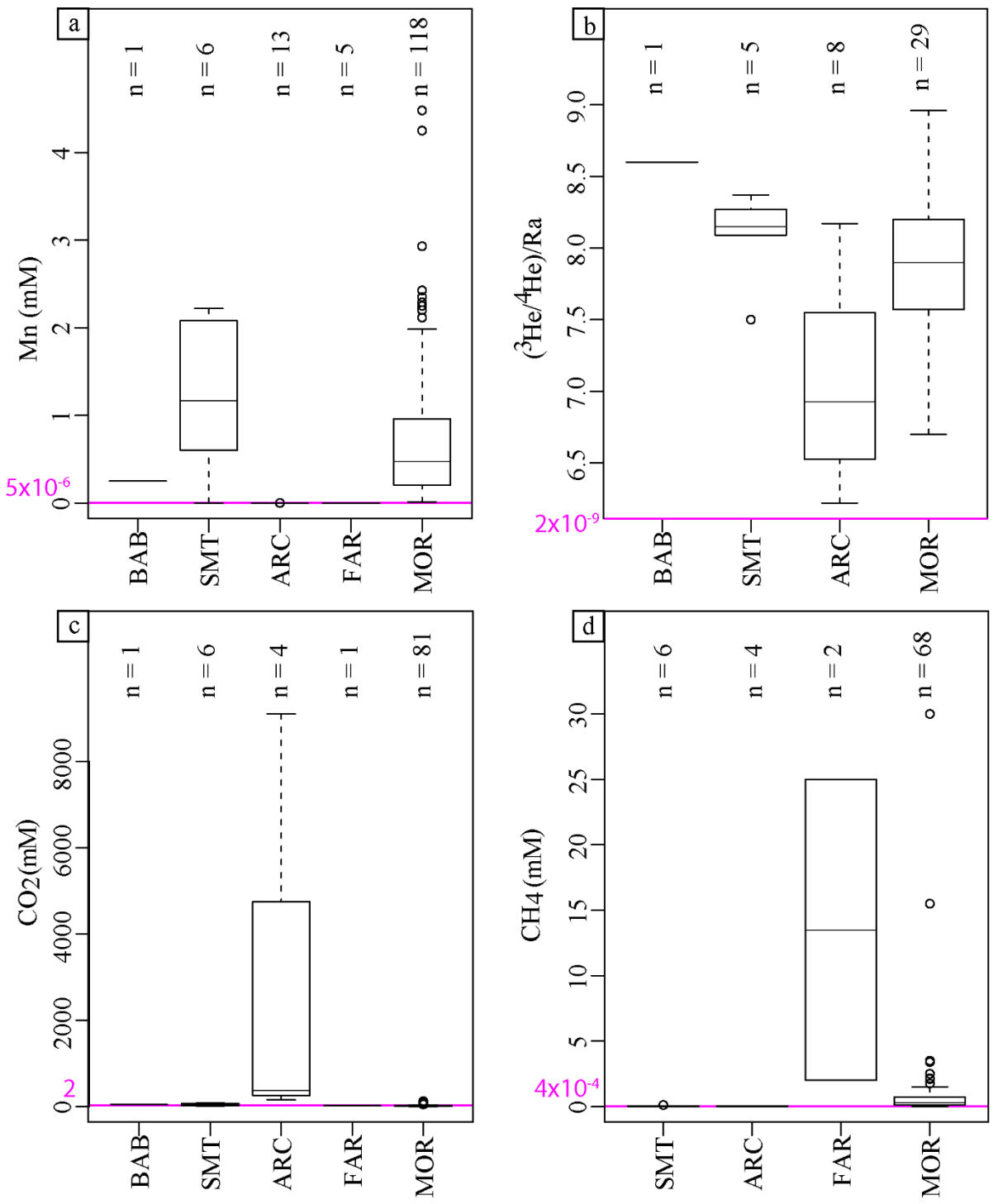

Fig. 2.12: Selected vent parameters grouped according to ridge segment spreading rate. Box and whisker plots for vent parameters (a) Mn (b) ($^3He/^4He$)/R_a (c) CO_2 (d) CH_4; n - represents the total number of individual vents considered.

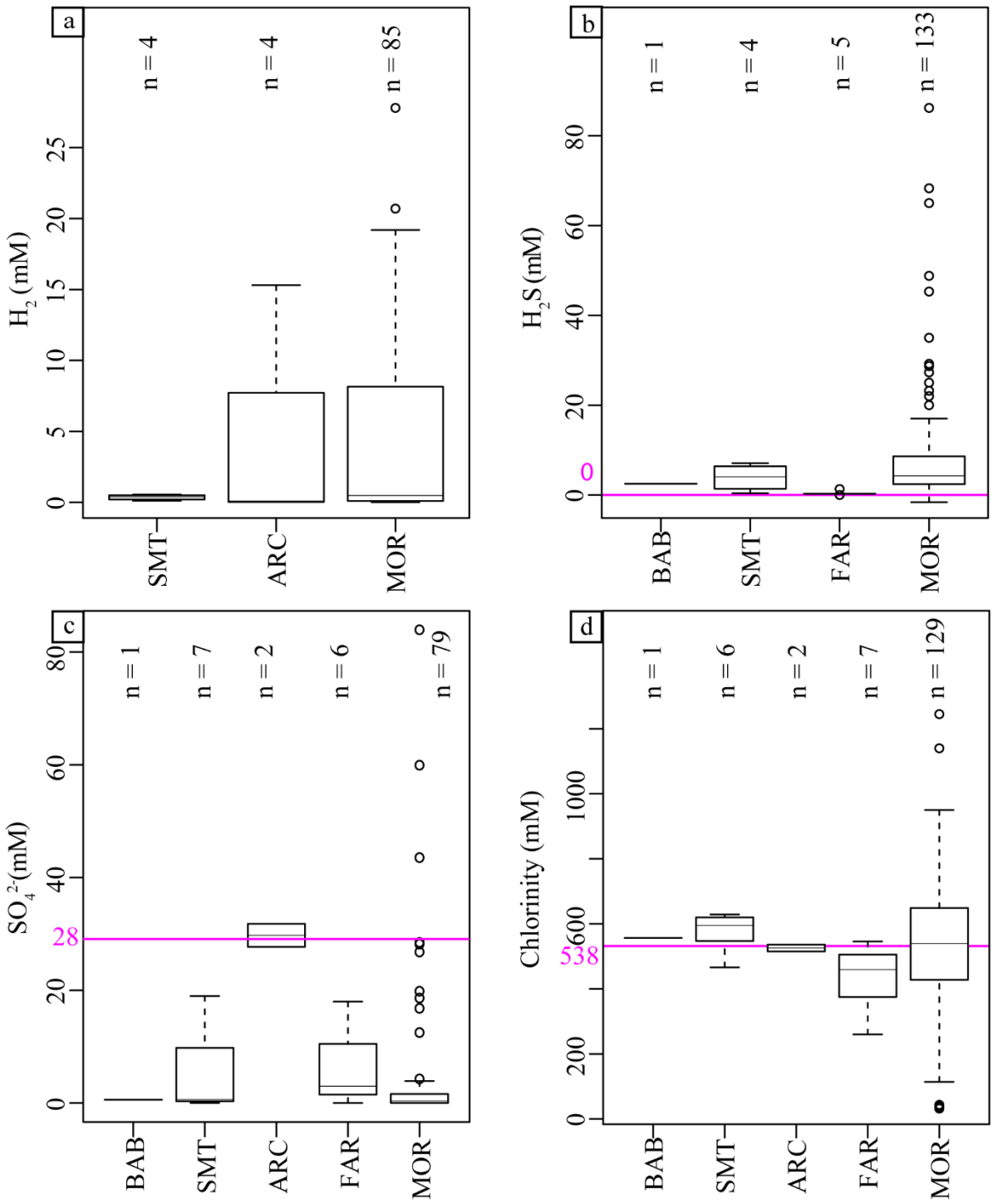

Fig. 2.13: Selected vent parameters grouped according to ridge segment spreading rate. Box and whisker plots for vent parameters (a) H_2 (b) H_2S (c) SO_4^{2-} ions (d) Chlorinity; n - represent the total number of individual vents considered.

to seawater in which average SO_4^{2-} concentrations are 28 mmol/kg (Table 2.1). Arc fluids have significantly different SO_4^{2-} ion content than MOR fluids (Table B.2).

2.5.2. Analyses of Vent Biota

Cold, alkaline forearc vent habitats vs. hot, acidic arc-backarc basin habitats are the first order controls on vent ecosystems in the Mariana convergent margin. Unsurprisingly, active venting correlates with colonization around the vents. Continuing exploration has discovered enormous biodiversity under the highest taxonomic rank of 3 main domains (Archaea, Bacteria and Eukarya; Woese, 1977). There are 39 eukaryotic genera and 19 prokaryotic genera that have been documented for Mariana vents. Under the prokaryotic domain Archaea, two different phyla so far are only recognized in Mariana forearc vents, namely Crenarchaeota and Euryarchaeota (Curtis et al., 2013; Takai et al., 2011). Five phyla of bacteria were reported in ARC, FAR and SMT vents (Aquificae, Proteobacteria, Bacteroidetes, Deferribacteres, Firmicutes). Out of 39 eukaryotic genera, 20 are reported in ARC, 15 in BAB, 5 in FAR and 15 in SMT (Table B.3).

Similarity coefficients obtained at the eukaryotic genera level for the four geographic provinces show that BAB vs SMT has the highest similarity (73%) (Table B.3). Surprisingly BAB shares more of its genera with CIR (42%), SWIR (34%) and ARC (23%). SMT also shares 30% of its genera with CIR, 29% with SWIR and 17% with ARC. ARC shares 21% of its genera with both CIR and MCR. FAR shares only 8% of its biota with ARC and shares no genera with BAB and SMT.

Our analysis reveals that out of 298 genera reported in Mariana and MOR segments, 21 genera are specific to Mariana vents. Squat lobster Genus Munidopsis is found in three Mariana

settings (BAB, SMT, ARC) and six of the MOR geographic provinces considered in this study. Neoverrcuca and Shinkailepas are also found in ARC, BAB and SMT. Alviniconcha, Austinograea, Bathymodiolus, Chorocaris, Desbruyeresia, Lepetodrilus, Phymorhynchus, Pseudorimula, Symmetromphalus and Ventsia are the other genera that can be found at least in 2 Mariana geographic provinces.

2.5.3. Analysis of Chimney Compositions

Our analysis reveals a diversity of chimney compositions: sulfur, sulfide-sulfate, carbonate/brucite (Fig. 2.14). In the Marianas, sulfide-sulfate chimneys (Fig. 2.4a) are the most common type in BAB and SMT (Nakagawa et al., 2006; NOAA Submarine Ring of Fire, 2014), similar to most MOR vents. Sulfur chimneys are also found in three of the arc volcanoes (Daikoku, Nikko and NW Eifuku) and one in the SMT-Toto Caldera (Nakagawa et al., 2006). However, sulfur chimneys are not documented for MOR vents. Carbonate (Fryer et al., 1999) and brucite (Ohara et al., 2011) chimneys (Fig. 2.4b) are only found in FAR (e.g., Shinkai Seep). Common minerals found in Mariana chimneys are sulfur, pyrite, marcasite, sphalerite, chalcopyrite, barite and minor silicates (Moore et al., 1990; Nakagawa et al., 2006; Stüben et al., 1994). Dominant minerals in FAR chimneys are calcite, aragonite, and brucite (Mottl et al., 2004) and minor amorphous silica. Chimneys can be either carbonate-dominant or brucite-dominant or a mixture of both, as is documented for the Shinkai Seep Field, where active chimneys composed of brucite transform to dead chimneys composed of carbonate (Okumura et al., 2016).

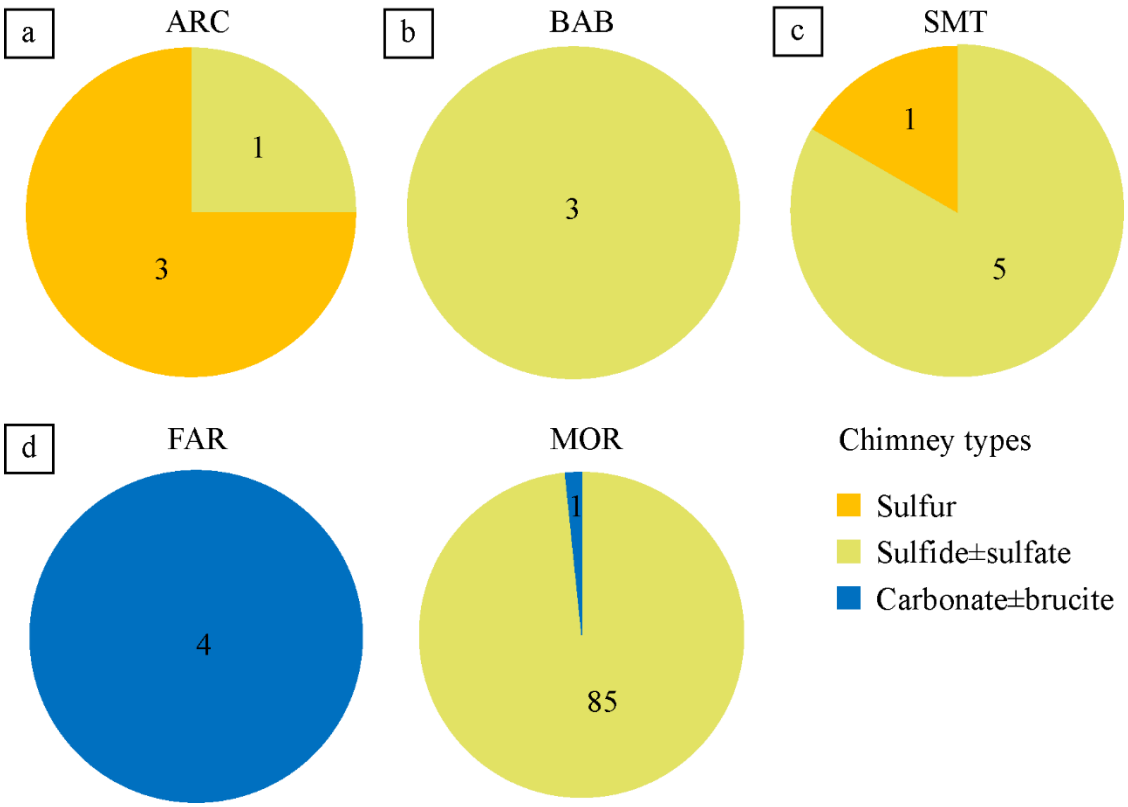

Fig. 2.14: Compositions of Mariana (a-d) and MOR (e) chimneys. (a) ARC chimneys (b) BAB chimneys (c) SMT chimneys (d) FAR chimneys. Number in each indicate numbers of occurrences listed in Supplemental Table S3.

2.6.DISCUSSION

2.6.1. How hydrothermally diverse Mariana vent system compared to MOR vent system.

Systematics of Mariana convergent margin vents provide a good foundation for understanding other submarine convergent margin vents. Mariana convergent margin vents show much more diversity in tectonic settings, fluid chemistry and biology than MOR vents. It is true for most of the hydrothermal systems that the vent fluid chemistry is controlled by rock type, temperature, residence time, depth of reaction zone and age of the hydrothermal system (Alt, 1995; German and Seyfried, 2014; Von Damm et al., 1985). In addition, convergent margins are controlled by variety

of tectonic processes in contrast to MOR where simple divergence is dominating. This asymmetry in tectonics and related magmatic processes are reflected through the differences in the bathymetry of the four tectonic regimes, and this is reflected through variable bathymetry and deep lying heat source found in the arc, whereas deeper vents with shallow lying heat source observed in the Mariana trough. Furthermore, at convergent margins, water and other volatiles lost by the deeply-rooted subduction-related processes are recycled through FAR vents and indirectly via arc, BAB, and SMT vents, providing strong asymmetry in vent fluid chemistry which is absent in mid-ocean ridge vents in which the only contribution is made through interactions of seawater with MORB. Unlike the MOR where these processes are mostly restricted to ridge axis (about 2 km across the ridge and about 5 km beneath the seafloor), the subduction zones run deep into the mantle and have their effect over 300 km across the convergent margin. The effect of the pressure sensitive dehydration of the slab prevails up to about several hundreds of kilometers (70 km for hot slabs and 300 km for cold slabs) (Schmidt and Poli, 1998) and water is continuously released through the slab while dropping most of it (30-70%) below the forearc supporting the serpentinization of the mantle wedge beneath the forearc. Schmidt and Poli (1998) inferred that another 18–37% of the subducted water will carry to depths where it might help generate arc magmas and make wetter BAB basalts (Stern, 2002). In addition to dehydration, decarbonation reactions also take place, and the influence of the both processes are visible in arc magmas which contains up to 6 wt % H_2O, compared MORB (0.4 wt % H2O) (Johnson et al., 1994). Conversely some arc vent fluids display very high CO_2 concentrations (2700 mm/kg of CO_2 observed in NW Eifuku volcano) compared to MOR systems (3-200 mmol/kg) indicating contributions from subducted carbonate bearing marine sediments (Lupton et al., 2008). Conversely CO2 concentration is highly variable and may reflect

degassing of different magma compositions (Lupton et al., 2006). This is further confirmed from our analysis where we observed significantly different ($p < 0.0001$) CO_2 concentrations for arc vs MOR fluids. SMT fluids also carry high concentrations of CO_2 and differs significantly from MOR, suggesting its arc-like nature. In addition to volatiles; comparatively less ($^3He/^4He$)/Ra ratios (average 7.05) of arc fluids with respect to MOR (R/Ra ~8) may reflect; recycling of atmospheric helium isotopes (richer in 4He) from the subduction slab or melting of new mantle as suggested by Sano and Marty, (1995). Variably low to moderate arc fluid temperatures are accounted for temporal variations and enhanced degassing of volatile-rich arc magmas in shallow magma chambers as indicated by sulfur and carbon dioxide. This contrasts with the situation for BAB and SMT fluids which are hotter than arc vent fluids due to their greater depth; BAB and SMT vent fluids are similar in this regard to MOR vent fluids. Acidity of arc, BAB, and SMT vent fluids is partly caused by the addition of magmatic gases such as CO_2, SO_2, which produces highly acidic fluids with H_2SO_4 and S_2 by interacting with water (Lupton et al., 2008; Toki et al., 2015). In addition, hot rocks associated with SMT and BAB vents, heat circulating seawater to produce hot fluids that are very effective in leaching metals and sulfur from mafic rocks (Alt, 1995) like MOR system. Reverse is observed in the FAR fluids which are cold, thus less effective in leaching metals from the rocks and therefore contain very little total Fe and Mn than MOR vent groups. Other fluid parameters of the forearc vents also greatly differ from MOR vents. Cooler alkaline fluids in Mariana forearc vents reflect subduction of the old, cold Pacific slab and addition of slab-derived fluids to the forearc lithosphere. pH is mainly controlled by the addition of CO_3^{2-} and HCO_3^- that come from carbonate dissolution reactions in the subducting slab (Frezzotti et al., 2011), and by anaerobic sulfate reduction to S_2^- that helps increase the pH (Mottl et al., 2004).

Abiotic production, thermogenesis and biological activity are possible mechanisms for producing vent CH_4 (McCollom and Seewald, 2007; Peacock, 1990; Fryer, 1992). Abiotic production via reduction of CO_2 (or other organic compounds) in the presence of H_2, is very effective in ultramafic substrates where low-T hydrothermal alteration produces strongly reducing conditions with high concentrations of H_2 (McCollom and Seewald, 2007). However, we were unable to find a correlation between CH_4 and H_2, as none of the FAR vents have measured H_2 contents. Significantly less H_2S content of FAR fluids are explained by the low contents of sulfur in forearc ultramafic rocks (McCollom, 2007).

2.6.2. SMT vent fluid chemistry provide more evidence to existing theory of seafloor spreading in southernmost Mariana

The trench, forearc, volcanic arc, and backarc are well known, geophysically established tectonic regimes of the Marianas from east to west. But the southernmost Mariana cusp (SMT) has a distinctive tectonic regime where strong extension has disrupted the typical forearc, arc and backarc observed farther north in the Marianas. Strong SMT extension is demonstrated as initial rifting followed by true seafloor spreading (Martinez et al., 2000) in response to regional tensional stresses in the overriding plate due to multiple processes. One mechanism is the combined effect of the sea anchor force due to the steep slab which resists the lateral motion of the plate and rapid convergence between Philippine-Eurasian plates (Scholz and Campos, 1995). Another possible cause is different rates of slab roll back (Miller et al., 2006) resulting from the N-S trending slab tears S of Guam (Gvirtzman and Stern, 2004) and an E-W trending slab tear N of Guam ~14.5°N (Miller et al., 2006) creating N-S extensional faulting and deformations in the overriding plate

(Fryer, 1996; Miller et al., 2006). A short video outlining the unique tectonomagmatic setting of this region can be found at https://www.youtube.com/watch?time_continue=1&v=IKGI6t7VM3g&feature=emb_logo (Stern et al., 2019). Consequently, SMT arc volcanoes are distorted by strong extension (Brounce et al., 2016) and vent fluid chemistry reflects MOR-like interactions, consistent with seafloor spreading as evidenced by dredged MORB-like basaltic glasses from the southernmost Marianas (Ribeiro et al., 2013). This is also supported by similar vent fluid chemistry observed in SMT and MOR vents. Our results indicate that for vent parameters considered in this study; depth, fluid temperature, pH, total Fe, Mn, ($^3He/^4He$)/Ra, H_2S, SO_4^{2-}, H_2 and chlorinity show the strongest similarities and the results are well explained from non-parametric ANOVA (Table B.2).

2.6.3. Diversity of Biology

Our analysis of Mariana vent biology is impeded by uneven and incomplete datasets for the biota around these vents. Clearly, future efforts to comprehensively catalog the biology around Mariana vents is needed. Nevertheless, a few key points can be made based on the data in hand. As expected, the variety of water depths and fluid compositions results in an exceptionally diverse distribution of vent organisms and communities among the different Mariana vent tectonic settings. The observed similarity between organisms at BAB and SMT vents to each other and to CIR and SWIR vents likely reflects similar fluid temperature and chemical signatures, although the great distance from the Marianas to the nearest active spreading ridges raises questions about how these larvae were dispersed. Similarities between BAB and SMT vents can be expected, given that the tectonic and geological conditions of basaltic volcanism and strong extension are similar.

In addition, ARC vent organisms also show similarities to those of BAB and SMT vents. The reasons for this are unclear, but we can imagine two scenarios: first that because BAB rifting initiated in the arc and second, because SMT magmas, rocks, and vent fluids have sufficiently arc-like features that some larvae from near-by arc vents can adapt to SMT and BAB vent conditions.

2.7.CONCLUSIONS

We conclude that convergent margin hydrothermal and cold seep vents at the Mariana convergent margin show great heterogeneity and that this diversity exceeds that of the much better known and globally more widespread MOR vents. Heterogeneity is reflected in many aspects such as the regional scales of the two tectonic regimes, in which Mariana vent fluids are being modified from the slab derived components in variable extents depending on where they are located with respect to the trench. Differences in the tectonic forces and magma supply affect their depths unlike the simple divergence observed for MOR. Fluid chemistries, especially in arc and FAR, are highly variable than the MOR, given the influence by slab contributions for arc magma and cold-alkaline nature of the forearc. These differences, the depths and variable fluid compositions help sustaining unique convergent margin vent animals. Further, distribution of vent animals is influenced by vent proximity and similar tectonics.

The Mariana vents can be categorized into four main groups as FAR, ARC, BAB and SMT following four different types of venting associated with three different types of chimney compositions. Besides the diversity shown for well-established distinct tectonic realms of FAR, ARC, and BAB, the southern portion of the Mariana Trough (SMT) is exceptional in resembling

MOR vent fluid chemistry and biology. This in turn provides further evidence that very strong extension is going on in this region, similar to MOR type seafloor spreading.

We have only begun efforts to assess and understand the strong heterogeneity of biological communities in this convergent margin. Similar heterogeneity is expected to be documented in other convergent margins. We need a more complete and uniform assessments of biota around convergent margin hydrothermal vents if we are to make progress in understanding these complex geobiological systems.

2.8.ACKNOWLEDGMENTS

We appreciate reviews by Bill Chadwick and XXX on a previous version of this manuscript. This is UTD Geosciences Dept. contribution number 1315.

Appendix B: Statistical analyses of fluid parameters and vent macro organisms in Mariana convergent margin hydrothermal system.

Table B.1: Kendall's tau coefficients (τ) and corresponding p-value for vent parameters with depth, temperature and chlorinity.

Variable	Statistics	Depth (m bsl)	Temperature (^{0}C)	pH	Total Fe (mM)	Mn (mM)	(^{3}He/^{4}He)/Ra
Depth (m bsl)	Tau	1.0000	0.2694	0.1783	0.2931	0.1633	0.4420
	p-value	****	*	ns	*	ns	*
Temperature (^{0})	Tau	0.2694	1.0000	-0.4268	0.4502	0.5978	0.5032
	p-value	*	****	*	*	***	*
pH	Tau	0.1783	-0.4268	1.0000	-0.1711	-0.2895	-0.1069
	p-value	ns	*	****	ns	ns	ns
Chlorinity (mM)	Tau	-0.3333	0.3818	-0.5042	0.3484	0.5549	-0.2928
	p-value	ns	ns	6.79E-03	ns	**	ns

Table B.1 (continued).

Variable	Statistics	CO_2 (mM)	CH_4 (mM)	H_2 (mM)	H_2S (mM)	SO_4^{2-} (mM)	Chlorinity (mM)
Depth (m bsl)	Tau	-0.5152	0.5152	0.2857	0.5438	-0.3727	-0.3333
	p-value	*	*	ns	***	ns	ns
Temperature (^{0})	Tau	-0.2121	0.0000	0.2143	0.2873	-0.3098	0.3818
	p-value	ns	ns	ns	ns	ns	ns
pH	Tau	-0.0909	0.3206	-0.4286	0.0000	-0.0193	-0.5042
	p-value	ns	ns	ns	ns	ns	**
Chlorinity (mM)	Tau	0.1429	-0.4286	-0.6667	0.4308	-0.0096	1.0000
	p-value	ns	ns	ns	ns	ns	****

§ ≥0.8 High correlation, ≤0.45-0.8> moderate correlation, ≤0.25-0.45> weak correlation, <0.25 no correlation; * Significant at $p < 0.05$, ** significant at $p < 0.01$, *** significant at $p < 0.001$, **** significant at $p < 0.0001$, ns – not significant.

Table B.2: p-Values of multiple comparisons from nonparametric Analysis of Variance (ANOVA) with Bonferroni correction.

Comparison	Depth (m bsl)	Temperature (^{0}C)	pH	Total Fe (mM)	Mn (mM)	(^{3}He/^{4}He)/R_a
BAB-SMT	****	ns	n/a	n/a	n/a	n/a
BAB-ARC	****	ns	n/a	n/a	n/a	n/a
BAB-FAR	ns	ns	n/a	n/a	n/a	n/a
BAB-MOR	****	ns	n/a	n/a	n/a	n/a
SMT-MOR	ns	ns	ns	ns	ns	ns
ARC-MOR	****	***	ns	****	****	*
FAR-MOR	*	*	****	****	****	n/a
SMT-ARC	***	ns	ns	*	**	ns
SMT-FAR	ns	ns	**	ns	ns	n/a
ARC-FAR	***	ns	**	ns	ns	n/a

Table B.2 (continued).

Comparison	CO_2 (mM)	CH_4 (mM)	H_2S (mM)	SO_4^{2-}(mM)	H_2 (mM)	Chlorinity (mM)
BAB-SMT	n/a	n/a	n/a	n/a	n/a	n/a
BAB-ARC	n/a	n/a	n/a	n/a	n/a	n/a
BAB-FAR	n/a	n/a	n/a	n/a	n/a	n/a
BAB-MOR	n/a	n/a	n/a	n/a	n/a	n/a
SMT-MOR	*	***	ns	ns	ns	ns
ARC-MOR	****	***	n/a	*	ns	ns
FAR-MOR	n/a	ns	***	ns	n/a	ns
SMT-ARC	ns	ns	n/a	ns	ns	ns
SMT-FAR	n/a	ns	ns	ns	n/a	*
ARC-FAR	n/a	ns	n/a	ns	n/a	ns

*ARC- arc; BAB- backarc; FAR- forearc; SMT- southern Mariana trough; MOR- mid ocean ridge; n/a - not available; p-value < 0.05 indicate that two settings are significantly different for the parameter considered; * Significant at $p < 0.05$, ** significant at $p < 0.01$, *** significant at $p < 0.001$, **** significant at $p < 0.0001$, ns – not significant.

Table B.3: Sörensen similarity indices for geographic provinces of Mariana vents and mid ocean ridge vents at genus level.

Setting		Mariana				Mid Ocean Ridges						
		ARC	BAB	FAR	SMT	NEP	EPR	GSC	MAR	SWIR	CIR	MCR
Mariana	ARC	100%	23%	8%	17%	5%	5%	17%	8%	13%	21%	21%
	BAB	23%	100%	0%	73%	11%	10%	0%	11%	34%	42%	17%
	FAR	8%	0%	100%	0%	3%	3%	50%	2%	6%	9%	0%
	SMT	17%	73%	0%	100%	5%	7%	0%	11%	29%	30%	8%
Mid Ocean Ridges	NEP	5%	11%	3%	5%	100%	23%	3%	14%	12%	20%	6%
	EPR	5%	10%	3%	7%	23%	100%	4%	24%	20%	28%	6%
	GSC	17%	0%	50%	0%	3%	4%	100%	4%	7%	15%	17%
	MAR	8%	11%	2%	11%	14%	24%	4%	100%	26%	26%	6%
	SWIR	13%	34%	6%	29%	12%	20%	7%	26%	100%	59%	11%
	CIR	21%	42%	9%	30%	20%	28%	15%	26%	59%	100%	17%
	MCR	21%	17%	0%	8%	6%	6%	17%	6%	11%	17%	100%

* ARC- arc; BAB- backarc; FAR- forearc; SMT- southern Mariana trough; CIR-Central Indian Ridge; EPR- East Pacific Rise; GSC- Galapagos Spreading Center; MCR- Mid Cayman Rise; MAR- Mid Atlantic Ridge; NEP- Northeast Pacific Ridges (Explorer Ridge/ Juan de Fuca Ridge and Gorda Ridge); SWIR- Southwest Indian Ridge.

REFERENCES

Alt, J. C. (1995). Subseafloor Processes in Mid-Ocean Ridge Hydrothermal Systems. Seafloor Hydrothermal Systems: Physical, chemical, biological, and geological interactions, Geophysical Monograph 91, 85-114.

Alt, J. C., Shanks III, W. C., & Jackson, M. C. (1993). Cycling of sulfur in subduction zones: The geochemistry of sulfur in the Mariana Island Arc and back-arc trough. Earth and Planetary Science Letters, 119(4), 477-494.

Anderson, M. O., W. W. Chadwick, Jr., M. D. Hannington, S. G. Merle, J. A. Resing, E. T. Baker, D. A. Butterfield, S. L. Walker, and N. Augustin (2017), Geological interpretation of volcanism and segmentation of the Mariana back-arc spreading center between 12.7°N and 18.3°N, Geochem. Geophys. Geosyst., 18, doi:10.1002/2017GC006813.

Baker, E. T., Embley, R. W., Walker, S. L., Resing, J. A., Lupton, J. E., Nakamura, K. I., ... & Massoth, G. J. (2008). Hydrothermal activity and volcano distribution along the Mariana arc. Journal of Geophysical Research: Solid Earth, 113(B8) doi:10.1029/2007JB005423.

Baker, E. T., S. L. Walker, J. A. Resing, W. W. Chadwick Jr., S. G. Merle, M. O. Anderson, D. A. Butterfield, N. J. Buck, and S. Michael (2017), The effect of arc proximity on hydrothermal activity along spreading centers: New evidence from the Mariana back-arc (12.7°–18.3°N), Geochem. Geophys. Geosyst., 18(11), 4211–4228, doi:10.1002/2017GC007234.

Bischoff, J. L., Clancy, J. J., & Booth, J. S. (1975). Magnesium removal in reducing marine sediments by cation exchange. Geochimica et Cosmochimica Acta, 39(5), 559-568.

Bloomer, S. H., Stern, R. J., Fisk, E., and Geschwind, C. H., 1989. Shoshonitic volcanism in the northern Mariana Arc: 1. Petrographic and major and trace element characteristics. Journal of Geophysical Research, B94, 4469-4496.

Brounce, M.N., Kelley, K., Stern, R. J., Martinez, F., and Cottrell, E., 2016. The Fina Nagu Volcanic Complex: Unusual submarine arc volcanism in the rapidly deforming southern Mariana margin. Geochemistry, Geophysics, Geosystems DOI: 10.1002/2016GC006457

Brunner, E., Konietschke, F., Pauly, M., & Puri, M. L. (2016). Rank-based procedures in factorial designs: hypotheses about non-parametric treatment effects. Journal of the Royal Statistical Society: Series B (Statistical Methodology). Journal of the Royal Statistical Society 79(5), 1463-1485.

Butterfield, D. A., Jonasson, I. R., Massoth, G. J., Feely, R. A., Roe, K. K., Embley, R. E., ... & Delaney, J. R. (1997). Seafloor eruptions and evolution of hydrothermal fluid chemistry.

Philosophical Transactions of the Royal Society of London A: Mathematical, Physical and Engineering Sciences, 355(1723), 369-386.

Corliss, J. B., Dymond, J., Gordon, L. I., Edmond, J. M., von Herzen, R. P., Ballard, R. D., ... & van Andel, T. H. (1979). Submarine thermal springs on the Galapagos Rift. Science, 203(4385), 1073-1083.

Craig, H. (1987). Hydrothermal vents in the Mariana Trough: Results of the first Alvin dives. Eos, Transactions, American Geophysical Union, 68, 1531.

Curtis, A. C., Wheat, C. G., Fryer, P., & Moyer, C. L. (2013). Mariana forearc serpentinite mud volcanoes harbor novel communities of extremophilic archaea. Geomicrobiology Journal, 30(5), 430-441.

Embley, R. W., Baker, E. T., Butterfield, D. A., Chadwick, W. W., Lupton, J. E., Resing, J. A., ... & Merle, S. G. (2007). Exploring the submarine ring of fire: Mariana Arc-Western Pacific. Oceanography, 20(4), 68-79.

Embley, R. W., Baker, E. T., Chadwick, W. W., Lupton, J. E., Resing, J. A., Massoth, G. J., & Nakamura, K. (2004). Explorations of Mariana Arc volcanoes reveal new hydrothermal systems. Eos, Transactions American Geophysical Union, 85(4), 37-40.

Frezzotti, M. L., Selverstone, J., Sharp, Z. D., & Compagnoni, R. (2011). Carbonate dissolution during subduction revealed by diamond-bearing rocks from the Alps. Nature Geoscience, 4(10), 703.

Fryer, P. (1995). Geology of the Mariana trough. In Backarc Basins (pp. 237-279). Springer US.

Fryer, P. (1996). Evolution of the Mariana convergent plate margin system. Reviews of Geophysics, 34(1), 89-125.

Fryer, P., & Mottl, M. J. (1992). Lithology, mineralogy, and origin of serpentine muds recovered from Conical and Torishima forearc seamounts: results of Leg 125 drilling. In Fryer, P., Pearce, JA, Stokking, LB, et al., Proc. ODP, Sci. Results. Vol. 125, pp. 343-362.

Fryer, P., (1990). Recent Marine Geological Research in the Mariana and Izu-Bonin Island Arcs. Pacific Science 44, 95-114.

Fryer, P., Ambos, E.L., and Hussong, D.M., (1985) Origin and emplacement of Mariana forearc seamounts. Geology 13, 774-777.

Fryer, P., Pearce, J. A., & Stokking, L. B. (1992). 36. A synthesis of Leg 125 drilling of serpentine seamounts on the Mariana and Izu–Bonin forearcs. In Proceedings of the Ocean Drilling Program, Scientific Results, Vol. 125, pp. 593-614.

Fryer, P., Wheat, C. G., & Mottl, M. J. (1999). Mariana blueschist mud volcanism: Implications for conditions within the subduction zone. Geology, 27, 103-106.

German, C. R., & Seyfried Jr, W. E. (2014). 8.7-hydrothermal processes. Treatise on Geochemistry, 2nd Edn, eds HD Holland and KK Turekian (Oxford: Elsevier), 191-233.

Gvirtzman, Z., & Stern, R. J. (2004). Bathymetry of Mariana trench-arc system and formation of the Challenger Deep as a consequence of weak plate coupling. Tectonics, 23(2).

Hawkins, J. W., Lonsdale, P. F., Macdougall, J. D., & Volpe, A. M. (1990). Petrology of the axial ridge of the Mariana Trough backarc spreading center. Earth and Planetary Science Letters, 100(1-3), 226-250.

Iwaida, C., & Ueno, H. (2005). Ore and gangue minerals of seafloor hydrothermal deposits in the Mariana trough. JAMSTEC Report of Research and Development, 1, 1-12.

Johnson, M. C., J. A. T. Anderson, and M. J. Rutherford, Pre-eruptive volatile contents of magmas, in Volatiles in Magmas, Rev. Mineral., vol. 30, edited by M. R. Carroll and J. R. Holloway, pp. 281–330, Mineral. Soc. of Am., Washington D. C., 1994.

Lin, P.-N., Stern, R. J., and Bloomer, S. H., 1989. Shoshonitic Volcanism in the Northern Mariana Arc: 2. Large-Ion Lithophile and Rare Earth Element Abundances - Evidence for the Source of Incompatible Element Enrichments in Intra-Oceanic Arcs. Journal of Geophysical Research 94B, 4497-4514.

Lowell, R. P. (2010). Hydrothermal circulation at slow spreading ridges: analysis of heat sources and heat transfer processes. Diversity of hydrothermal systems on slow spreading ocean ridges. Geophysical Monograph, 188, 11-26.

Lowell, R. P., Rona, P. A., & Von Herzen, R. P. (1995). Seafloor hydrothermal systems. Journal of Geophysical Research: Solid Earth, 100(B1), 327-352.

Lupton, J., Lilley, M., Butterfield, D., Evans, L., Embley, R., Massoth, G., ... & Schmidt, M. (2008). Venting of a separate CO2-rich gas phase from submarine arc volcanoes: Examples from the Mariana and Tonga-Kermadec arcs. Journal of Geophysical Research: Solid Earth, 113(B8).

Martinez, F., Fryer, P., and Becker, N. (2000), Geophysical Characteristics of the Southern Mariana Trough, 11°50'N-13°40'N, Journal of Geophysical Research: Solid Earth, 105(B7), 16591-16607.

McCollom, T. M. (2007). Geochemical constraints on sources of metabolic energy for chemolithoautotrophy in ultramafic-hosted deep-sea hydrothermal systems. Astrobiology, 7(6), 933-950.

McCollom, T. M., & Seewald, J. S. (2007). Abiotic synthesis of organic compounds in deep-sea hydrothermal environments. Chemical Reviews, 107(2), 382-401.

Miller, M. S., Gorbatov, A., & Kennett, B. L. (2006). Three-dimensional visualization of a near-vertical slab tear beneath the southern Mariana arc. Geochemistry, Geophysics, Geosystems, 7(6).

Moore, W. S., & Stakes, D. (1990). Ages of barite-sulfide chimneys from the Mariana Trough. Earth and Planetary Science Letters, 100(1-3), 265-274.

Mottl, M. J., Wheat, C. G., Fryer, P., Gharib, J., & Martin, J. B. (2004). Chemistry of springs across the Mariana forearc shows progressive devolatilization of the subducting plate. Geochimica et Cosmochimica Acta, 68(23), 4915-4933.

Nakagawa, T., Takai, K., Suzuki, Y., Hirayama, H., Konno, U., Tsunogai, U., & Horikoshi, K. (2006). Geomicrobiological exploration and characterization of a novel deep-sea hydrothermal system at the TOTO caldera in the Mariana Volcanic Arc. Environmental Microbiology, 8(1), 37-49.

Ohara, Y., Reagan, M. K., Fujikura, K., Watanabe, H., Michibayashi, K., Ishii, T., ... & Ribeiro, J. (2012). A serpentinite-hosted ecosystem in the Southern Mariana Forearc. Proceedings of the National Academy of Sciences, 109(8), 2831-2835.

Okumura, T., Ohara, Y., Stern, R. J., Yamanaka, T., Onishi, Y., Watanabe, H., ... & Ishii, T. (2016). Brucite chimney formation and carbonate alteration at the Shinkai Seep Field, a serpentinite-hosted vent system in the southern Mariana forearc. Geochemistry, Geophysics, Geosystems, 17(9), 3775-3796.

Peacock, S. M. (1990). Fluid processes in subduction zones. Science, 248(4953), 329-337.

Pettibone, M. H. (1989). New species of scale-worms (Polychaeta: Polynoidae) from the hydrothermal rift-area of the Mariana Back-arc Basin in the Western Central Pacific. Proceedings of the Biological Society of Washington, 102(1), 137-153.

Plank, T., & Langmuir, C. H. (1993). Tracing trace elements from sediment input to volcanic output at subduction zones. Nature, 362(6422), 739-743.

Ribeiro, J. M., Stern, R. J., Kelley, K. A., Martinez, F., Ishizuka, O., Manton, W. I., & Ohara, Y. (2013). Nature and distribution of slab-derived fluids and mantle sources beneath the Southeast Mariana forearc rift. Geochemistry, Geophysics, Geosystems, 14(10), 4585-4607.

Sakai, R., Kusakabe, M., Noto, M., & Ishii, T. (1990). Origin of waters responsible for serpentinization of the Izu-Ogasawara-Mariana forearc seamounts in view of hydrogen and oxygen isotope ratios. Earth and Planetary Science Letters, 100(1-3), 291-303.

Sano, Y., & Marty, B. (1995). Origin of carbon in fumarolic gas from island arcs. Chemical Geology, 119(1-4), 265-274.

Schmidt, M. W., and S. Poli, Experimentally based water budgets for dehydrating slabs and consequences for arc magma generation, Earth Planet. Sci. Lett., 163, 361–379, 1998.

Scholz, C. H., & Campos, J. (1995). On the mechanism of seismic decoupling and back arc spreading at subduction zones. Journal of Geophysical Research: Solid Earth, 100(B11), 22103-22115.

Seyfried Jr, W. E., Berndt, M. E., & Janecky, D. R. (1986). Chloride depletions and enrichments in seafloor hydrothermal fluids: Constraints from experimental basalt alteration studies. Geochimica et Cosmochimica Acta, 50(3), 469-475.

Shipboard Scientific Party, 1990. Introduction. In Fryer, P., Pearce, J.A., Stokking, L.B., et al., Proc. ODP, Init. Repts., 125: College Station, TX (Ocean Drilling Program), 5–14. doi: 10.2973/odp.proc.ir.125.101.1990

Smoot, N. C. (1990). Mariana Trough by multi-beam sonar. Geo-Marine Letters, 10(3), 137-144.

Stein, C. A., & Stein, S. (1994). Constraints on hydrothermal heat flux through the oceanic lithosphere from global heat flow. Journal of Geophysical Research: Solid Earth, 99(B2), 3081-3095.

Stern, R. J. (2002). Subduction zones. Reviews of Geophysics, 40(4).

Stern, R. J. (2010). The anatomy and ontogeny of modern intra-oceanic arc systems. Geological Society, London, Special Publications, 338(1), 7-34.

Stern, R. J., Fouch, M. J., & Klemperer, S. L. (2003). An overview of the Izu-Bonin-Mariana subduction factory. Inside the Subduction Factory, Washington, DC: American Geophysical Union, ©2003. 175-222.

Stern, R. J., Jackson, M. C., Fryer, P., & Ito, E. (1993). O, Sr, Nd and Pb isotopic composition of the Kasuga cross-chain in the Mariana arc: a new perspective on the K-h relationship. Earth and Planetary Science Letters, 119(4), 459-475.

Stern, R.J., Ohara, Y., Martinez, F., and Lin, J. (2019). Deep Challenges in the Southern Marianas. AGU Fall Meeting (abstract)

Stern, R. J., Ren, M., Kelley, K. A., Ohara, Y., Martinez, F., & Bloomer, S. H. (2014). Basaltic volcaniclastics from the Challenger Deep forearc segment, Mariana convergent margin: Implications for tectonics and magmatism of the southernmost Izu–Bonin–Mariana arc. Island Arc, 23(4), 368-382.

Stern, R. J., Tamura, Y., Masuda, H., Fryer, P., Martinez, F., Ishizuka, O., & Bloomer, S. H. (2013). How the Mariana volcanic arc ends in the south. Island Arc, 22(1), 133-148.
Stern, R., & Smoot, N. C. (1998). A bathymetric overview of the Mariana forearc. Island Arc, 7(3), 525-540.

Stüben, D., Taibi, N. E., McMurtry, G. M., Scholten, J., Stoffers, P., & Zhang, D. (1994). Growth history of a hydrothermal silica chimney from the Mariana backarc spreading center (southwest Pacific, 18 13′ N). Chemical Geology, 113(3-4), 273-296.

Takai, K., & Nakamura, K. (2011). Archaeal diversity and community development in deep-sea hydrothermal vents. Current opinion in microbiology, 14(3), 282-291.

Toki, T., Ishibashi, J. I., Noguchi, T., Tawata, M., Tsunogai, U., Yamanaka, T., & Nakamura, K. (2015). Chemical and isotopic compositions of hydrothermal fluids at Snail, Archaean, Pika, and Urashima sites in the Southern Mariana Trough. In Subseafloor Biosphere Linked to Hydrothermal Systems (pp. 587-602). Springer Japan.

Van Dover, C. L. (2002). Community structure of mussel beds at deep-sea hydrothermal vents. Marine Ecology Progress Series, 230, 137-158.

Von Damm, K. L. (1988). Systematics of and postulated controls on submarine hydrothermal solution chemistry. Journal of Geophysical Research: Solid Earth, 93(B5), 4551-4561.

Von Damm, K. L., Edmond, J. M., Grant, B., Measures, C. I., Walden, B., & Weiss, R. F. (1985). Chemistry of submarine hydrothermal solutions at 21 N, East Pacific Rise. Geochimica et Cosmochimica Acta, 49(11), 2197-2220.

Woese, C. R., & Fox, G. E. (1977). Phylogenetic structure of the prokaryotic domain: the primary kingdoms. Proceedings of the National Academy of Sciences, 74(11), 5088-5090.

BIOGRAPHICAL SKETCH

Diluni Hetti Pathirannehelage was born in Sri Lanka. After completing her school education, she pursued a bachelor's degree in Geology from Faculty of Science, University of Peradeniya, Sri Lanka from 2007 to 2011. Following graduation, she worked in the Department of Geosciences as a Teaching Assistant until mid-2012. Then, she received the opportunity to pursue her graduate studies at the University of Texas at Dallas (UTD), in the Department of Geosciences in January 2015. She started working as a Teaching Assistant in the department in August 2015. As a graduate student, she had the privilege of participating in a research expedition to the Mariana trench in 2016. In addition, she participated in the AAPG Imperial Barrel Award Competition (Southwest Section) as part of the team that represented UTD in 2018. She was awarded the Best Teaching Assistant Award in Fall 2018 by the UTD Department of Geosciences.

CURRICULUM VITAE

Diluni Ayeshika Wimalaratne, Hetti Pathirannehelage
Hayward, CA. | Email: dah130130@utdallas.edu
LinkedIn: https://www.linkedin.com/in/diluni-hetti-110877152/

TEACHING AND WORKING EXPERIENCE

Graduate Teaching Assistant

Department of Geosciences, University of Texas at Dallas 2015 – Present

- Conducting laboratories of Stratigraphy and Sedimentology, Physical Geology, Paleobiology, History of Earth and Life, and The Oceans.
- Conducting field trips.
- Evaluating student performance, including grading examinations, quizzes, assignments and papers.
- Communicating with students in-person as needed.
- Promptly responding to student inquiries regarding grades, assignments, attendance and course materials.
- Planning, scheduling and facilitating review sessions for examinations as requested by course instructors.

Teaching Assistant

Department of Geology, University of Peradeniya, Sri Lanka 2011 – 2012

- Conducted Optical Mineralogy lectures for second year undergraduates.
- Conducted laboratories of Structural Geology, Crystallography and Mineralogy, Optical Mineralogy, Petrology (Metamorphic/Igneous/Sedimentary) and Hydrology.
- Assisted in field visits and assessments.
- Received and promptly responded to student inquiries regarding grades, assignments, attendance and course materials.

Trainee Geologist, Moragahakande Hydro Power Project, Sri Lanka 2011

- Participated in field mapping program of Moragahakande Hydro Power Project, Sri Lanka.
- Produced maps of geology and geological structures.

In-Plant Trainee Geologist, Dankotuwa Porcelain PLC, Sri Lanka 2010

- Analyzed the behavior of clay (Bentonite) materials in industrial porcelain production process.

Trainee Geologist, National Building Resource Organization, Sri Lanka 2009

- Participated in the field mapping program in landslide prone areas of Central Province of Sri Lanka.
- Produced digitized maps using ArcGIS.
- Generated professional reports.

EDUCATION

The University of Texas at Dallas

Ph.D. in Geosciences 2015 – Present

- Multivariate statistical analysis of seafloor hydrothermal vents
- Expedition to the Mariana trench in Western Pacific Ocean
- PhD Research Small Grants Travel Award – 2019
- Developed and maintains the Global Magmatic and Tectonic Laboratory (GMTL) University of Texas at Dallas website.

M.S. in Geosciences 2015 - 2017

University of Peradeniya, Sri Lanka

B.Sc. (Special) in Geology 2007 – 2011

- Field relations, geochemistry and petrography of Augen Gneiss in Sri Lanka

---

PUBLICATIONS

- Hetti, D. A., Stern, R. J., (2019) Global Mid Ocean Ridge Hydrothermal Vents and Their Biota: A Review (Manuscript Submitted to Marine Geology)

- Hetti, D. A., Gunawardana, A, M., Konietschke, F., Stern, R. J., (2019) A Compilation of Hydrothermal and Cold-Seep Vents in the Mariana Convergent Margin: Tectonics, Fluid Chemistry and Biology (Manuscript in preparation)
- Hetti, D. A., Stern, R. J., (2019) Multivariate Statistical Analysis for Global Mid Ocean Ridge Hydrothermal Vents. AGU Fall Meeting (abstract)
- D. Wimalaratne, L.R.K.Perera and Rohana Chandrajith (2012) Geology of Augen Gneiss at Minneriya, Sri Lanka. Proceedings of the 28th Annual Sessions - Geological Society of Sri Lanka (abstract)

SOFTWARE, SKILLS AND EXPERTISE

- ArcGIS 10.3
- R, MATLAB and MS Excel
- Adobe Illustrator CS6
- Paradigm
- Scanning Electron Microscope (SEM)
- Atomic Absorbance Spectrophotometry (AAS)
- Kingdom
- ERDAS IMAGINE
- GEOMAPAPP
- Adobe Illustrator CS6

HONORS AND AWARDS

- PhD Research Small Grant Program at UTD – Travel Award ($1000)
  2019
- Best Teaching Assistant – Department of Geosciences, University of Texas at Dallas
  2018

PROFESSIONAL MEMBERSHIP

- American Geophysical Union (AGU)

- American Association for Petroleum Geoscientists (AAPG)
- Geological Society of Sri Lanka (GSSL)

LEADERSHIP AND EXTRACURRICULAR ACTIVITIES

- Core logging workshop 2017 – Texas Christian University Core Facility
- 3D seismic interpretation workshop 2017 – Pioneer Natural Resources
- Historian of the UTD AAPG Student Chapter (2017 – 2018)